

AD-A182 622

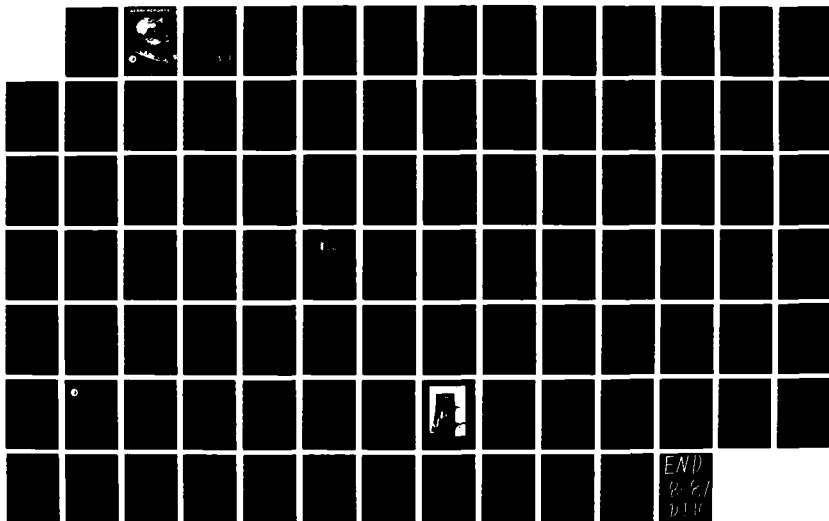
AFFRI (ARMED FORCES RADIOBIOLOGY RESEARCH INSTITUTE)  
REPORTS JANUARY FEBRUARY MARCH 1967(U) ARMED FORCES  
RADIOBIOLOGY RESEARCH INST BETHESDA MD APR 67

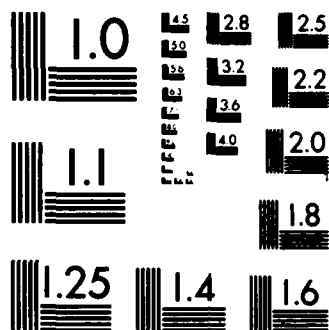
1/1

UNCLASSIFIED

F/G 6/7

NL





# AFRRI REPORTS

②

DTIC FILE COPY

Jan  
Feb  
Mar  
1987

AD-A182 622



Defense Nuclear Agency  
Armed Forces Radiobiology Research Institute

Bethesda, Maryland 20814-5145

This document has been approved  
for public release and sale; its  
distribution is unlimited.

87

003

DTIC  
ELECTE  
JUL 10 1987

UNCLASSIFIED

SECURITY CLASSIFICATION OF THIS PAGE

ADA182622

## REPORT DOCUMENTATION PAGE

|   |       |  |  |   |                                   |
|---|-------|--|--|---|-----------------------------------|
| 1a. REPORT SECURITY CLASSIFICATION<br><b>UNCLASSIFIED</b>   |       |  | 1b. RESTRICTIVE MARKINGS   |   |                                   |
| 2a. SECURITY CLASSIFICATION AUTHORITY   |       |  | 3. DISTRIBUTION/AVAILABILITY OF REPORT<br>Approved for public release; distribution unlimited. |   |                                   |
| 2b. DECLASSIFICATION/DOWNGRADING SCHEDULE   |       |  |  |   |                                   |
| 4. PERFORMING ORGANIZATION REPORT NUMBER(S)<br><b>SR87-1 through SR87-9 and TR86-4</b>  |       |  | 5. MONITORING ORGANIZATION REPORT NUMBER(S)  |   |                                   |
| 6a. NAME OF PERFORMING ORGANIZATION<br><b>Armed Forces Radiobiology Research Institute</b>  |       | 6b. OFFICE SYMBOL<br>(If applicable)<br><b>AFRRI</b> | 7a. NAME OF MONITORING ORGANIZATION  |   |                                   |
| 6c. ADDRESS (City, State and ZIP Code)<br><b>Defense Nuclear Agency<br/>Bethesda, Maryland 20814-5145</b>   |       |  | 7b. ADDRESS (City, State and ZIP Code)   |   |                                   |
| 8a. NAME OF FUNDING/SPONSORING ORGANIZATION<br><b>Defense Nuclear Agency</b>  |       | 8b. OFFICE SYMBOL<br>(If applicable)<br><b>DNA</b>   | 9. PROCUREMENT INSTRUMENT IDENTIFICATION NUMBER  |   |                                   |
| 8c. ADDRESS (City, State and ZIP Code)<br><b>Washington, DC 20305</b>   |       |  | 10. SOURCE OF FUNDING NOS.   |   |                                   |
|   |       |  | PROGRAM ELEMENT NO.<br><b>NWED QAXM</b>  | PROJECT NO.   | TASK NO.                          |
| 11. TITLE (Include Security Classification)<br><b>AFRRI Reports, Jan-Mar 1987</b>   |       |  |  |   |                                   |
| 12. PERSONAL AUTHOR(S)  |       |  |  |   |                                   |
| 13a. TYPE OF REPORT<br><b>Reprints/Technical</b>  |       | 13b. TIME COVERED<br>FROM _____ TO _____             |  | 14. DATE OF REPORT (Yr., Mo., Day)<br><b>1987 April</b> |                                   |
| 15. PAGE COUNT<br><b>94</b>   |       |  |  |   |                                   |
| 16. SUPPLEMENTARY NOTATION  |       |  |  |   |                                   |
| 17. COSATI CODES  |       |  | 18. SUBJECT TERMS (Continue on reverse if necessary and identify by block number)              |   |                                   |
| FIELD   | GROUP | SUB. GR.   |  |   |                                   |
|   |       |  |  |   |                                   |
|   |       |  |  |   |                                   |
| 19. ABSTRACT (Continue on reverse if necessary and identify by block number)<br><br>This volume contains AFRRI Scientific Reports SR87-1 through SR87-9 and Technical Report TR86-4 for Jan-Mar 1987. |       |  |  |   |                                   |
| 20. DISTRIBUTION/AVAILABILITY OF ABSTRACT<br><b>UNCLASSIFIED/UNLIMITED</b> <input type="checkbox"/> SAME AS RPT. <input checked="" type="checkbox"/> DTIC USERS <input type="checkbox"/>              |       |  | 21. ABSTRACT SECURITY CLASSIFICATION<br><b>UNCLASSIFIED</b>                                    |   |                                   |
| 22a. NAME OF RESPONSIBLE INDIVIDUAL<br><b>Junith A. Van Deusen</b>  |       |  | 22b. TELEPHONE NUMBER<br>(Include Area Code)<br><b>(202)295-3536</b>                           |   | 22c. OFFICE SYMBOL<br><b>ISDP</b> |

DD FORM 1473, 83 APR

EDITION OF 1 JAN 73 IS OBSOLETE

UNCLASSIFIED  
SECURITY CLASSIFICATION OF THIS PAGESDTIC  
ELECTE  
JUL 10 1987  
E

UNCLASSIFIED

SECURITY CLASSIFICATION OF THIS PAGE

UNCLASSIFIED

SECURITY CLASSIFICATION OF THIS PAGE

## CONTENTS

### Scientific Reports

**SR87-1:** Brook, I., Walker, R. I., and MacVittie, T. J. Effect of radiation dose on the recovery of aerobic and anaerobic bacteria from mice;

**SR87-2:** Moran, A. Sodium-hydrogen exchange system in LLC-PK<sub>1</sub> epithelium;

**SR87-3:** Moran, A., Biber, J., and Murer, H. A sodium-hydrogen exchange system in isolated apical membrane from LLC-PK<sub>1</sub> epithelia;

**SR87-4:** Mullin, M. J., and Hunt, W. A. Effects of ethanol on the functional properties of sodium channels in brain synaptosomes;

**SR87-5:** Neta, R., Douches, S. D., and Oppenheim, J. J. Radioprotection by interleukin-1;

**SR87-6:** Neta, R., Vogel, S. N., Oppenheim, J. J., and Douches, S. D. Cytokines in radioprotection. Comparison of the radioprotective effects of IL-1 to IL-2, GM-CSF and IFN $\gamma$ ;

**SR87-7:** Tolliver, J. M., and Pellmar, T. C. Dithiothreitol elicits epileptiform activity in CA<sub>1</sub> of the guinea pig hippocampal slice;

**SR87-8:** Warnick, J. E., and Pellmar, T. C. Resistance of afterhyperpolarizations in hippocampal pyramidal cells to prostaglandins and vasoactive intestinal polypeptide (VIP);

**SR87-9:** Yoshida, H., and Swenberg, C. E. Kinetic flow dichroism study of conformational changes in supercoiled DNA induced by ethidium bromide and noncovalent and covalent binding of benzo[a]pyrene diol epoxide; a.i.w.

### Technical Report

**TR86-4:** Dooley, M., Eagleson, D. M., Mohaupt, T. H., Kazi, A. H., and Zeman, G. H. Reference dosimetry for 1986 NATO battlefield dosimetry intercomparison at Army Pulsed Radiation Facility.

|                    |  |
|--------------------|--|
| Accession For      |  |
| NTIS GRA&I         | <input checked="checked" type="checkbox"/> |
| DTIC TAB           | <input type="checkbox"/>                   |
| Unannounced        | <input type="checkbox"/>                   |
| Justification      |  |
| By                 |  |
| Distribution/      |  |
| Availability Codes |  |
| Dist               | Avail and/or<br>Special                    |
| A-1                |  |



# Effect of radiation dose on the recovery of aerobic and anaerobic bacteria from mice<sup>1</sup>

ITZHAK BROOK,<sup>2</sup> RICHARD I. WALKER, AND THOMAS J. MACVITTIE

Naval Medical Research Institute and Armed Forces Radiobiology Research Institute, Bethesda, MD, U.S.A. 20814

Accepted June 3, 1986

BROOK, I., R. I. WALKER, and T. J. MACVITTIE. 1986. Effect of radiation dose on the recovery of aerobic and anaerobic bacteria from mice. *Can. J. Microbiol.* 32: 719-722.

The presence of aerobic and anaerobic bacteria in the blood, spleen, and liver was investigated in mice that were exposed to 7, 8, 9, or 10 Gy <sup>60</sup>Co radiation. Microorganisms were detected more often in animals exposed to higher doses of radiation. The number of mice that were culture positive and the number of isolates in one site increased with increasing dose. Bacteria were recovered in mice killed at various times after radiation, in 3 of 100 mice exposed to 7 Gy, in 13 of 100 irradiated with 8 Gy, in 23 of 90 exposed to 9 Gy, and in 34 of 87 irradiated with 10 Gy. The predominant organisms recovered were *Escherichia coli*, anaerobic Gram-positive cocci, *Proteus mirabilis*, *Staphylococcus aureus*, and *Bacteroides* spp. *Escherichia coli* and anaerobes were more often isolated in animals exposed to 10 Gy, while *S. aureus* was more often recovered in those irradiated with 9 Gy. These data demonstrate a relationship between the dose of radiation and the rate of infection due to enteric aerobic and anaerobic bacteria.

BROOK, I., R. I. WALKER et T. J. MACVITTIE. 1986. Effect of radiation dose on the recovery of aerobic and anaerobic bacteria from mice. *Can. J. Microbiol.* 32: 719-722.

Chez des souris exposées à des radiations de 7, 8, 9, et 10 de Gy de <sup>60</sup>Co nous avons recherché la présence de bactéries aérobies et anaérobies au niveau du sang, de la rate et du foie. Les bactéries se retrouvaient plus souvent chez les animaux qui avaient reçu les plus fortes doses de radiation. Le nombre de souris qui donnaient des cultures positives et le nombre d'isolements à un site anatomique augmentaient avec la dose de radiation. Des bactéries ont été isolées chez des souris sacrifiées à différents temps après l'irradiation soit chez 3 des 100 souris exposées à 7 Gy, 13 des 100 exposées à 8 Gy, 23 des 90 exposées à 9 Gy et 34 des 87 irradiées avec 10 Gy. Les principales espèces observées étaient *Escherichia coli*, *Proteus mirabilis*, *Staphylococcus aureus*, des coques anaérobies gram-positifs et des *Bacteroides* spp. *Escherichia coli* et les anaérobies étaient plus souvent isolés chez les souris irradiées avec 10 Gy alors que *S. aureus* était plus souvent isolé chez les souris irradiées avec 9 Gy. Ces résultats confirment qu'il existe une relation entre la dose de radiation et la fréquence des infections dues à des bactéries entériques aérobies et anaérobies.

[Traduit par la revue]

## Introduction

Increased dose of whole-body irradiation is associated with greater mortality in animals (Gordon et al. 1955; Miller et al. 1951). These animals show increased susceptibility to various endogenous or exogenous pathogens (Benacerraf 1960). The majority of the endogenous pathogens are of enteric origin and can be recovered from lymphatic organs as well as from the blood stream of these animals.

Most previous studies of infections in irradiated animals did not utilize methodologies for recovery of anaerobic bacteria. When we employed methods for recovery of anaerobic as well as aerobic bacteria, we were able to recover both types of microorganisms from animals irradiated with a fatal dose of radiation (Brook, Hunter et al. 1984); We have extended our previous studies to evaluate the effect of graded doses of radiation on the incidence of isolation of anaerobic and aerobic bacteria from the blood, spleen, and liver.

## Materials and methods

### Animals

Mice (female C3H/ebFeJ, 10-12 weeks old; Jackson Laboratories, Bar Harbor, ME) were quarantined and acclimated to laboratory

conditions for 21 weeks before experimentation, during which time samples from each shipment were examined and found to be free of murine pneumonia complex, oropharyngeal *Pseudomonas* sp., and mouse hepatitis virus. Six mice were housed in each cage before and after radiation.

### Experimental design

Mice in well-aerated, perforated Plexiglass restrainers were exposed to bilateral, whole-body radiation from the AFRRRI cobalt-60 source at a rate of 1.5 Gy per min at ambient temperature. The midline absorbed dose was 7, 8, 9, or 10 Gy (1 Gy = 100 rads) measured by dosimetry. The distance to the radiation source was 376 cm. Each group of 90 mice was divided into groups of 40 and 50 mice each. The group of 40 mice was used for monitoring mortality, and the other was used for sacrifice for the purpose of obtaining cultures. The experiment was done two times.

After irradiation, the mice were observed for mortality and symptoms of disease between days 0 and 21. As long as there were living animals present in a group, five animals were selected at random from each irradiation group on days 1, 3, 5, 7, 9, 11, 13, 15, 17, and 21. Samples were also obtained from 10 nonirradiated mice who served as a control. Animals were sacrificed by cervical dislocation. The spleens and livers were removed aseptically, were immediately homogenized, and then swabbed onto media for aerobic and anaerobic bacteria. Through open heart puncture, 0.3-0.5 mL of blood was obtained and plated on media for aerobic and anaerobic bacteria (Lennette et al. 1980; Sutter et al. 1980).

The time between collection and inoculation of media never exceeded 5 min. The media used for aerobes were blood, chocolate, and MacConkey agars. For anaerobic bacteria, pre-reduced media were used which included vitamin K<sub>1</sub> enriched brucella blood agar, and a selective blood agar plate containing kanamycin and vancomycin were used (Sutter et al. 1980). The plates were immediately incubated in anaerobic GasPak jars (BBL, Cockeysville, MD). The aerobic plates were incubated in air and 5% carbon dioxide and were read at 24 and 48 h. The GasPak jars were not opened until after 48 h incubation and were

<sup>1</sup>This work was supported in part by the Naval Medical Research and Development Command work unit No. 3M463750D808.AB.062 and the Armed Forces Radiobiology Research Institute MIPR No. 820023. The opinions and assertions contained herein are the private ones of the writer and are not to be construed as official or reflecting the views of the Navy Department, the naval services at large, or the Defense Nuclear Agency.

<sup>2</sup>Author to whom reprint requests should be addressed. Present address: Experimental Hematology Department, Armed Forces Radiobiology Research Institute, Bethesda, MD, U.S.A. 20814-5145.

TABLE 1. Bacteria recovered from mice irradiated with different doses

| ORGANISMS                           | Days after irradiation |   |   |    |   |   |   |    |    |   |   |    |    |   |   |    | Total no. of mice exhibiting recoverable microorganisms |    |   |   |   |    |   |   |     |    |  |  |  |
|-------------------------------------|------------------------|---|---|----|---|---|---|----|----|---|---|----|----|---|---|----|---|----|---|---|---|----|---|---|-----|----|--|--|--|
|                                     | 7                      |   |   |    | 9 |   |   |    | 11 |   |   |    | 13 |   |   |    |   | 15 |   |   |   | 17 |   |   |     | 21 |  |  |  |
|                                     | 7 <sup>a</sup>         | 8 | 9 | 10 | 7 | 8 | 9 | 10 | 7  | 8 | 9 | 10 | 7  | 8 | 9 | 10 |   | 7  | 8 | 9 | 7 | 8  | 9 | 7 | 8   |    |  |  |  |
| <b>Aerobic</b>                      |                        |   |   |    |   |   |   |    |    |   |   |    |    |   |   |    |   |    |   |   |   |    |   |   |     |    |  |  |  |
| <i>Escherichia coli</i>             |                        |   | 1 | 1  |   |   |   | 1  |    |   | 2 | 6  |    | 2 | 3 | 7  |   | 2  |   |   | 4 |    |   | 4 | 33  |    |  |  |  |
| <i>Enterobacter cloacae</i>         |                        |   |   |    | 1 |   |   |    |    |   |   |    |    |   | 2 |    |   | 1  |   |   |   |    |   |   | 4   |    |  |  |  |
| <i>Proteus mirabilis</i>            |                        |   |   |    |   |   |   |    |    | 4 | 4 |    |    |   | 2 | 4  |   |    |   |   |   |    |   |   | 14  |    |  |  |  |
| <i>Pseudomonas aeruginosa</i>       |                        |   |   |    |   |   |   | 1  | 1  |   |   |    |    |   |   |    |   |    |   |   |   |    |   |   | 2   |    |  |  |  |
| <i>Staphylococcus aureus</i>        |                        |   | 1 |    |   |   | 2 |    |    |   | 3 | 1  |    |   | 2 | 2  |   |    |   |   |   |    |   |   | 11  |    |  |  |  |
| <i>Staphylococcus epidermidis</i>   |                        |   |   |    |   |   |   |    |    |   |   |    |    |   |   | 2  |   |    |   |   |   |    |   |   | 2   |    |  |  |  |
| Alpha hemolytic streptococcus       |                        |   |   |    |   |   |   | 2  |    |   |   |    |    |   | 1 |    |   |    |   |   |   |    |   |   | 3   |    |  |  |  |
| Subtotal                            |                        |   |   |    |   |   |   |    |    |   |   |    |    |   |   |    |   |    |   |   |   |    |   |   | 69  |    |  |  |  |
| <b>Anaerobic</b>                    |                        |   |   |    |   |   |   |    |    |   |   |    |    |   |   |    |   |    |   |   |   |    |   |   |     |    |  |  |  |
| <i>Peptococcus</i> spp.             |                        |   |   | 1  |   |   |   | 4  |    |   |   | 5  |    |   |   | 5  |   |    |   |   |   |    |   |   | 15  |    |  |  |  |
| <i>Peptostreptococcus</i> spp.      |                        |   |   |    |   |   |   |    |    |   |   | 5  |    |   |   | 1  |   |    |   |   |   |    |   |   | 6   |    |  |  |  |
| <i>Propionibacterium acnes</i>      |                        |   | 1 |    |   |   | 1 |    |    | 1 | 1 |    | 1  |   |   |    |   |    |   |   |   |    |   |   | 5   |    |  |  |  |
| <i>Bacteroides asaccharolyticus</i> |                        |   |   |    |   | 1 |   |    |    |   |   |    |    |   |   |    |   |    |   |   |   |    |   |   | 1   |    |  |  |  |
| <i>Bacteroides distasonis</i>       |                        |   | 1 |    |   |   |   |    |    |   | 1 |    |    |   |   | 2  |   |    |   |   |   |    |   |   | 4   |    |  |  |  |
| <i>Fusobacterium necrogenes</i>     |                        |   |   |    |   | 1 |   |    |    |   |   |    |    |   |   | 1  |   |    |   |   |   |    |   |   | 2   |    |  |  |  |
| Subtotal                            |                        |   |   |    |   |   |   |    |    |   |   |    |    |   |   |    |   |    |   |   |   |    |   |   | 33  |    |  |  |  |
| Total                               |                        |   |   |    |   |   |   |    |    |   |   |    |    |   |   |    |   |    |   |   |   |    |   |   | 102 |    |  |  |  |

NOTE: Data are given as the number of mice from whom bacteria were recovered from at least one site. An isolate had to be recovered from at least one site for the mouse to be culture positive. Mice were subject to 7, 8, 9, and 10 Gy of irradiation. A total of 80 mice were included in each irradiation group, and a maximal number of 10 mice were sacrificed per day from each group.

<sup>a</sup>Dose of irradiation in Grays. Data for 10 Gy was previously published (Brook, MacVittie et al. 1984) and is presented here for comparison.

held for 7 days. A thioglycolate broth was incubated aerobically for 14 days. Aerobic isolates were identified by conventional criteria (Lennette et al. 1980). Anaerobes were identified on the basis of Gram-stain morphology, gas-liquid chromatography of metabolic by-products, and the Minitek (BBL) anaerobic identification scheme (Sutter et al. 1980).

#### Statistical analysis

Statistical analysis was done utilizing the chi-square and Mann-Whitney tests (Sokal and Rohlf 1975). A mouse was considered to be culture positive when a bacterial isolate was recovered from at least one site, and each bacterial isolate was counted only once irrespective of site location.

### Results

#### Mortality

Mortality did not occur in any irradiated groups until 9 days postirradiation. In animals irradiated with 10 Gy, mortality was first noted on day 9 and all animals died by day 13. In animals irradiated with 9 Gy, mortality was first noted on day 10 and all animals died by day 18. In animals irradiated with 8 Gy, mortality was first noted on day 11 and 54 (67.5%) of the 80 expired by day 21. In animals irradiated with 7 Gy, mortality was first noted on day 10, and 29 (36%) animals died by day 21.

#### Isolation of microorganisms

No bacterial growth was noted in the cultures obtained from the nonirradiated mice. Infection was not detected until 7 days postirradiation and was first noted in the animals exposed to 9 and 10 Gy. The results of bacterial cultures of blood, spleen, and liver are summarized in Table 1 and represent a summary of the two experiments totalling 100 mice per inoculation group. Cultures were obtained from 377 mice. Most organisms were recovered concomitantly in all three sites: liver, spleen, and blood. Each bacterial isolate was counted only as one even when it was recovered from more than one site in a mouse. There was

a total of 102 isolates, 69 aerobic and 33 anaerobic. The predominant aerobic organisms were *Escherichia coli* (recovered from 33 mice), *Proteus mirabilis* (14 isolates), and *Staphylococcus aureus* (11 isolates). The most frequently isolated anaerobes were Gram-positive cocci (21 isolates), *Bacteroides* spp. and *Propionibacterium acnes* (5 isolates of each).

Different organisms were isolated from the various groups. Although of statistical borderline significance, *E. coli* was recovered more often in mice exposed to 10 Gy than 9 Gy (15 in 34 vs. 6 in 23 culture-positive mice;  $P = 0.0519$ ). On the other hand, *S. aureus* was recovered more often in the group exposed to 9 Gy compared with those exposed to 10 Gy (8 in 23 vs. 3 in 34;  $P = 0.015$ ). Anaerobic bacteria were isolated more often in those exposed to 10 Gy compared with those exposed to 9 Gy (25 of 34 vs. 2 in 23;  $P = 0.001$ ).

Most of the organisms were recovered from mice irradiated with 10 and 9 Gy (Table 2). Sixty different organisms were recovered from 34 animals exposed to 10 Gy (1.25 organisms per culture-positive animal), 26 organisms from 23 animals exposed to 9 Gy (1.13 organisms per animal), 13 organisms from 13 animals exposed to 8 Gy (1 organism per animal), and 3 organisms were found in 3 animals irradiated with 7 Gy (1 organism per animal).

The total number of mice in which organisms were recovered and the distribution of aerobic and anaerobic bacteria also varied (Table 2). In the group irradiated with 10 Gy, a total of 34 (60%) of the 57 sacrificed mice had bacterial isolates in at least one site. Aerobic bacteria were recovered exclusively in 9 (27%) of the 34 culture-positive mice; anaerobic bacteria were recovered exclusively in 15 (44%), and mixed aerobic and anaerobic flora were recovered in 10 mice (29%). Thus, anaerobic bacteria were recovered from a total of 73% of the culture-positive mice, and aerobic bacteria were recovered from 71%.



TABLE 2. Number of bacterial isolates per mouse<sup>a</sup> and type of bacteria recovered in the irradiated mice

| Dose of irradiation, Gy | Aerobes only (%) | Anaerobes only (%) | Aerobes and anaerobes (%) | No. of isolates per mouse |    |   | Total no. of isolates | No. of culture-positive mice | Total no. of cultured mice |
|-------------------------|------------------|--------------------|---------------------------|---------------------------|----|---|-----------------------|------------------------------|----------------------------|
|                         |                  |                    |                           | 1                         | 2  | 3 |                       |                              |                            |
| 7.00                    | 2(67)            | 1(33)              | —                         | 3                         | —  | — | 3                     | 3                            | 100                        |
| 8.00                    | 13(100)          | —                  | —                         | 13                        | —  | — | 13                    | 13                           | 100                        |
| 9.00                    | 21(91)           | —                  | 2(9)                      | 20                        | 3  | — | 26                    | 23                           | 90                         |
| 10.00                   | 9(27)            | 15(44)             | 10(29)                    | 14                        | 14 | 6 | 60                    | 34                           | 87                         |

<sup>a</sup>Including isolates from liver, spleen, and blood.

In a group exposed to 9 Gy a total of 23 (38%) of the 60 sacrificed mice had bacterial isolates in at least one of their sites. Aerobic bacteria were recovered in 21 (91%), and anaerobic bacteria in 2 (9%). The mice irradiated with 8 Gy had bacteria (all aerobes) recovered in only 13 of the 70 (19%) of the sacrificed mice, and the animals exposed to 7.00 Gy had bacteria recovered from 3 (4%) of the 70 sacrificed animals.

### Discussion

These data demonstrate a relationship between the amount of radiation and the number and type of organisms recovered from mice. *Escherichia coli* and anaerobic bacteria were more often isolated from mice irradiated with 10 Gy as compared with those exposed to 9 Gy, while *S. aureus* were more often recovered from animals exposed to 9 Gy. Polymicrobial infections, due mostly to mixed aerobic and anaerobic organisms, were also found more than in animals exposed to 10 Gy.

Our findings support the clinical observations of the high frequency of similar infections in severely immunocompromised individuals (Kramer et al. 1982). The recovery of the enteric Gram-negative organisms from lethally irradiated mice confirms previous studies (Gordon et al. 1955; Miller et al. 1951), but anaerobic organisms have been less often described. Bennett et al. (1951) recovered *Clostridium* species and aerobic bacteria from irradiated dogs. We were not able to isolate clostridial species; however, we used a different animal model, and did not employ specific media for selection of clostridial species (such as yeast extract agar), and this may account for their absence.

The recovery of anaerobes when host defenses are suppressed is not surprising, because they outnumber aerobic flora in the intestine by the ratio of 1000 to 1 (Gorbach 1971). These endogenous organisms might invade the body in a manner similar to that of the aerobic enteric organisms. The recovery of most of the isolates between days 9 to 13 coincides with the irradiation-induced leukopenia and damage to the enteric mucosa (Bennett et al. 1951). The damaged mucosa may therefore become permeable to the enteric bacteria, which thereafter can invade the blood (Benacerraf 1960; Carter and Collins 1974; Miller 1956). The local mucosal defenses may also become ineffective in limiting the spread of the infection (Gorbach 1971; Carter and Collins 1974).

Infrequent isolation of anaerobes in animals exposed to lower levels of radiation also supports the hypothesis that greater damage to the gastrointestinal mucosa and immune system promotes the spread of more varieties of enteric organisms, since exposure to such levels do not induce as severe damage to the gastrointestinal mucosa or the immune system (Collins 1979). This is consistent with the concomitant decrease in recovery of *E. coli* that also originates from the gastrointestinal tract in animals exposed to less radiation. It is possible that when

the animal is exposed to smaller amounts of radiation its gastrointestinal mucosa is less permeable to enteric aerobic and anaerobic bacteria, and (or) its immune system is capable of preventing infection with these organisms (Benacerraf 1960; Carter and Collins 1974; Miller 1956; Collins 1979; Hale and McCarthy 1984; Shechmeister et al. 1953; Volkman and Collins 1968). The observation of intestinal bacteria in the lamina propria following irradiation may also be due to invasion of radiation-damaged mucosal cells by the normal flora (Miller 1956; Porvaznik 1979).

Our findings suggest that a polymicrobial aerobic-anaerobic mixed infection can occur more often in animals exposed to higher dosages of irradiation. Because of the reported synergy between these organisms (Brook, Hunter et al. 1984; Brook, MacVittie et al. 1984), our data indicate that antimicrobial therapy should include coverage for all bacterial components of the infections.

### Acknowledgements

The authors gratefully acknowledge J. E. Perry for technical assistance, W. E. Jackson for statistical analysis, and Ms. Gloria Contreras and Mrs. Mariann Waldbillig for secretarial assistance.

- BENACERRAF, B. 1960. Influence of irradiation on resistance to infection. *Bacteriol. Rev.* 24: 35-40.
- BENNETT, L. R., P. E. REKERS, and J. HOWLAND. 1951. Influence of infection on hematological effects and mortality following mid-lethal roentgen irradiation. *Radiology*, 57: 99-105.
- BROOK, I., V. HUNTER, and R. I. WALKER. 1984. Synergistic effect of anaerobic cocci, *Bacteroides*, *Clostridia*, *Fusobacteria*, and aerobic bacteria on mouse mortality and induction of subcutaneous abscess. *J. Infect. Dis.* 149: 924-928.
- BROOK, I., T. J. MACVITTIE, and R. I. WALKER. 1984. Recovery of aerobic and anaerobic bacteria from irradiated mice. *Infect. Immun.* 46: 270-271.
- CARTER, P. B., and F. M. COLLINS. 1974. The route of enteric infection in normal mice. *J. Exp. Med.* 139: 1189-1203.
- COLLINS, F. M. 1979. Mucosal defenses against *Salmonella* infection in the mouse. *J. Infect. Dis.* 129: 503-510.
- GORBACH, S. L. 1971. Intestinal microflora. *Gastroenterology*, 60: 1110-1129.
- GORDON, L. E., D. RUMI, H. J. DAHNE, and C. P. MILLER. 1955. Studies on susceptibilities to infection following ionizing irradiation. IV. The pathogenesis of the endogenous bacteremia in mice. *J. Exp. Med.* 102: 413-424.
- HALE, M. L., and K. F. MCCARTHY. 1984. Effect of sublethal ionizing radiation on rat Peyer's patch lymphocytes. *Radiat. Res.* 99: 151-164.
- KRAMER, B. S., P. A. PIZZO, K. J. ROBICHAUD, F. WITESBSKY, and R. WESLEY. 1982. Role of serial microbiologic surveillance and clinical evaluation in the management of cancer patients with fever and granulocytopenia. *Am. J. Med.* 72: 561-568.

- LENNETTE, E. H., A. BALOWS, A. W. HAUSLER, JR., and J. P. TRUANT (Editors). 1980. Manual of clinical microbiology. 3rd ed. American Society for Microbiology, Washington, DC.
- MILLER, C. P. 1956. The effect of irradiation on natural resistance to infection. *Ann. N.Y. Acad. Sci.* 66: 250-291.
- MILLER, C. P., C. W. HAMMOND, and M. J. TOMKINS. 1951. The role of infection in radiation injury. *J. Lab. Clin. Med.* 38: 331-343.
- PORVAZNIK, M. 1979. Tight junction disruption and recovery after sublethal gamma irradiation. *Radiat. Res.* 78: 233-250.
- SHECHMEISTER, I. L., L. J. PAULISSEN, and M. FISHMAN. 1953. Sublethal total body x-radiation and susceptibility of mice to *Salmonella enteritidis* and *Escherichia coli*. *Proc. Soc. Exp. Biol. Med.* 83: 205-209.
- SOKAL, R. R., and F. J. ROHLF. 1975. Biometry. W. H. Freeman and Company, San Francisco.
- SUTTER, V. L., D. M. CITRON, and S. M. FINEGOLD. 1980. Wadsworth anaerobic bacteriology manual. 3rd ed. The C. V. Mosby Company, St. Louis.
- VOLKMAN, A., and F. M. COLLINS. 1968. Recovery of delayed-type hypersensitivity in mice following suppressive doses of x-radiation. *J. Immunol.* 101: 846-859.

# Sodium-hydrogen exchange system in LLC-PK<sub>1</sub> epithelium

A. MORAN

*Department of Physiology, Armed Forces Radiobiology Research Institute,  
Bethesda, Maryland 20814-5145; and Department of Physiology,  
Ben-Gurion University of the Negev, Beer-Sheva, Israel*

MORAN, A. Sodium-hydrogen exchange system in LLC-PK<sub>1</sub> epithelium. *Am. J. Physiol.* 252 (*Cell Physiol.* 21): C63-C67, 1987.—Sodium influx into LLC-PK<sub>1</sub> cells has been characterized. The main amiloride-sensitive pathway for sodium entry through the apical membrane in this cell line is sodium-hydrogen exchange with an apparent  $K_m$  for sodium of 19 mM. Influx is pH dependent and is amiloride sensitive with  $K_{1/2}$  of 30  $\mu$ M. Inhibition of the sodium transport by protons (at 1 mM external sodium) is consistent with an interaction of H<sup>+</sup> ions at a single site having an apparent pK<sub>H</sub> of 7.2. These data are similar to those reported previously for brush border membrane (BBM) isolated from kidney proximal tubule. However, in contrast to previously published reports, H<sup>+</sup> does not compete with amiloride in blocking Na<sup>+</sup> influx and exhibits a mixed inhibition with sodium ions. The latter, together with a direct and independent assessment of amiloride and sodium interaction, indicates that amiloride does not compete with sodium for the same site. Possible explanations for the discrepancy in the literature concerning the interaction of Na<sup>+</sup>, H<sup>+</sup>, and amiloride with the Na<sup>+</sup>-H<sup>+</sup> exchanger and the characteristics of the Na<sup>+</sup>-H<sup>+</sup> exchange system in LLC-PK<sub>1</sub> are discussed.

renal cells in culture; proximal tubule acidification

MOST, IF NOT ALL, mammalian cells have a higher cytoplasmic pH than would be expected if H<sup>+</sup> ions distributed passively across the plasma membrane (19). This implies that active mechanisms compensate for any passive lack of H<sup>+</sup> ions into the cells, maintaining pH above the electrochemical equilibrium. Sodium-hydrogen exchange and chloride bicarbonate countertransport are two mechanisms that have been shown to be involved in the regulation and homeostasis of intracellular pH (1, 19). Na<sup>+</sup>-H<sup>+</sup> exchange is of particular interest since it is postulated to be involved in the regulation of several other cellular functions. For example, Na<sup>+</sup>-H<sup>+</sup> exchanger activity is stimulated by various growth factors, including serum, phorbol esters, and epidermal growth factor (12, 17, 18, 20, 21). In lymphocytes, red blood cells, and gallbladder this system is involved in volume regulation and is activated when cells recover from hyperosmotic shrinkage (6, 7, 22).

In the kidney, Na<sup>+</sup>-H<sup>+</sup> exchange is believed to be the primary mechanism for acidification in the proximal tubule (2). Most of the kinetic data available on this transport system in the kidney come from experiments utilizing isolated brush border membranes (2, 4, 10). As

with studies of Na<sup>+</sup>-H<sup>+</sup> exchange in other systems, substantial work has been done on the effect of the diuretic drug amiloride on this system. However, the interactions of the drug with sodium transport systems of the proximal tubule of the kidney are not completely understood. Conflicting reports exist in the literature concerning inhibition of the transporter by amiloride. Both competitive (4) and mixed inhibition (10) of sodium influx have been documented. Through the use of the established cell line LLC-PK<sub>1</sub>, it is possible to study transport systems localized to the apical membrane in whole cells as well as in isolated apical membranes (5, 15). This paper characterizes Na<sup>+</sup>-H<sup>+</sup> exchange in the apical membrane of LLC-PK<sub>1</sub> epithelia, focusing on its pH and sodium dependence. The effect of the diuretic drug amiloride and its interaction with sodium were also investigated. The experimental findings are consistent with noncompetitive inhibition of Na<sup>+</sup>-H<sup>+</sup> exchange by amiloride.

## MATERIALS AND METHODS

**Cell culture.** LLC-PK<sub>1</sub> cells were grown as previously described (16). Briefly, cells (passages 190-220) were subcultured 1:10 from 2- to 3-wk-old stock cultures into cluster 12 wells (4 cm<sup>2</sup>, Costar). The cells were grown in Dulbecco's Modified Eagle Medium supplemented with 10% fetal bovine serum (Gibco), 0.03% glutamine, and 10 units of penicillin and 10  $\mu$ g streptomycin/ml. Experiments were conducted on epithelia 7-12 days after subculture.

**Uptake procedure.** Prior to the uptake measurements the epithelia were depleted of sodium as follows. After washing three times with *N*-Methylglucamine (NMG) medium (130 mM NMG, 4 mM KCl, 2 mM MgCl<sub>2</sub>, 0.5 mM CaCl<sub>2</sub>, 0.1 mM NaCl,  $2 \times 10^{-4}$  M ouabain, and 20 mM HEPES-tris(hydroxymethyl)aminomethane (Tris), pH 7.4) cells were incubated in the NMG medium for 2-3 h at room temperature. During this period the domes usually visible on these cultures collapsed. Cell viability as determined by trypan blue exclusion showed no apparent damage to the cells treated with ouabain as compared with control cells. The rate of Na<sup>+</sup> influx was determined by 1 min <sup>22</sup>Na<sup>+</sup> uptake measurements at room temperature. Na<sup>+</sup> flux was linear for >3 min at all pHs and sodium concentrations used (data not shown). At the end of the incubation period, epithelia were washed five times with ice-cold phosphate-buffered sa-

line (PBS). The cells were then solubilized in 0.5% Triton-X 100 in water and sampled for radiolabeled sodium counting and for protein determination (Bio-Rad). Four, six, or eight washes resulted in the same amount of sodium trapped in the cells, an indication that there was essentially no efflux during the wash period. Addition of amiloride ( $10^{-4}$  M) to the PBS used to wash the cells did not change the results (data not shown). The contribution to uptake measurements of incubation medium trapped in extracellular spaces was found to be negligible by correcting for residual supernatant in some experiments using [<sup>3</sup>H]raffinose as an extracellular marker.

Data are corrected for the amiloride insensitive flux (flux in the presence of 1 mM amiloride), which accounted for 10–20% of the total flux (data not shown).

Depletion of sodium has been shown to cause intracellular acidification, thus stimulating activity of the Na<sup>+</sup>-H<sup>+</sup> exchange system (19). It should be noted, however, that a smaller, amiloride-sensitive flux has been observed even without depleting the cells of sodium.

**Materials.** [<sup>22</sup>Na]Cl and [<sup>3</sup>H]raffinose were purchased from New England Nuclear. NMG was purchased from Sigma. Amiloride was a gift from Merck, Sharp, and Dhorne. All other materials were of the highest purity available commercially.

Representative experiments are shown. Each point represents a mean and standard deviation of at least three determinations. All experiments were repeated at least three times with the same qualitative results. Some quantitative differences were obtained among different experiments.

## RESULTS

Figure 1 depicts the initial Na<sup>+</sup> influx into the epithelium in the presence of 10 mM sodium as a function of amiloride concentration. The  $K_{1/2}$  of amiloride inhibition

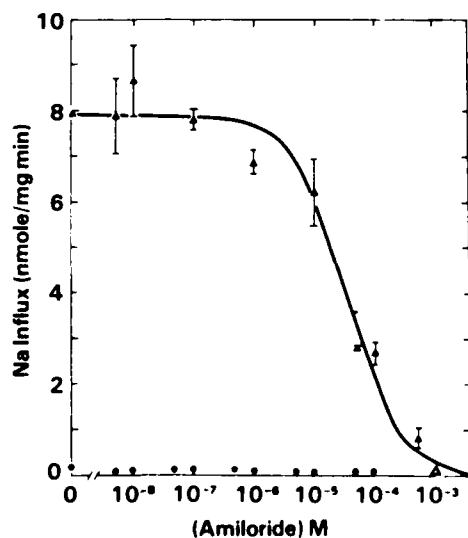


FIG. 1. Amiloride sensitive Na influx into sodium-depleted epithelia (closed triangles). One-minute uptake in presence of 10 mM sodium, pH 7.4. Nonlinear curve fitted to a single Michaelis-Menten equation yields  $K_{1/2}$  of 30  $\mu$ M. Uptake in presence of 1 mM harmaline (closed circles).

(calculated from the nonlinear curve fitted to the experimental points) is 30  $\mu$ M. Similar sensitivity to amiloride has been reported for the Na<sup>+</sup>-H<sup>+</sup> exchange system in BBM isolated from kidney proximal tubule (2). Harmaline (1 mM), which is known to inhibit Na<sup>+</sup>-H<sup>+</sup> exchange but has no effect on the sodium channel in epithelia (3, 8), totally abolished the amiloride-sensitive Na<sup>+</sup> influx.

To evaluate the effect of extracellular pH on Na<sup>+</sup> influx, the rate of Na<sup>+</sup> uptake was measured at external pHs ranging from 6.8 to 8.9. Preincubation conditions were identical to those described above. Na<sup>+</sup> uptake remained linear during the 1-min uptake measurement; thus it is likely that intracellular pH was constant during the measured uptake and therefore that the increase in Na<sup>+</sup> influx observed with increasing external pH (Fig. 2) results solely from differences in extracellular pH. When the data are replotted on a Dixon plot (Fig. 3) a linear relationship results, as was found for BBM from kidney proximal tubule (2). The data are consistent with H<sup>+</sup>

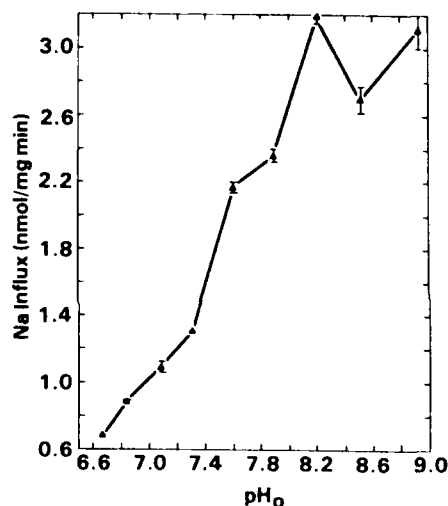


FIG. 2. Effect of external pH on Na influx. Different pHs applied only during 1-min uptake period in presence of 1 mM sodium. Preincubation was at pH 7.4 for all points.

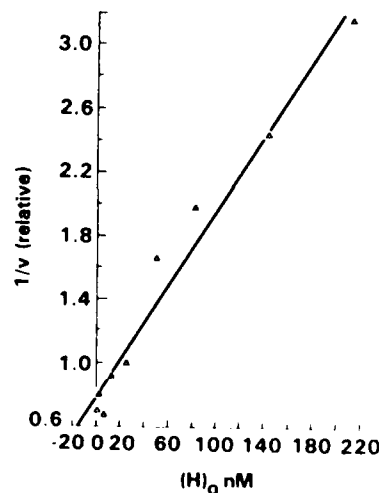


FIG. 3. Inhibition of Na influx by external H<sup>+</sup> ions. Data taken from Fig. 2 were replotted in form of 1/V vs. [H<sup>+</sup>]. Data are expressed relative to Na influx with external pH of 7.59. Regression line calculated by method of least-squares yields an intercept of 66 nM (at 7.2 pH).

ions interacting with the transport system at a single site with an apparent  $K_H$  of 66 nM, equivalent to an apparent  $P_K$  of 7.2.

The effect of external pH on the amiloride dose-response relationship is depicted in Fig. 4. Uptake measurements were performed in the presence of 1 mM NaCl for 1 min. The results of nonlinear curve fitting to the Michaelis-Menten equation show that extracellular pH affects the magnitude of the uptake without any detectable changes in the affinity for amiloride. Figure 5 depicts the effect of extracellular pH on the sodium dependence of this transport system. The experimental points are fitted to a single Michaelis-Menten equation yielding an apparent  $K_m$  of 20 mM for sodium at pH 7.4, in good agreement with data found for isolated kidney BBM (2). In contrast to the effect of extracellular pH on the amiloride dose response, both the affinity and the max-

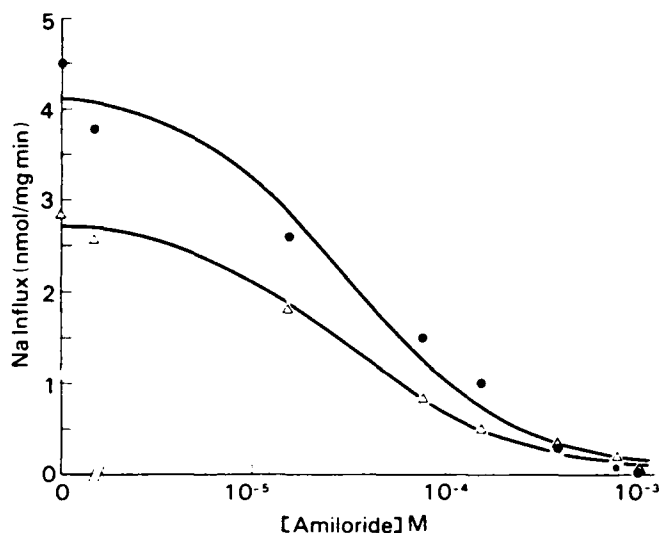


FIG. 4. Amiloride dose response as a function of extracellular pH. Lines are from a nonlinear fit to a single Michaelis-Menten equation yielding  $K_{1/2}$  of 3 and  $3.2 \times 10^{-5}$  M and maximum velocity of 2.8 and 4.2 nmol/mg min for pH 7.4 (open triangles) and 8.0 (closed circles), respectively.

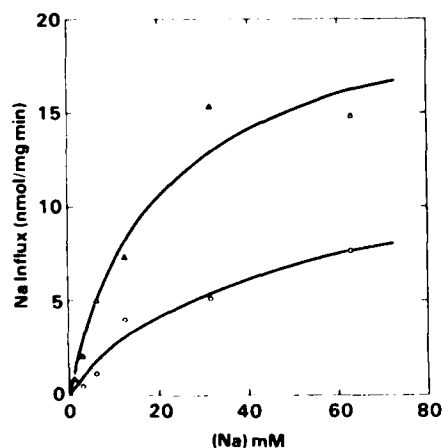


FIG. 5. Effect of extracellular pH on the sodium dependence of Na influx. Solid lines are a nonlinear fit to Michaelis-Menten equation that yields  $K_{1/2}$  of 39 and 20 mM and maximum velocity of 12 and 21 nmol/mg min for pH 6.4 (open circles) and 7.4 (open triangles), respectively.

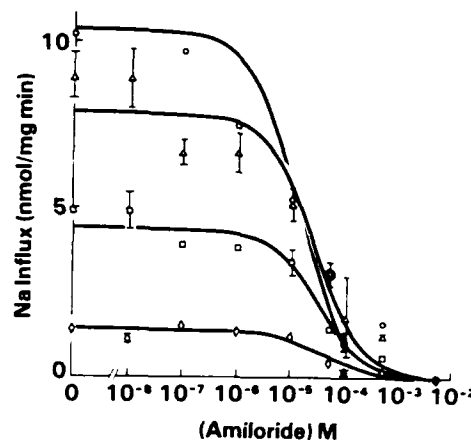


FIG. 6. Amiloride dose response at different sodium concentrations. Nonlinear curve fit yields  $K_{1/2}$  of 11.7, 26, 27, and 27  $\mu$ M and maximum velocity of 10.4, 7.9, 4.48, and 1.38 nmol/mg min for sodium concentrations of 21.2 (open circles), 12.7 (open triangles), 6.35 (open squares), and 1.27 mM (open diamonds), respectively.

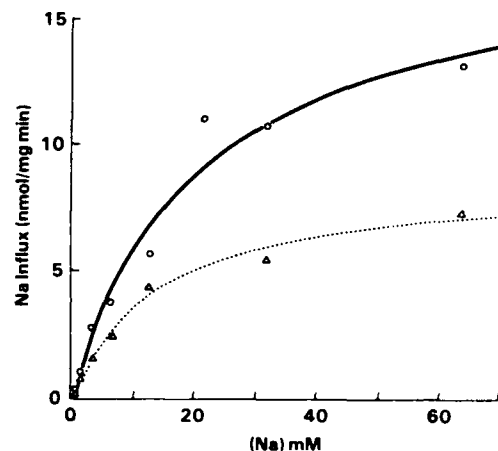


FIG. 7. Sodium dependence of Na influx and effect of  $10^{-5}$  M amiloride. Lines are a nonlinear fit to experimental points yielding  $K_{1/2}$  of 19.9 and 15 and maximum velocity of 17.9 and 8.8 for the control (open circles) and the amiloride (open triangles) inhibited curves, respectively.

imum transport capacity for sodium are affected by changes in the extracellular pH. This suggests that the interaction of sodium and amiloride with this system is not competitive as previously reported for some kidney preparations (2, 4).

To further study the interaction between amiloride and sodium with the Na<sup>+</sup>-H<sup>+</sup> exchanger, amiloride inhibition was evaluated at different sodium concentrations. Figure 6 depicts the result of such an experiment. No change in affinity for amiloride is observed at the Na<sup>+</sup> concentrations studied (1.27–21.2 mM); this is consistent with a system in which amiloride and sodium react with the exchanger at different sites. Similarly, in the reciprocal experiment examining sodium dependence of Na<sup>+</sup> influx with and without amiloride (Fig. 7), a change in maximum velocity ( $V_{max}$ ) is observed, whereas there is no change in the affinity for sodium.

## DISCUSSION

In this paper the characteristics of Na<sup>+</sup> influx into a monolayer of the established cell line LLC-PK<sub>1</sub> have

been studied. As found for other transport systems identified in this cell line (5, 14), it seems that the Na<sup>+</sup> influx mechanism resembles in many respects the system described in the proximal tubule of the kidney. First, Na<sup>+</sup> influx is a saturable, amiloride-sensitive process with a  $K_m$  for sodium similar to that observed in the BBM of the proximal kidney tubule. Second, as extracellular pH increases, Na<sup>+</sup> influx increases. Third, as in the kidney, H<sup>+</sup> ions seem to act via a single site with a  $pK_a$  of 7.2.

However, not all the properties of Na<sup>+</sup>-H<sup>+</sup> exchange found in the apical membrane of the LLC-PK<sub>1</sub> are similar to the properties of this system in BBMs isolated from the proximal tubule. In several previous reports (2, 4) on Na<sup>+</sup>-H<sup>+</sup> exchange in the kidney, sodium, amiloride, and hydrogen ions appeared to compete at the same site. This does not seem to be the case in LLC-PK<sub>1</sub> cells, since decreases in extracellular pH reduce Na<sup>+</sup> uptake without changing the affinity for amiloride, yet affect both affinity and maximum transport capacity for sodium. This indicates that H<sup>+</sup> ions are not simply competing with both sodium and amiloride. Moreover, direct evaluation of the interaction between sodium and amiloride in this cell line supports the notion that amiloride inhibits sodium uptake noncompetitively. This was established in experiments in which the sodium dependence of Na<sup>+</sup> influx was tested in the presence and absence of amiloride and in experiments in which the amiloride dose-response relationship was evaluated at various sodium concentrations. In both cases only the  $V_{max}$  changed while the affinity for either sodium or amiloride was not affected.

A previous study by Haggerty et al. (9) reported competitive interaction of amiloride and sodium in rapidly growing LLC-PK<sub>1</sub> cells. The difference in the results reported in their study and the present one may indicate changes in the Na<sup>+</sup>-H<sup>+</sup> exchanger following confluency. This notion, suggested in their paper, is supported by the present work utilizing confluent monolayers, which exhibit minimal cell division as determined by radiolabeled thymidine incorporation, measured both as cumulative net incorporation and by autoradiography as proportion of cells in a monolayer incorporating thymidine (13, 14).

It is more difficult to reconcile the finding of noncompetitive interaction of sodium and amiloride with other reports in the literature (10-12). It is unlikely that the discrepancy results from systematic error in the methods used in the present study. First, using the pH stat technique to measure Na<sup>+</sup> dependence of amiloride sensitive H<sup>+</sup> efflux, the observed  $K_m$  for sodium was 17 mM (R. Lynch and A. Moran, unpublished observations). This value is in good agreement with the value (20 mM) found in the Na<sup>+</sup> influx measurements. Second, it is unlikely that the discrepancy arises from changes in the cells during the preincubation period. Similar results were obtained in isolated BBM vesicles from LLC-PK<sub>1</sub> cells that had not been preincubated and in which intravesicular conditions were strictly controlled (A. Moran, J. Biber, and H. Murer, unpublished observation).

It is possible that the differences in the kinetics of Na<sup>+</sup> and amiloride interaction observed in this study reflect

inherent differences between the Na<sup>+</sup>-H<sup>+</sup> exchange system of LLC-PK<sub>1</sub> and the exchange system in isolated BBM of rabbit kidney origin due to genetic changes in the cell culture or species differences. In this regard, it should be noted that many of the previous studies utilized kidney tissue of rabbits rather than pigs, from which LLC-PK<sub>1</sub> was derived. However, though speculative, a more attractive explanation is that not one but two different Na<sup>+</sup>-H<sup>+</sup> exchange systems exist along the nephron, one of which is competitively inhibited by amiloride, whereas the other is noncompetitively inhibited. If this were the case, the type of inhibition observed in a preparation would depend on the section of the nephron from which it was isolated. The transporter found in the apical membrane of the LLC-PK<sub>1</sub> cells probably would be found in the S2 or S3 segment of the proximal tubule (15). Properties of the sodium-coupled glucose transporter in LLC-PK<sub>1</sub> such as 1:2 stoichiometry of sodium-to-glucose are similar to the properties of this part of the nephron. It is thus conceivable that this cell line will express other properties localized to the same nephron segments. Therefore, unless specific attempts are made to dissect this portion of the proximal tubule, the relative amount of this fraction in a whole kidney cortex preparation would be small and variable.

In conclusion, a Na<sup>+</sup>-H<sup>+</sup> exchange system has been described in the apical membrane of LLC-PK<sub>1</sub> cells with some characteristics of the exchanger found in the proximal tubule. However in contrast to past studies of BBM prepared from kidneys, this transporter exhibits a non-competitive inhibition of Na<sup>+</sup> influx by amiloride.

The author would like to thank Drs. Gunter-Smith and Foskett for critically reviewing the manuscript.

This work was supported by the Armed Forces Radiobiology Research Institute, Defense Nuclear Agency, under Research Work Unit MJ 00107.

The views presented in this paper are those of the author; no endorsement by the Defense Nuclear Agency has been given nor should be inferred.

Received 25 September 1985; accepted in final form 12 August 1986.

## REFERENCES

1. AICKIN, C. C., AND R. C. THOMAS. An investigation of the ionic mechanism of intracellular pH regulation in mouse soleus muscle fibers. *J. Physiol. Lond.* 273: 295-316, 1977.
2. ARONSON, P. S. Mechanism of active H<sup>+</sup> secretion in the proximal tubule. *Am. J. Physiol.* 245 (Renal Fluid Electrolyte Physiol. 14): F647-F659, 1983.
3. ARONSON, P. S., AND S. E. BOUNDS. Harmaline inhibition of Na<sup>+</sup>-dependent transport in renal microvillus membrane vesicles. *Am. J. Physiol.* 240 (Renal Fluid Electrolyte Physiol. 9): F1-F11, 1981.
4. ARONSON, P. S., M. A. SUHM, AND J. NEE. Interaction of external H<sup>+</sup> with the Na<sup>+</sup>-H<sup>+</sup> exchanger in renal microvillus membrane vesicles. *J. Biol. Chem.* 258: 6767-6771, 1983.
5. BROWN, C. D. A., M. BODMER, J. BIBER, AND H. MURER. Sodium-dependent phosphate transport by apical membrane vesicles from a cultured renal epithelial cell line (LLC-PK<sub>1</sub>). *Biochim. Biophys. Acta* 769: 471-478, 1984.
6. CALA, P. M. Volume regulation of *amphitoma* red blood cells: the membrane potential and its implications regarding the nature of the ion flux pathways. *J. Gen. Physiol.* 76: 683-708, 1980.
7. GRINSTEIN, S., A. D. CLARKE, AND A. ROTHSTEIN. Activation of Na<sup>+</sup>-H<sup>+</sup> exchange in lymphocytes by osmotically induced volume changes and cytoplasmic acidification. *J. Gen. Physiol.* 82: 619-638, 1983.

8. GROSSO, A., AND R. C. DE SOUSA. Vasopressin-like effect of psychotropic drugs in amphibian epithelia. *J. Membr. Biol.* 40: 305-321, 1978.
9. HAGGERTY, J. G., E. J. CRAGOE, C. W. SLAYMAN, AND E. A. ADELBURG. Na<sup>+</sup>/H<sup>+</sup> exchange activity in the pig kidney epithelial cell line, LLC-PK<sub>1</sub>: inhibition by amiloride and its derivatives. *Biochem. Biophys. Res. Commun.* 127: 759-768, 1985.
10. IVES, H. E., V. J. YEE, AND D. G. WARNOCK. Mixed type inhibition of the renal Na<sup>+</sup>/H<sup>+</sup> antiporter by Li<sup>+</sup> and amiloride. Evidence for a modifier site. *J. Biol. Chem.* 258: 9710-9716, 1983.
11. L'ALLEMAIN, G., S. PARIS, AND J. POUYSSÉGUR. Role of Na<sup>+</sup> dependent Cl<sup>-</sup>/HCO<sub>3</sub><sup>-</sup> exchange in regulation of intracellular pH in fibroblasts. *J. Biol. Chem.* 260: 4877-4883, 1985.
12. MOOLENAAR, W. H., L. G. J. TERTOOLEN, AND S. W. DE LAAT. Phorbol ester and diacylglycerol mimic growth factors in raising cytoplasmic pH. *Nature Lond.* 312: 371-374, 1984.
13. MORAN, A., L. DAVIS, AND M. HAGAN. Effect of radiation on the regulation of sodium-dependent glucose transport in LLC-PK<sub>1</sub> epithelial cell line: possible model for gene expression. *Radiat. Res.* 105: 201-210, 1986.
14. MORAN, A., J. S. HANDLER, AND M. HAGAN. Role of cell replication in regulation of Na<sup>+</sup> coupled hexose transport in LLC-PK<sub>1</sub> epithelial cells. *Am. J. Physiol.* 250 (Cell Physiol. 19): C314-C318, 1986.
15. MORAN, A., J. S. HANDLER, AND R. J. TURNER. Na<sup>+</sup>-dependent transport in vesicles from cultured renal epithelial cell line. *Am. J. Physiol.* 243 (Cell Physiol. 12): C293-C298, 1982.
16. MORAN, A., R. J. TURNER, AND J. S. HANDLER. Regulation of sodium-coupled glucose transport by glucose in a cultured epithelium. *J. Biol. Chem.* 258: 15087-15090, 1983.
17. OWEN, N. E., AND M. L. VILLEREAL. Lys-bradykinin stimulates Na<sup>+</sup> influx and DNA synthesis in cultured human fibroblasts. *Cell* 32: 979-985, 1983.
18. POUYSSÉGUR, J., J. C. CHAMBAR, A. FRANCHI, S. PARIS, AND E. VAN OBERGHEEN-SCHILLING. Growth factor activation of an amiloride-sensitive Na<sup>+</sup>/H<sup>+</sup> exchange system in quiescent fibroblasts: coupling to ribosomal protein S6 phosphorylation. *Proc. Natl. Acad. Sci.* 79: 3935-3939, 1982.
19. ROOS, A., AND W. F. BORON. Intracellular pH. *Physiol. Rev.* 61: 296-434, 1981.
20. SCHULDINER, S., AND E. ROZENGURT. Na<sup>+</sup>/H<sup>+</sup> antiport in Swiss 3T3 cells: mitogenic stimulation leads to cytoplasmic alkalization. *Proc. Natl. Acad. Sci.* 79: 7778-7782, 1982.
21. VILLEREAL, M. L. Sodium fluxes in human fibroblasts: effect of serum, Ca<sup>++</sup> and amiloride. *J. Cell. Physiol.* 107: 359-369, 1981.
22. WEINMAN, S. A., AND L. REUSS. Na<sup>+</sup> H<sup>+</sup> exchange at the apical membrane of *Necturus* gallbladder. *J. Gen. Physiol.* 80: 299-321, 1982.

# A sodium-hydrogen exchange system in isolated apical membrane from LLC-PK<sub>1</sub> epithelia

A. MORAN, J. BIBER, AND H. MURER

*Department of Physiology, Armed Forces Radiobiology Research Institute, Bethesda, Maryland 20814-5145; and Department of Physiology, Ben-Gurion University of the Negev, Beer-Sheva 84105, Israel; and Institute of Physiology, University of Zurich-Irchel 8057, Zurich, Switzerland*

MORAN, A., J. BIBER, AND H. MURER. A sodium-hydrogen exchange system in isolated apical membrane from LLC-PK<sub>1</sub> epithelia. *Am. J. Physiol.* 251 (Renal Fluid Electrolyte Physiol. 20): F1003-F1008, 1986. We have monitored transmembrane pH gradients using acridine orange fluorescence quenching and traced Na<sup>+</sup> flux to study the properties of Na<sup>+</sup>-H<sup>+</sup> exchange in apical membrane vesicles isolated from LLC-PK<sub>1</sub> epithelia. The membranes have low conductance for Na<sup>+</sup>, H<sup>+</sup>, and K<sup>+</sup> ions. An outwardly directed K<sup>+</sup> gradient in the presence of valinomycin and carbonyl cyanide *p*-trifluoromethoxyphenyl hydrazone produced intravesicular acidification. This pH gradient was collapsed by addition of extravesicular Na<sup>+</sup> or Li<sup>+</sup> ions but not by tetramethylammonium. Amiloride (10<sup>-4</sup> M) inhibited the effect of both Na<sup>+</sup> and Li<sup>+</sup>. An outwardly directed Na<sup>+</sup> gradient stimulated H<sup>+</sup> influx, which was also inhibited by 10<sup>-4</sup> M amiloride. Membrane short-circuit conditions affected neither Na<sup>+</sup> nor H<sup>+</sup> flux, consistent with transport mediated by an electroneutral process. The interaction of amiloride and sodium is consistent with noncompetitive inhibition with  $K_i = 100 \pm 10 \mu\text{M}$  for amiloride and an apparent  $K_m$  for Na<sup>+</sup> of ~20 mM. This finding is in agreement with previous studies of intact LLC-PK<sub>1</sub> epithelia but differs from observations in brush-border membrane vesicles isolated from kidney proximal tubule in which competitive and mixed inhibition have been reported. These observed differences can be reconciled if two types of Na<sup>+</sup>-H<sup>+</sup> exchange systems exist along the nephron, one with competitive and the other with noncompetitive inhibition, and if only the latter is expressed in the homogeneous cultured cells.

Na<sup>+</sup>-H<sup>+</sup> exchange; renal tissue culture; brush-border membrane; proximal tubule acidification

RECENTLY, studies on intact LLC-PK<sub>1</sub> cells have identified a Na<sup>+</sup>-H<sup>+</sup> exchange system that is noncompetitively inhibited by amiloride (10). This system was assumed to be located at the apical membrane of the epithelial cells (2, 6). However, in low resistance epithelial layers such as the LLC-PK<sub>1</sub>, the localization of a transport system is always in doubt; substrates offered only to one surface may gain access to the other via penetration through the junctional complexes. Moreover, intact cells may contain regulatory mechanisms that complicate the qualitative properties of a transport system under study. The isolation of specific fractions of membrane vesicles, a procedure developed over the last decade (8, 11, 13), provides an experimental system that overcomes many of the disadvantages inherent in study-

ing an intact cell system. A specific transport system can be localized with enzyme markers by identifying whether a fraction of membrane manifesting the transporter is derived from the apical or basolateral surface of the cell. Moreover, the transport system can be analyzed under well-defined conditions, and the contribution of conducting pathways can be evaluated using the appropriate ionophores and salt gradient conditions (15).

In experiments with apical membrane vesicles from LLC-PK<sub>1</sub> using the acridine orange (AO) quench technique to monitor intravesicular pH, as well as by the analysis of Na<sup>+</sup> tracer fluxes, we have established the existence of Na<sup>+</sup>-H<sup>+</sup> exchange in the apical membrane. The results indicate that the apical membranes isolated from LLC-PK<sub>1</sub> cells have low conductance for K<sup>+</sup>, H<sup>+</sup>, and Na<sup>+</sup>. The Na<sup>+</sup>-H<sup>+</sup> exchange system we have studied is electroneutral, as has been observed in apical membrane preparations isolated from the kidney proximal tubule (7). However, in contrast to findings in brush-border membrane (BBM) isolated from proximal tubule (1, 6), but in agreement with observations in intact LLC-PK<sub>1</sub> cells (10), amiloride noncompetitively inhibits Na<sup>+</sup> flux in isolated apical membrane preparations from these cells.

## MATERIALS AND METHODS

**Cell culture.** LLC-PK<sub>1</sub> were grown in 75 cm<sup>2</sup> flasks (Costar) for 8-10 days before 1:10 subculture into glass roller bottles. These bottles were infused with 10% CO<sub>2</sub> in air, sealed, and rotated continuously on a rolling apparatus at 37°C. Dulbecco's modified Eagle's medium was supplemented with 10% fetal bovine serum, 0.03% L-glutamine, 100 U penicillin, and 100 μg streptomycin per milliliter.

**Membrane preparation.** BBMs were prepared from scrapings of the epithelial layer using the Mg<sup>2+</sup> precipitation technique of Brown et al. (3). The membrane preparations used were enriched in the apical membrane marker enzyme trehalase 7.8 ± 0.1-fold and 0.7-fold of the basolateral membrane enzyme marker Na<sup>+</sup>-K<sup>+</sup>-ATPase relative to the initial LLC-PK<sub>1</sub> cell homogenate. The compositions of the various buffers used for vesicle loading and suspension and for the incubation media are presented in Figs. 1-7. To ensure that the intravesicular space contained the appropriate buffer, the vesicles were suspended in the desired buffer, passed through a 30-



gauge needle, then incubated in that buffer for 2 h at 37°C.

**AO fluorescence measurements.** As previously described (4, 14, 16), changes in transmembrane pH gradients were analyzed by continuous recording of AO fluorescence at 37°C. Briefly, a spectrofluorometric cuvette was filled with 2.03 ml of buffer containing 6  $\mu$ M of AO. Ionophores were added from ethanol-based stock solutions (alcohol content never exceeded 0.5%). Fluorescence was induced with excitation at 493 nm and emission monitored at 535 nm with a Shimadzu RF510 spectrofluorometer. To allow comparison of the fluorescence signal under different conditions, gain was altered to give an emission reading in the absence of vesicles of 90 arbitrary units (AU), then remained constant throughout the experiment. To initiate each trial, 20  $\mu$ l of a vesicle suspension, adjusted to give a final protein concentration in the cuvette of 350  $\mu$ g/ml, were injected into the chamber. To test the effect of amiloride, amiloride in ethanol (5  $\mu$ l) was added to the incubation mixture prior to injection of the vesicles to give a final concentration of  $10^{-4}$  M.

**Tracer measurements.** <sup>22</sup>Na fluxes were measured using the rapid filtration method as previously described (12). Briefly, 10  $\mu$ l of vesicles (3–5 mg/ml protein) were rapidly mixed with the appropriate incubation medium containing 10  $\mu$ Ci/ml <sup>22</sup>Na. The flux was stopped with 1.2 ml of ice-cold stop solution [200 mM KCl, 20 mM tris(hydroxymethyl)aminomethane (Tris)-Cl, pH 7.4], and the vesicles were recovered on a 0.65  $\mu$ m filter (Millipore) and rinsed free of residual incubation media by aspirating two additional stop solution washes through the filter. Except for the time course, the uptake incubation period was 15 s, and all uptakes were performed at room temperature. Uptake was found to be linear up to 30 s and extrapolated to zero for a zero incubation period under all experimental conditions (all ranges of pH and Na<sup>+</sup> concentration; data not shown).

**Materials.** AO was obtained from Eastman Kodak (Rochester, NY). Valinomycin and FCCP (carbonyl cyanide *p*-trifluoromethoxyphenyl hydrazone) were purchased from Boehringer (Mannheim, FRG). All other reagents were of the highest purity commercially available. Tetramethylammonium (TMA)-gluconate was made by titrating a solution of TMA-hydroxide with gluconic acid.

Representative experiments are shown. Each point of the tracer uptake measurements represents a mean and standard deviation from at least three filters. Amiloride insensitive component of the Na<sup>+</sup> flux was defined as the flux in the presence of 1 mM amiloride. This component accounted for 10–20% of the total flux. All experiments were repeated at least three times with the same qualitative results, although we obtained some quantitative differences ( $\pm 25\%$ ) in the transport rates between the different membrane preparations used.

## RESULTS

Figure 1 depicts the effects of valinomycin and FCCP on intravesicular pH of K<sup>+</sup>-loaded vesicles, with AO fluorescence plotted as a function of time. The vesi-

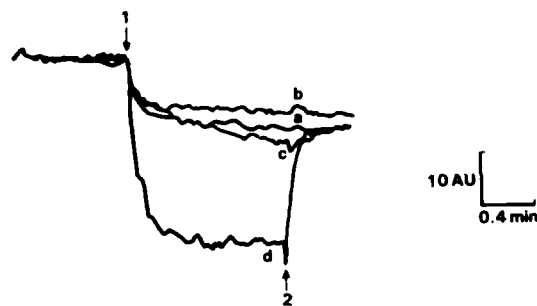


FIG. 1. K<sup>+</sup> gradient-dependent formation of pH. Vesicles were pre-loaded with 150 mM K<sup>+</sup>-gluconate and 10 mM HEPES-Tris, pH 7.4. 20  $\mu$ l of vesicles were injected (1) into 2.03 ml of buffer containing 150 mM tetramethylammonium (TMA) 10 mM HEPES-Tris, pH 7.4, 6  $\mu$ M acridine orange and 0.5% ethanol. Fluorescence traces are expressed in arbitrary units (AU) as a function of time. Trace a, control; absence of ionophores. Trace b, 0.1  $\mu$ M of carboxyl cyanide *p*-trifluoromethoxyphenyl hydrazone (FCCP). Trace c, 0.1  $\mu$ M of valinomycin. Trace d, 0.1  $\mu$ M of FCCP and 0.1  $\mu$ M of valinomycin. 50  $\mu$ l of 1 M K<sup>+</sup>-gluconate were injected (2) to collapse transmembrane K<sup>+</sup> gradients.

cles are loaded with 150 mM K-gluconate, 10 mM *N*-2-hydroxyethylpiperazine-*N'*-2-ethanesulfonic acid (HEPES)-Tris pH 7.4, and suspended in TMA-gluconate medium of the same pH. Valinomycin and FCCP should cause marked acidification of the intravesicular space due to their combined activity as a K<sup>+</sup>-H<sup>+</sup> exchanger. The expected behavior is observed and AO fluorescence is quenched due to H<sup>+</sup> influx into the vesicles driven by the outwardly directed K<sup>+</sup> flux (Fig. 1d). As expected, addition of K-gluconate to the extravesicular medium, which reduces the K<sup>+</sup> gradient, collapses the valinomycin/FCCP-generated pH gradient as revealed by the recovery of the quenched fluorescence.

In the presence of valinomycin alone, the negative potential established by increased outwardly directed K<sup>+</sup> flux induced proton influx and intracellular acidification via intrinsic H<sup>+</sup> conductance; hence, we expect AO quenching. On the other hand, the intrinsic K<sup>+</sup>-conductive pathway creates a negative internal membrane potential, which, in the presence of FCCP, should drive H<sup>+</sup> influx, and again we expect AO quenching. However, in the presence of valinomycin alone (Fig. 1c) or FCCP alone (Fig. 1b), the observed AO quenching is small and cannot be reversed by abolishing the K<sup>+</sup> gradient. This indicates that intrinsic conductances for K<sup>+</sup> and for H<sup>+</sup> are small in these vesicles, in comparison to vesicles isolated from kidney tissue, and do not contribute significantly to intravesicular acidification. The effectiveness of a combination of these two ionophores in inducing K<sup>+</sup>-H<sup>+</sup> exchange, however, is illustrated by the large fluorescence quenching in trace d. The decrease in fluorescence observed immediately after addition of vesicles to the fluorescence chamber is most probably related to nonspecific acridine orange quenching by the membrane added. This nonspecific quenching is also apparent in the incomplete recovery of AO fluorescence after external K<sup>+</sup> collapses the FCCP-valinomycin-induced pH gradient (Fig. 1d), and is observed in other experiments (2–4) after vesicles are added to the chamber.

The existence of Na<sup>+</sup>-H<sup>+</sup> exchange activity and its sensitivity to amiloride is exhibited in Fig. 2. Vesicles loaded with Na-gluconate (150 mM) and HEPES-Tris

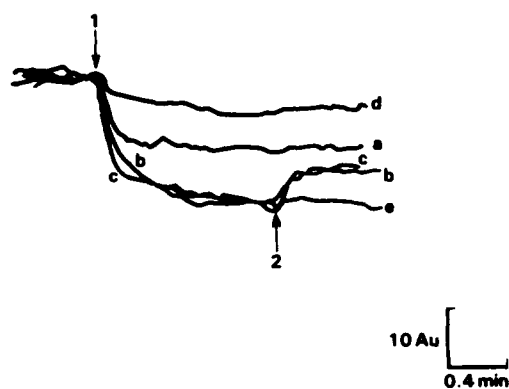


FIG. 2. Na<sup>+</sup> gradient-dependent formation of  $\Delta$ pH. Vesicles were preloaded with 150 mM Na<sup>+</sup>-gluconate, 50 mM K<sup>+</sup>-gluconate and 10 mM HEPES-Tris, pH 7.4. Twenty microliters of vesicles were injected (1) into 2.03 ml of a buffer containing 150 mM tetramethylammonium (TMA)-gluconate, 50 mM K<sup>+</sup>-gluconate, 10 mM HEPES-Tris, pH 7.4, and 6  $\mu$ M acridine orange except in trace a, in which extravesicular buffer was identical to internal buffer + 6  $\mu$ M acridine orange. At (2) in traces a-d, 100  $\mu$ l of 1 M Na<sup>+</sup>-gluconate was injected into the external buffer. In trace e at (2), 100  $\mu$ l of 1 M TMA-gluconate was injected. In traces a and b, no ionophore added. Trace c, 0.1  $\mu$ M valinomycin. Trace d, amiloride (final concentration  $10^{-4}$  M) was added prior to addition of vesicles; no ionophore added.

(10 mM) at pH 7.4 are injected into TMA-gluconate (150 mM) solution at the same pH. This outwardly directed Na<sup>+</sup> gradient causes a gradual acidification of the intravesicular space (b, c, and e), presumably due to the activity of the Na<sup>+</sup>-H<sup>+</sup> exchanger allowing Na<sup>+</sup> efflux, since the quenching is completely blocked by amiloride ( $10^{-4}$  M, trace d). The steady-state acidification level achieved depends on the relative fluxes through the H<sup>+</sup> "pump" (Na<sup>+</sup>-H<sup>+</sup>, or K<sup>+</sup>-H<sup>+</sup> in the presence of valinomycin and FCCP). Thus, the apparently lower level of acidification reached in this experiment, compared with the study depicted in Fig. 1, is probably due to the higher efficiency of the FCCP-valinomycin acidification mechanism as opposed to intrinsic Na<sup>+</sup> exchange. Fluorescence quenching can be reversed by addition of extravesicular Na<sup>+</sup> (b and c) but not by TMA<sup>+</sup> (e). In trace d, addition of extravesicular Na<sup>+</sup> (arrow 2) produced no significant reduction in AO fluorescence quenching, further evidence that  $10^{-4}$  M amiloride inhibited Na<sup>+</sup> gradient-dependent intravesicular acidification, and hence that the Na<sup>+</sup> gradient-dependent acidification observed in traces b, c, and e is due to amiloride-sensitive Na<sup>+</sup>-H<sup>+</sup> exchange.

To examine the role of membrane potential in Na<sup>+</sup> gradient-induced acidification we "short circuited" the membrane potential with valinomycin in the presence of high K<sup>+</sup> concentrations on both sides of the membrane. The elimination of membrane potential had essentially no effect on the AO quenching (compare traces b and c). Thus Na<sup>+</sup> gradient-induced acidification is entirely related to Na<sup>+</sup>-H<sup>+</sup> exchange and not to electrodiffusional coupling of conductive pathways. Furthermore, as expected from the stoichiometry previously described (2, 7), this Na<sup>+</sup>-H<sup>+</sup> exchange is electroneutral. As a control to establish the degree to which the observed signal was due to Na<sup>+</sup>-H<sup>+</sup> cotransport, AO quenching was measured for vesicles loaded with Na<sup>+</sup>, as before, but injected into

a cuvette solution with the same Na<sup>+</sup> concentration, i.e., in the absence of a transmembrane Na<sup>+</sup> gradient. As expected of a system driven by Na<sup>+</sup> gradient, only the nonspecific AO quenching was observed under this condition (a).

Because the membrane under study is relatively impermeable (see Fig. 1), it is difficult to alter the intravesicular buffer content or pH in a predicted manner after vesicle formation. We overcame these difficulties by loading them at the time of homogenization with a high concentration of K<sup>+</sup>; loading with protons was then achieved by incubation in a K<sup>+</sup>-free solution containing valinomycin and FCCP (see Fig. 1). Figure 3 depicts the effect of extravesicular Na<sup>+</sup> ions on the collapse of the pH gradient established by this H<sup>+</sup> loading technique (b), and the inability of TMA (c) to substitute for Na<sup>+</sup> in restoring the intravesicular pH. In each case, a collapse of the outward-directed K<sup>+</sup> gradient by addition of extravesicular K<sup>+</sup> abolished the pH gradient completely (b and c).

Figure 4 illustrates again the collapse of the K<sup>+</sup> gradient-supported pH gradient when Na<sup>+</sup> ions are injected into the extravesicular solution (a). Amiloride at a concentration of  $10^{-4}$  M substantially diminishes this effect of Na<sup>+</sup> (b). Collapsing the K<sup>+</sup> gradient by addition of K<sup>+</sup>-gluconate to the outside compartment resulted in further collapse of the pH gradient (Fig. 3c; Figure 4, a and b). Amiloride had little effect on the magnitude of the acidification (i.e., the difference between the fluorescence at the maximum acidification and fluorescence after reduction of the K<sup>+</sup> gradient). This observation rules out nonspecific effects of amiloride.

The ability of NaCl, Na<sup>+</sup> gluconate, and LiCl to collapse the pH gradient in the presence and absence of  $10^{-4}$  M amiloride is summarized in Table 1. As expected for a Na<sup>+</sup>-H<sup>+</sup> exchange system, external Li<sup>+</sup> collapses

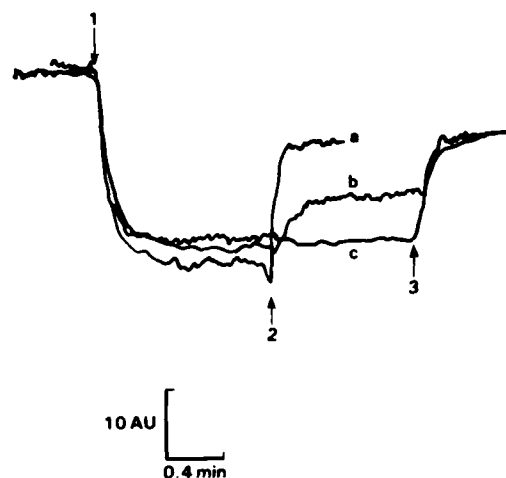


FIG. 3. Dissipation, by Na<sup>+</sup>-H<sup>+</sup> exchange, of a  $\Delta$ pH induced by K<sup>+</sup> gradient, valinomycin, and carboxyl cyanide *p*-trifluoromethoxyphenyl hydrazone (FCCP). Twenty microliters of vesicles preloaded with 150 mM K<sup>+</sup>-gluconate, 10 mM HEPES-Tris, pH 7.4 were injected (1) into 2.03 ml of buffer containing 150 mM tetramethylammonium (TMA)-gluconate, 10 mM HEPES-Tris, pH 7.4, 6  $\mu$ M acridine orange, 0.1  $\mu$ M valinomycin, and 0.1  $\mu$ M FCCP. One-hundred microliters of 1 M K<sup>+</sup>-gluconate (a), Na<sup>+</sup>-gluconate (b), or TMA-NO<sub>3</sub> (c) were injected into extravesicular solution at (2). One-hundred microliters of 1 M K<sup>+</sup>-gluconate was injected at (3).

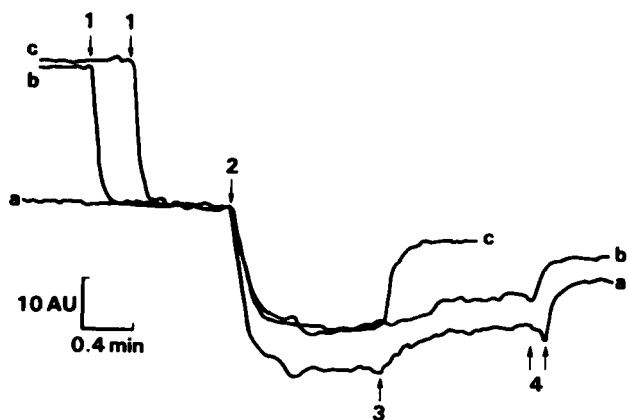


FIG. 4. Effect of amiloride on the Na<sup>+</sup>-H<sup>+</sup> exchange-mediated pH gradient collapse. Experimental conditions were identical to those in Fig. 3. Five microliters of amiloride solution were added at 1 to give a final concentration of 10<sup>-4</sup> M caused fluorescence quenching (traces b and c). Trace a was recorded in absence of amiloride and was aligned for convenience. At point 2, 20  $\mu$ l of vesicles preloaded with 150 mM K<sup>+</sup>-gluconate and 10 mM HEPES-Tris, pH 7.4, were injected into 2.03 ml of buffer containing 150 mM tetramethylammonium (TMA)-gluconate, 10 mM HEPES-Tris, pH 7.4, 6  $\mu$ M of acridine orange, 0.1  $\mu$ M valinomycin, and 0.1  $\mu$ M carboxyl cyanide *p*-trifluoromethoxyphenyl-hydrazone (FCCP). At arrows, 100  $\mu$ l of 1 M Na<sup>+</sup>-gluconate (3 in traces a and b) or K<sup>+</sup>-gluconate (3 in trace c and 4 in traces a and b) were injected into extravesicular solution. Amiloride (final concentration 10<sup>-4</sup> M) was injected prior to injection of vesicles (1, traces b and c).

TABLE 1. Rate of  $\Delta$ pH dissipation induced by Na<sup>+</sup> and Li<sup>+</sup> in presence and absence of amiloride

|              | Control,<br>AU·min <sup>-1</sup> | n | +10 <sup>-4</sup> Amiloride,<br>AU·min <sup>-1</sup> | n |
|--------------|----------------------------------|---|--|---|
| Na-gluconate | 0.955 $\pm$ 0.08                 | 5 | 0.17 $\pm$ 0.08                                      | 4 |
| Na-Cl        | 0.76 $\pm$ 0.09                  | 3 | 0.28 $\pm$ 0.04                                      | 2 |
| Li-Cl        | 0.147 $\pm$ 0.04                 | 3 | 0.075 $\pm$ 0.007                                    | 2 |

Values are means  $\pm$  SE for *n* = number of experiments. The experimental conditions were identical to those given in Fig. 4. The rate of  $\Delta$ pH dissipation was estimated from the slope of the initial change in the fluorescence trace after addition of Na<sup>+</sup>- or Li<sup>+</sup>-containing solution indicated as (3) in Fig. 4. AU, arbitrary units.

the pH gradient, but at a much slower rate than do Na<sup>+</sup> ions at the same concentration. Amiloride markedly decreased the effect of Li<sup>+</sup> as well as the effect of Na<sup>+</sup> in collapsing the pH gradient. The slight differences found in the ability of gluconate and chloride salts to collapse the pH gradient may indicate the existence of a Cl<sup>-</sup>-coupled OH<sup>-</sup> transport system, which is as yet unidentified.

To confirm that the pH changes we measured with the AO quench technique were indeed due to a direct exchange of Na<sup>+</sup> and H<sup>+</sup> mediated by the Na<sup>+</sup>-H<sup>+</sup> transport system, we directly monitored Na<sup>+</sup> flux using <sup>22</sup>Na. Figure 5 presents the time-course of Na<sup>+</sup> influx into LLC-PK<sub>1</sub> BBM vesicles in the presence (open squares) or absence (open circles) of pH gradient. Typical "overshoot" was observed only when a pH gradient was present to provide a driving force for the accumulation of Na<sup>+</sup> ions above equilibrium levels in the intravesicular space. No such "overshoot" is observed in the absence of pH gradient, indicating that Na<sup>+</sup> was driven by the H<sup>+</sup> gradient. Valinomycin (0.1  $\mu$ M) did not change the observed Na<sup>+</sup> influx, consistent with the data depicted in

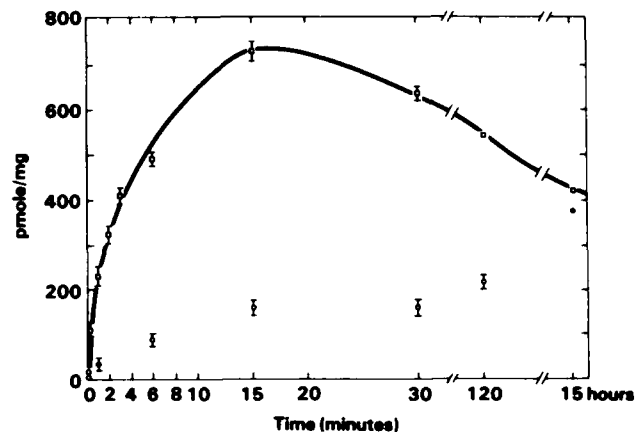


FIG. 5. Time dependence of uptake of <sup>22</sup>Na into brush-border vesicles. Vesicles were preloaded with 150 mM *N*-methyl-D-glucamine (NMG), titrated with 2-(*N*-morpholino)ethanesulfonic acid (MES) to pH 6.0, 50 mM K<sup>+</sup>-gluconate, and 20 mM mannitol. Incubation media contained 149 mM NMG adjusted to pH 7.4 (open squares) or 6.0 (open circles) with Tris or MES, respectively, 20 mM mannitol, 50 mM K<sup>+</sup>-gluconate, 0.1  $\mu$ M valinomycin, and 1 mM <sup>22</sup>NaCl.

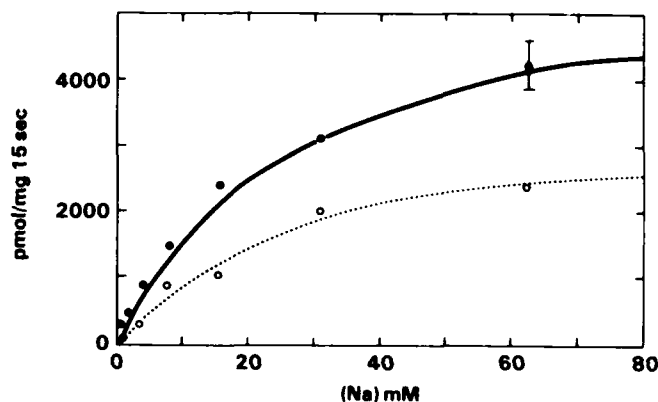
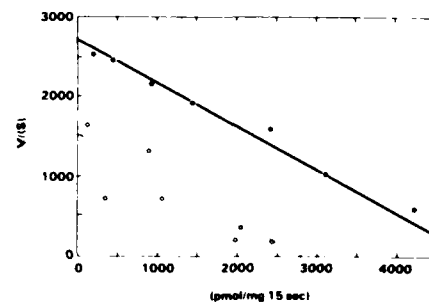


FIG. 6. Na<sup>+</sup> dependence of amiloride-sensitive Na<sup>+</sup> influx. Vesicles and incubation media (pH 7.4) were as in Fig. 5 except for different NaCl concentrations. Amiloride (open circles, final concentration of 10<sup>-5</sup> M) was added only to incubation media. Inset depicts Scatchard plot of data fitted by linear regression yielding *V*<sub>max</sub> of 5,058 and 2,800 pmol·mg<sup>-1</sup>·15 s<sup>-1</sup> and apparent *K*<sub>m</sub> of 19.2 and 18 mM for control (filled circles) and amiloride (open circles)-treated membranes, respectively.

Fig. 2, indicating an electroneutral process and the absence of electrodiffusional coupling of Na<sup>+</sup> and proton flux (data not shown). The intravesicular space was calculated from the equilibrium uptake values to be 0.5  $\mu$ l·mg protein<sup>-1</sup>, which is in the range of volumes reported in the literature for such a preparation.

Figure 6 illustrates the amiloride-sensitive Na<sup>+</sup> de-

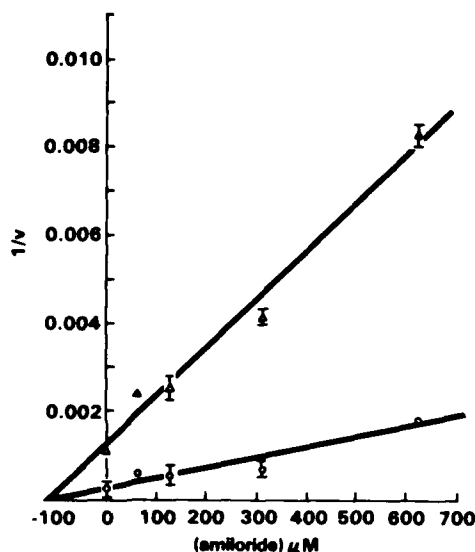


FIG. 7. Dixon plot of amiloride inhibition at 2 Na<sup>+</sup> concentrations. Vesicles and incubation media (pH 7.4) were as in Fig. 5. Amiloride dose-response of amiloride-sensitive Na<sup>+</sup> flux at 4 mM (open triangles) and 30 mM (open circles) Na<sup>+</sup> (substituted with *N*-methyl-D-glucamine in buffer for osmotic consistency). Line fitted by linear regression yields a  $K_i$  of  $100 \pm 10$   $\mu$ M amiloride.

pendence of the initial Na<sup>+</sup> influx into the apical membrane vesicles in the presence (open circles) or absence (closed circles) of  $10^{-5}$  M amiloride. Michaelis-Menten analysis of the rates of Na<sup>+</sup> flux at various Na<sup>+</sup> concentrations yields an apparent  $K_m$  of 19 mM and  $V_{max}$  of 5,058 pmol·mg protein<sup>-1</sup>·15 s<sup>-1</sup>. Amiloride ( $10^{-5}$ ) reduces the  $V_{max}$  to 2,800 pmol·mg protein<sup>-1</sup>·15 s<sup>-1</sup> with no change in the affinity of the system for Na<sup>+</sup> (apparent  $K_m = 18.1$ ). These findings are consistent with the data obtained in the fluorescence measurements under similar conditions (vesicles loaded with K-salts and incubation media containing NaCl), as illustrated in Fig. 4 and Table 1, and are in agreement with findings in whole-cell studies showing amiloride to be a noncompetitive inhibitor of Na<sup>+</sup> flux mediated by the Na<sup>+</sup>-H<sup>+</sup> transporter (10). Due to the scatter of the points, and since only one amiloride concentration was used, this experiment is unsuitable to evaluate the  $K_i$  for amiloride.

To allow direct measurement of the  $K_i$  we measured its dose-response at 4 and 30 mM of Na<sup>+</sup>. Figure 7 presents a Dixon plot of amiloride inhibition at these external Na<sup>+</sup> concentrations. Again, in agreement with the above findings, amiloride and Na<sup>+</sup> do not compete for a common site on the transporter. Linear regression reveals a  $K_i$  of  $100 \pm 10$   $\mu$ M for amiloride.

## DISCUSSION

We have established the activity of Na<sup>+</sup>-H<sup>+</sup> exchange in apical membrane vesicles of LLC-PK<sub>1</sub> cells by studying Na<sup>+</sup> and H<sup>+</sup> fluxes. This Na<sup>+</sup>-H<sup>+</sup> exchange activity does not result from electrodiffusional coupling, but from a direct coupled flux (antiporter). It should be emphasized that these two fluxes, although complimentary, cannot be directly compared without a precise measurement of the intravesicular volume and buffer capacity, which has not been done here. The system is apparently

electroneutral as membrane potential clamping caused no alteration in the Na<sup>+</sup> gradient-induced development of a pH gradient (monitored by AO quench) nor in pH-driven Na<sup>+</sup> ion flux (measured using <sup>22</sup>Na<sup>+</sup>); similar results have been observed in other laboratories in studies with BBM vesicles prepared from proximal kidney tubule tissue (1).

The LLC-PK<sub>1</sub> system under study here is similar to such kidney tissue preparations in that Na<sup>+</sup> influx and H<sup>+</sup> efflux are amiloride sensitive and saturable with increasing Na<sup>+</sup> concentration. Li<sup>+</sup> can partially substitute for Na<sup>+</sup> in inducing amiloride-sensitive H<sup>+</sup> efflux, though the rate of H<sup>+</sup> efflux induced by Li<sup>+</sup> is much lower than that induced by Na<sup>+</sup> (Table 1).

Vesicles made from membranes isolated from the LLC-PK<sub>1</sub> and incubated in Na<sup>+</sup> solution reach equilibrium with the outside solution only after 15 h (Fig. 5). The low permeability of these membranes relative to other vesicle preparations is further illustrated by the low conductances observed for K<sup>+</sup> and protons, as presented in Fig. 1. This may explain the difficulty we have encountered in loading the vesicles with desired buffers, a problem seen also in renal BBM. Membranes isolated from rabbit cortex and incubated for 2 h at 37°C with a buffer at pH 6.0 reached an internal pH of only 7.0, as measured by the AO technique at different extravesicular pH (data not shown). We have circumvented the difficulties of preloading with different buffers by acidification of the intravesicular space via ionophore-induced K<sup>+</sup>-H<sup>+</sup> exchange.

Conflicting reports are found in the literature concerning the relationship of amiloride and Na<sup>+</sup> and their effects on the Na<sup>+</sup>-H<sup>+</sup> exchange system. Both competitive and mixed inhibition have been documented (1, 6). Studying rapidly growing cells, Haggerty et al. (5) found that Na<sup>+</sup>-H<sup>+</sup> exchange system is expressed only when the cells are acidified. In that system Na<sup>+</sup> and amiloride compete for the same site. Haggerty et al. (5) suggested, however, that confluent monolayer behaved differently. Indeed, characterization of the Na<sup>+</sup> and amiloride interaction in confluent monolayer of LLC-PK<sub>1</sub> cells (which expresses minimal cell division as determined by thymidine incorporation and autoradiography, 9) showed that amiloride and Na<sup>+</sup> interact in a noncompetitive fashion with the Na<sup>+</sup>-H<sup>+</sup> exchanger (10). Because apical membrane vesicles and whole-cell preparations of LLC-PK<sub>1</sub> exhibit very similar Na<sup>+</sup>-H<sup>+</sup> behavior under defined conditions, we conclude that the observed Na<sup>+</sup>-H<sup>+</sup> exchange, as well as its properties in the whole cell, is an intrinsic behavior of a specific transporter, and not an artifactual phenomenon stemming from unknown regulatory mechanisms altered during the experimental procedures. It is conceivable that a similar Na<sup>+</sup>-H<sup>+</sup> exchange system exists along the nephron in addition to the exchanger that is competitively inhibited by amiloride. The coexistence of the two systems at different locations along the nephron may reconcile the conflicting reports in the literature, in which both competitive and mixed inhibition have been documented (1, 6).

In conclusion, a Na<sup>+</sup>-H<sup>+</sup> exchange system, similar to the system described in BBM from kidney proximal

tubule, has been characterized in the apical membrane of LLC-PK<sub>1</sub> cells. In this membrane, in contrast to BBM prepared from kidney, amiloride and Na<sup>+</sup> do not compete for a common site on Na<sup>+</sup>-H<sup>+</sup> exchange.

This work was supported by Armed Forces Radiobiology Research Institute, Defense Nuclear Agency, under Work Unit MJ 00107 and the Swiss National Science Foundation Grant No. 3.226.082. C.D.A.

The views presented in this paper are those of the authors; no endorsement by the Defense Nuclear Agency has been given nor should be inferred.

Received 7 October 1985; accepted in final form 29 July 1986.

## REFERENCES

1. ARONSON, P. S. Mechanisms of active H<sup>+</sup> secretion in the proximal tubule. *Am. J. Physiol.* 245 (*Renal Fluid Electrolyte Physiol.* 14): F647-F659, 1983.
2. ARONSON, P. S., M. A. SUHAM, AND J. NEE. Interaction of external H<sup>+</sup> with the Na<sup>+</sup>-H<sup>+</sup> exchanger in renal microvillus membrane vesicles. *J. Biol. Chem.* 258: 6767-6771, 1983.
3. BROWN, C. D. A., M. BODMER, J. BIBER, AND H. MURER. Sodium-dependent phosphate transport by apical membrane vesicles from a cultured renal epithelial cell line (LLC-PK<sub>1</sub>). *Biochim. Biophys. Acta* 769: 471-478, 1984.
4. CASSANO, G., B. STIEGE, AND H. MURER. Na/H and Cl/OH exchange in rat jejunal and rat proximal tubular brush border membrane vesicles. *Pfluegers Arch.* 400: 309-317, 1984.
5. HAGGERTY, J. G., E. J. CRAGOE, C. W. SLYMAN, AND E. A. ADELBERG. Na<sup>+</sup>/H<sup>+</sup> exchanger activity in the pig kidney epithelial cell line, LLC-PK<sub>1</sub>; inhibition by amiloride and its derivatives. *Biochem. Biophys. Res. Comm.* 127: 759-767, 1985.
6. IVES, H. E., V. J. YEE, AND D. G. WARNOCK. Mixed type inhibition of renal Na<sup>+</sup>-H<sup>+</sup> antiporter by Li<sup>+</sup> and amiloride. *J. Biol. Chem.* 258: 9710-9716, 1983.
7. KINSELLA, J. L., AND P. S. ARONSON. Determination of the coupling ratio of Na<sup>+</sup>-H<sup>+</sup> exchange in renal microvillus membrane vesicles. *Biochim. Biophys. Acta* 689: 161-164, 1982.
8. MIRCHEFF, A. K., C. C. LU, AND C. N. CONTEAS. Resolution of apical and basolateral plasma membrane populations from rat exorbital gland. *Am. J. Physiol.* 245 (*Gastrointest. Liver Physiol.* 8): G661-G667, 1983.
9. MORAN, A., L. DAVIS, AND M. HAGAN. Effect of radiation on the regulation of sodium-dependent glucose transport in LLC-PK<sub>1</sub> epithelial cell line: possible model for gene expression. *Rad. Res.* 105: 201-210, 1986.
10. MORAN, A. Sodium hydrogen exchange system in LLC-PK<sub>1</sub> epithelium. *Am. J. Physiol.* 252 (*Cell Physiol.* 21): C63-C68, 1987.
11. MURER, H., J. BIBER, P. GMAJ, AND B. STIEGER. Cellular mechanism in epithelial transport: advantage and disadvantage of studies with vesicles. *Mol. Physiol.* 6: 55-82, 1984.
12. MURER, H., U. HOPFER, AND R. KINNE. Sodium/proton antiport in brush-border-membrane vesicles isolated from rat small intestine and kidney. *Biochem. J.* 154: 597-604, 1976.
13. MURER, H., AND R. KINNE. The use of isolated membrane vesicles to study epithelial transport processes. *J. Membr. Biol.* 55: 81-95, 1980.
14. REENSTRA, W. W., D. G. WARNOCK, V. J. YEE, AND J. G. FORTE. Proton gradients in renal cortex brush-border membrane vesicles. *J. Biol. Chem.* 256: 11663-11666, 1981.
15. SABOLIC, I., AND G. BURCKHARD. Effect of the preparation method on Na<sup>+</sup>-H<sup>+</sup> exchange and ion permeabilities in rat renal brush-border membranes. *Biochim. Biophys. Acta* 772: 140-148, 1984.
16. WARNOCK, D. G., W. W. REENSTRA, AND V. J. YEE. Na<sup>+</sup>-H<sup>+</sup> antiporter of brush-border vesicles: studies with acridine orange uptake. *Am. J. Physiol.* 242 (*Renal Fluid Electrolyte Physiol.* 11): F733-F739, 1982.

## Effects of Ethanol on the Functional Properties of Sodium Channels in Brain Synaptosomes

Michael J. Mullin and Walter A. Hunt

**Abstract.** Voltage-sensitive sodium channels in excitable cell membranes are responsible for the rapid increase in permeability to sodium ions that occurs during depolarization. Neurotoxins that bind with high affinity and specificity to voltage-sensitive sodium channels have been widely used to identify and characterize the structure and function of sodium channels in nerve and skeletal muscle. This chapter describes the actions of ethanol on the functional properties of voltage-sensitive sodium channels in mammalian brain nerve endings. The effects of acute and chronic ethanol administration are also reviewed. Alterations in the function of neuronal membrane sodium channels may be involved in the depressant effect of ethanol.

### 1. Introduction

Since the turn of the century, general anesthetics have been believed to interact with excitable membranes to produce their depressant effects. In fact, aliphatic alcohols were used to formulate the well-known Meyer-Overton principal of anesthesia, stating that the potencies of anesthetics are directly related to their lipid solubility. (For a complete review of alcohol-membrane interactions, see Hunt.<sup>1</sup>)

An action of aliphatic alcohols on lipids is expected on physicochemical grounds based on the structure of alcohols. Since alcohols, such as ethanol, are molecules consisting of a single hydroxyl group on a hydrocarbon chain, they would be expected to be both lipophilic and hydrophilic, that is, amphiphiles. The concentration of an alcohol in a membrane would depend on its relative solubilities in membranes and water as expressed by the membrane/water partition coefficient.

Alcohols dissolve in membranes and as a result disorder lipid structure. This has been shown in a number of ways. In the presence of alcohols, the surface area of membranes increases, and the temperature at which mem-

Michael J. Mullin and Walter A. Hunt • Behavioral Sciences Department, Armed Forces Radiobiology Research Institute, Naval Medical Command National Capital Region, Bethesda, Maryland 20814-5145

branes undergo transition from a gel to a liquid phase decreases.<sup>2</sup> A more direct indication of lipid order can be determined with molecular probes that can report on the microenvironment in which they reside. Attached spin-labels or fluorescent molecules can be studied with electron paramagnetic resonance or fluorescence spectrometry.

With these methods aliphatic alcohols have been found to disorder or fluidize membranes at concentrations equivalent to those found in intoxicated animals.<sup>3,4</sup> The disordering occurs more in the lipid core of the membrane than at the surface and can be reduced by increasing the concentration of cholesterol in the membrane or by reducing its temperature.<sup>5</sup>

Cell membranes contain integral units that process various activities in support of the function of the cell. For the lipid-disordering effects of alcohols to have relevance to the pharmacological and behavioral effects of alcohols, these functional entities must in some way be modified. Many enzymes and ion channels depend for optimal activity on the lipid environment associated with them. Consequently, the lipid-disordering effect of alcohols may disrupt this environment with possibly substantial physiological consequences.

Neurons generate and transmit electrical impulses by moving various ions across membranes at precisely controlled intervals. As shown in the classic experiments of Hodgkin and Huxley,<sup>6</sup> electrical impulses or action potentials develop in neurons that have a resting membrane potential and result from an initial but transient increase in the inward movement of sodium ions, whose concentration is mostly extracellular. The cell depolarizes until there is a reversal in the polarity, allowing for depolarization of adjacent portions of the membrane. For the cell to repolarize, potassium ions, which are predominantly intracellular, flow out.

Alcohols can alter the movement of ions through membranes, thereby altering the electrical properties of neurons. Several electrophysiological studies have demonstrated that in invertebrates the height of the action potential and maximum sodium conductance are reduced.<sup>7-9</sup> However, high concentrations of ethanol are required to produce these changes. Similar results were observed with electrically stimulated brain slices.<sup>10,11</sup> In the presence of 105 mM ethanol, sodium uptake into intracellular spaces was significantly reduced.

A molecular approach can also be used to study ion movements. Ions move through pores in membranes called channels containing gates that open and close in response to physiological conditions. Recent advances have led to the isolation and characterization of some of these channels. In the case of sodium channels, various neurotoxins that are known from electrophysiological experiments to interact with sodium channels have been used to characterize the toxins in synaptosomes and cultured cells.

The sodium channel is a glycoprotein with multiple polypeptide subunits that traverses the neuronal membrane.<sup>12</sup> Studies in which purified channels were reconstituted in artificial membranes have demonstrated an absolute requirement of lipids for normal channel function.<sup>13</sup> At least three functional

**Table I.** Neurotoxin Binding Sites in the Sodium Channel

| Site | Neurotoxin        | Effect on ion influx                                | Effect of ethanol |
|------|-------------------|---|-------------------|
| I    | Saxitoxin         | Inhibits ion flux                                   | None              |
|      | Tetrodotoxin      |   |                   |
| II   | Batrachotoxin     | Promotes ion influx                                 | Inhibits          |
|      | Veratridine       |   |                   |
| III  | Scorpion venom    | Potentiates effect of neurotoxins acting at site II | None              |
|      | Sea anemone venom |   |                   |

sites within sodium channels have been identified<sup>14</sup> (Table I). Site I, located on the external surface of the neuronal membrane, binds tetrodotoxin and saxitoxin, drugs that block the generation of action potentials. Site II, located in the lipid core of the membrane, binds batrachotoxin and veratridine, lipid-soluble drugs that activate the sodium channels. And site III, located on the membrane surface but with projections down to site II, binds scorpion and sea anemone toxins that enhance the actions of toxins acting on site II but have no intrinsic activity of their own.

With these latest advances it has been possible to examine further the effects of alcohols at the molecular level on sodium channels in the mammalian brain. The research to date has explored the effects of ethanol on the uptake of radioactive sodium ions into synaptosomes that are stimulated with the neurotoxins batrachotoxin or veratridine. Synaptosomal preparations are incubated in a low-sodium or sodium-free physiological medium.<sup>15,16</sup> A preincubation in which ethanol and the toxin are added together or the toxin is added 2 min later lasts for 10 min after the toxin is added. Uptake of the labeled ion is then determined in incubations generally lasting 2–5 sec. Blanks to assess passive movement of sodium ions are performed similarly, except tetrodotoxin may be added to inhibit toxin-stimulated uptake.

## 2. Effects of Ethanol *in Vitro* on Neurotoxin-Stimulated Sodium Influx and Neurotoxin Binding

As mentioned previously, the lipid-disordering action of ethanol should result in changes in the functional properties of neuronal membranes. In recent years, a number of studies have examined the effects of ethanol on calcium,<sup>17–18</sup> potassium,<sup>19</sup> and sodium channels<sup>20,21</sup> in synaptosomes. This section reviews the changes in the properties of voltage-sensitive sodium channels that occur after incubation of ethanol with synaptosomes *in vitro*.

Initially, it was demonstrated that when whole rat brain synaptosomes were incubated with ethanol *in vitro* there was a concentration-dependent inhibition of veratridine-stimulated <sup>22</sup>Na<sup>+</sup> influx.<sup>20</sup> This effect of ethanol oc-



curred at sublethal, pharmacologically relevant concentrations and was fully reversible when the ethanol was removed from the membranes by centrifugation and washing. Pentobarbital (0.45 mM) also reduced the veratridine-stimulated  $^{22}\text{Na}^+$  influx. In addition, Harris<sup>21</sup> demonstrated that ethanol, ether, enflurane, halothane, pentobarbital, and phenytoin reduced the veratridine-dependent uptake of  $^{24}\text{Na}^+$  in a mouse brain synaptosomal preparation. Each of these intoxicant-anesthetic agents also increased the fluidity of mouse brain synaptic plasma membranes. Thus, it seemed reasonable to conclude that an increase in membrane fluidity could alter the functional properties of voltage-sensitive sodium channels in the brain. Since ion channels in the brain play an important role in the processing of information and the control of neuroexcitability, it was necessary to characterize further the effect of ethanol on sodium channel function.

Recently, it was shown that the concentration of ethanol required to inhibit neurotoxin-stimulated sodium influx by 50% ( $\text{IC}_{50}$ ) was dependent on which neurotoxin was used to activate the channel.<sup>22</sup> Batrachotoxin is a full agonist that activates nearly all sodium channels present in synaptosomes. In contrast, veratridine, a partial agonist, activates about 50% of the sodium channels present in rat brain synaptosomes. The  $\text{IC}_{50}$  values for ethanol were 345 and 583 mM for veratridine- and batrachotoxin-stimulated sodium influx, respectively. In an independent study, Harris and Bruno<sup>23</sup> described a similar difference in the potency of ethanol using mouse brain synaptosomes. Thus, although batrachotoxin and veratridine bind to the same site in the channel, there may be major differences in the manner in which each toxin affects the channel after binding occurs. It is interesting to note that the veratridine-stimulated cation influx in reconstituted sodium channels from skeletal muscle is sensitive to changes in temperature, whereas batrachotoxin-stimulated cation influx is rather insensitive to changes in temperature.<sup>24</sup>

When the effect of ethanol on sodium influx was measured over a range of concentrations of veratridine or batrachotoxin, we found that ethanol reduced the maximum effect of the toxin ( $V_{\text{max}}$ ) with no significant change in the affinity ( $K_{0.5}$ ) of the toxin for its receptor, as measured by modified Michaelis-Menten equations. In contrast, Harris and Bruno<sup>23</sup> reported that although ethanol reduced the maximum effect of both batrachotoxin and veratridine, the apparent affinity of veratridine for its receptor was also affected by ethanol in a temperature-dependent fashion. This difference may be caused by the different membrane preparations and assay conditions used in the two studies.

Whereas the neurotoxin-dependent influx of sodium is inhibited by ethanol, the influx of sodium in the presence of veratridine and tetrodotoxin is not affected by ethanol. In addition, the passive influx of sodium into synaptosomes in the absence of any neurotoxins is unchanged by ethanol. Thus, it appears that ethanol reduces the influx of sodium ions that occurs specifically through the voltage-sensitive sodium channel. Ethanol *in vitro* also has no effect on the inhibition of batrachotoxin-stimulated sodium influx by te-

trodotoxin. The presence of ethanol (400 mM) *in vitro* has no effect on the binding of [ $^3$ H]saxitoxin to its receptor in the channel.<sup>25</sup> This may be because the saxitoxin receptor is located at the extracellular side of the membrane, where the fluidizing effect of ethanol is rather weak. Ethanol may only affect certain specific areas in the channel. In addition to this apparent selectivity for different binding sites in the channel, specific brain areas also differ in sensitivity to the inhibitory effect of ethanol on sodium influx, with rat cortex being more sensitive than synaptosomes derived from the cerebellum.<sup>23</sup>

### 3. Effects of Acute and Chronic Ethanol Treatment on Sodium Channel Function

Most of the literature concerning the effects of ethanol on the properties of sodium channels deals with the direct effects of ethanol *in vitro*. However, it was also of interest to determine if acute or chronic ethanol treatment would alter the properties of voltage-sensitive sodium channels in rat brain synaptosomes. To study this question in some detail, dose-response and time-course studies were performed after a single dose of ethanol.<sup>25</sup>

In the time-course study, male Sprague-Dawley rats received a single dose of ethanol (4.5 g/kg) given orally, and cortical synaptosomes were prepared and blood ethanol concentrations were determined at 1, 2, 6, 18, and 24 hr after the dose of ethanol. For the first 6 hr after the single dose of ethanol, the blood ethanol concentrations were between 250 and 325 mg/dl. At 18 and 24 hr after the dose of ethanol, the blood ethanol concentrations were below 25 mg/dl. To assess the function of the channel, the cortical synaptosomes were incubated with batrachotoxin only, batrachotoxin plus ethanol (400 mM), and batrachotoxin plus tetrodotoxin to define the nonspecific influx of sodium. Acute ethanol treatment did not significantly alter the influx of sodium in the presence of batrachotoxin only or the nonspecific influx in the presence of batrachotoxin and tetrodotoxin at any of the time points examined. Thus, it appeared that the acute ethanol treatment did not impair the binding of the neurotoxins or affect the response (sodium influx) to the toxins in the absence of ethanol *in vitro*.

However, the inhibitory effect of ethanol *in vitro* was significantly reduced by the single dose of ethanol *in vivo*. The results shown in Table II demonstrate the reduction in the inhibitory effect of ethanol *in vitro* over the course of the experiment. Although the response to the *in vitro* addition of ethanol was reduced at 18 hr, recovery was essentially complete at 24 hr. The sodium channels present in the membranes from the ethanol-treated rats were tolerant to the inhibitory effect of ethanol on the neurotoxin-stimulated influx of sodium ions. The tolerance developed rapidly, was maximal 6 hr after the single dose of ethanol, and was still evident 18 hr after the acute treatment, a time when the blood ethanol concentrations in the whole animal were 25 mg/dl or less.

**Table II.** Effect of Acute Ethanol (4.5 g/kg, p.o.) Treatment on Neurotoxin-Stimulated Sodium Uptake

| Group         | Batrachotoxin-stimulated $^{22}\text{Na}^+$ uptake <sup>a</sup> |                     |
|---------------|---|---------------------|
|               | BTX <sup>a</sup> only   | BTX + EtOH (400 mM) |
| Control       | 7.61 ± 0.21   | 4.91 ± 0.21         |
| Ethanol 1 hr  | 7.16 ± 0.21   | 6.02 ± 0.21*        |
| Ethanol 2 hr  | 6.78 ± 0.33   | 5.94 ± 0.29*        |
| Ethanol 6 hr  | 8.00 ± 0.33   | 8.11 ± 0.22**       |
| Ethanol 18 hr | 6.73 ± 0.48   | 5.55 ± 0.38         |
| Ethanol 24 hr | 7.34 ± 0.10   | 5.00 ± 0.34         |

<sup>a</sup>Expressed in nanomoles per milligram protein. \* $P < 0.05$ , \*\* $P < 0.01$  versus corresponding control value. BTX, batrachotoxin; EtOH, ethanol.

To characterize this effect further, a dose-response study was performed. Animals received a single intubation of saline (controls) or ethanol at a dose of 1.5, 3.0, 4.5, or 6.0 g/kg, and synaptosomes were prepared from the cortex at 2 hr after the intubation. Blood ethanol concentrations were also determined at the same time. The influx of sodium in the presence of batrachotoxin only was unaffected by any dose of ethanol. The inhibition of the batrachotoxin-stimulated sodium influx by ethanol *in vitro* was significantly reduced by the acute ethanol treatment at doses of 3.0, 4.5, and 6.0 g/kg. The mechanism responsible for the acute tolerance is currently under study. It may be that the acute ethanol treatment *in vivo* affects the partitioning of ethanol added *in vitro* into a crucial site of the membrane. It is clear that the treatment of the whole animal with a single dose of ethanol exerts a dramatic effect on the action of ethanol added *in vitro* to the synaptosomes. The functional properties of sodium channels in nerve membranes are known to be regulated by a variety of factors including lipid composition and fluidity, protein phosphorylation, and the levels of calcium in the membrane. The elucidation of the mechanisms responsible for the acute tolerance that occurs could lead to a better understanding of the phenomenon of tolerance in general.

The administration of a liquid diet containing ethanol to mice for 7 days has been reported to have no significant effect on the resting or veratridine-stimulated influx of sodium or the ability of ethanol *in vitro* to inhibit the neurotoxin-stimulated influx of sodium.<sup>23</sup> This treatment regimen is known to produce tolerance, physical dependence, and signs of withdrawal when ethanol is removed from the diet. In contrast to these findings, the chronic administration of ethanol to rats by multiple intubations for a period of 4 days produced tolerance to the inhibitory effects of ethanol *in vitro* on the neurotoxin-stimulated influx of sodium ions. The reduction in the inhibitory effect of ethanol (400 mM) *in vitro* on the batrachotoxin-stimulated influx of sodium ions was apparent after 2 days of chronic ethanol treatment and lasted for at least 20 days after withdrawal. Thirty-five days after withdrawal, the effect

of ethanol *in vitro* was essentially identical in synaptosomes derived from control and chronically treated rats.<sup>25</sup>

It is interesting to note that the reduction in the inhibitory effect of ethanol is greatest during the induction period, while the rats are intoxicated and have a blood ethanol concentration of 225 mg/dl or more. After withdrawal, the inhibitory effect of ethanol *in vitro* recovers somewhat, although the degree of inhibition in the treated animals is still significantly smaller than the inhibition in synaptosomes derived from control rats. During the induction period, the effect of ethanol added *in vitro* closely resembles the effect in rats treated with a large single dose of ethanol and sacrificed 1 or 2 hr later. After withdrawal, ethanol added *in vitro* has an effect similar to the results seen at 18 hr after acute ethanol in the time-course study.

#### 4. Effects of Other Agents on Sodium Channels

In addition to ethanol, a number of physical and chemical agents have been studied to determine their effects on the properties of sodium channels using ion flux and receptor-binding techniques.

General anesthetics<sup>21</sup> have been shown to cause a significant inhibition of neurotoxin-stimulated sodium influx at or near the concentration of the drug that is required to produce anesthesia *in vivo*.<sup>21</sup> Additionally, in a series of chemically diverse anesthetics, there was a strong correlation between the potency for decreasing neurotoxin-stimulated sodium influx and the increase in membrane fluidity produced deep in the core of the membrane.<sup>26</sup> Local anesthetics<sup>27-28</sup> have also been shown to be competitive inhibitors of the binding of batrachotoxin and of the membrane depolarization caused by batrachotoxin. Alterations in the function of sodium channels may be related to the pharmacological actions of these agents.

Clinically effective concentrations of the antiepileptic drugs carbamazepine and phenytoin have been shown to inhibit neurotoxin-stimulated sodium influx and the binding of [<sup>3</sup>H]batrachotoxin in neuroblastoma cells and rat brain synaptosomes.<sup>29-30</sup> Sodium valproate, diazepam, and phenobarbital were without effect at concentrations that are effective *in vivo*.

Ultraviolet radiation also inhibits neurotoxin-stimulated sodium movements and has been shown to reduce the binding of [<sup>3</sup>H]saxitoxin to the channel.<sup>31</sup> Ionizing radiation has been reported to inhibit neurotoxin-stimulated sodium influx in a manner remarkably similar to the observed effects of ethanol.<sup>32</sup> Different mechanisms of action are probably involved, as ionizing radiation has no effect on the fluidity of rat brain synaptic plasma membranes. Thus, a number of chemical and physical agents can alter the functional properties of sodium channels, apparently through a variety of mechanisms of action. The sodium channel in excitable membranes may represent a common target for a variety of chemical and physical agents that depress the central nervous system.

## 5. Summary

The direct effects of ethanol added *in vitro* on the voltage-sensitive sodium channels in brain synaptosomes are concentration dependent and fully reversible. Potency for inhibition of neurotoxin-stimulated sodium influx was correlated with lipid solubility and the degree of membrane disordering. Brain regions also vary in sensitivity to the inhibitory effects of ethanol. In addition, ethanol appeared to have an effect only on the channel site for activation, where the toxins batrachotoxin and veratridine bind.

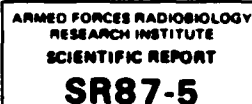
It seems likely that the direct effects of ethanol *in vitro* are a result of the membrane-disordering effect of ethanol. Also, acute and chronic administration of ethanol results in the development of tolerance to the inhibitory effect of ethanol *in vitro*. The tolerance develops rapidly and is long lasting. The mechanisms responsible for the membrane adaptation are not yet known but are currently under study.

In addition to ethanol a number of chemical agents including general and local anesthetics, some antiepileptics, and certain antiarrhythmics alter the function of brain sodium channels. Physical agents such as ultraviolet and ionizing radiation also have dramatic effects on the sodium channel. Further studies should improve our understanding of how the chemical and physical agents work and increase our knowledge of the structure and function of sodium channels in the brain.

## References

1. Hunt WA: *Alcohol and Biological Membranes*. New York, Guilford Press, 1985.
2. Rowe ES: Lipid chain length and temperature dependence of ethanol-phosphatidylcholine interactions. *Biochemistry* 22:3229-3305, 1983.
3. Chin JH, Goldstein DB: Effects of low concentrations of ethanol on the fluidity of spin-labeled erythrocyte and brain membranes. *Mol Pharmacol* 13:435-441, 1977.
4. Harris RA, Schroeder F: Ethanol and the physical properties of brain membranes: Fluorescence properties. *Mol Pharmacol* 20:128-137, 1981.
5. Chin JH, Goldstein DB: Membrane-disordering action of ethanol: Variation with membrane cholesterol content and depth of the spin label probe. *Mol Pharmacol* 19:425-431, 1981.
6. Hodgkin AL, Huxley AF: A quantitative description of membrane current and its application to conduction and excitation in nerve. *J. Physiol (Lond)* 117:500-544, 1952.
7. Armstrong CM, Binstock L: The effects of several alcohols on the properties of the squid giant axon. *J Gen Physiol* 48:265-277, 1964.
8. Moore JW, Ulbricht W, Takata M: Effect of ethanol on the sodium and potassium conductances of the squid giant axon membrane. *J Gen Physiol* 48:279-295, 1964.
9. Bergmann MC, Klee MW, Faber DS: Different sensitivities to ethanol of early transient voltage clamp currents of *Aplysia* neurons. *Pfluegers Arch* 348:139-153, 1974.
10. Nikander P, Wallgren H: Ethanol, electrical stimulation, and net movements of sodium and potassium in rat brain tissue *in vitro*. *Acta Physiol Scand* 80:29A, 1970.
11. Wallgren H, Nikander P, von Boguslawsky P, et al: Effects of ethanol, tert. butanol, and clomethiazole on net movements of sodium and potassium in electrically stimulated cerebral tissue. *Acta Physiol Scand* 91:83-93, 1974.

12. Catterall WA: The emerging molecular view of the sodium channel. *Trends Neurosci* 5:303-306, 1982.
13. Tamkun MM, Talvenheimo JA, Catterall WA: The sodium channel from rat brain: Reconstitution of neurotoxin-activated ion flux and scorpion toxin binding from purified components. *J Biol Chem* 259:1676-1688, 1984.
14. Catterall WA: Neurotoxin that act on voltage-sensitive sodium channels in excitable membranes. *Annu Rev Pharmacol Toxicol* 20:15-43, 1980.
15. Krueger BK, Blaustein MP: Sodium channels in presynaptic nerve terminals: Regulation by neurotoxins. *J Gen Physiol* 76:287-313, 1980.
16. Tamkun MM, Catterall WA: Ion flux studies of voltage-sensitive sodium channels in synaptic nerve-ending particles. *Mol Pharmacol* 19:78-86, 1981.
17. Harris RA, Hood WF: Inhibition of synaptosomal calcium uptake by ethanol. *J Pharmacol Exp Ther* 213:562-568, 1980.
18. Leslie SW, Barr E, Chandler J, et al: Inhibition of fast and slow-phase depolarization-dependent synaptosomal calcium uptake by ethanol. *J Pharmacol Exp Ther* 225:571-575, 1983.
19. Yamamoto H, Harris RA: Calcium-dependent  $^{86}\text{Rb}^+$  efflux and ethanol intoxication: Studies of human blood cells and rodent brain synaptosomes. *Eur J Pharmacol* 88:357-363, 1983.
20. Mullin MJ, Hunt WA: Ethanol inhibits veratridine-stimulated sodium uptake in synaptosomes. *Life Sci* 34:287-292, 1984.
21. Harris RA: Differential effects of membranes perturbants on voltage-activated sodium and calcium channels and calcium-dependent potassium channels. *Biophys J* 45:132-134, 1984.
22. Mullin MJ, Hunt WA: Actions of ethanol on voltage-sensitive sodium channels. Effects on neurotoxin-stimulated sodium uptake in synaptosomes. *J Pharmacol Exp Ther* 232:413-419, 1985.
23. Harris RA, Bruno P: Effects of ethanol and other intoxicant-anesthetics on voltage-dependent sodium channels of brain synaptosomes. *J Pharmacol Exp Ther* 232:401-406, 1985.
24. Tanaka JC, Eccleston JF, Barchi RL: Cation selectivity characteristics of the reconstituted voltage-dependent sodium channel purified from rat skeletal muscle sarcolemma. *J Biol Chem* 258:7519-7526, 1983.
25. Mullin MJ, Hunt WA, Dalton TK, et al: Alterations in neurotoxin-stimulated  $^{22}\text{Na}^+$  influx in synaptosomes after acute and chronic ethanol treatment. *Fed Proc* 44:4843, 1985.
26. Harris RA, Bruno P: Membrane disordering by anesthetic drugs. Relationship to synaptosomal sodium and calcium fluxes. *J Neurochem* 44:1274-1281, 1985.
27. Creveling CR, McNeal ET, Daly JW, et al: Batrachotoxin-induced depolarization and [ $^3\text{H}$ ]batrachotoxinin-A 20  $\alpha$ -benzoate binding in a vesicular preparation from guinea pig cerebral cortex. *Mol Pharmacol* 23:350-358, 1983.
28. Postma SW, Catterall WA: Inhibition of binding of [ $^3\text{H}$ ]batrachotoxinin A20- $\alpha$ -benzoate to sodium channels by local anesthetics. *Mol Pharmacol* 25:219-227, 1984.
29. Willow M, Catterall WA: Inhibition of binding of [ $^3\text{H}$ ]batrachotoxinin A20- $\alpha$ -benzoate to sodium channels by the anticonvulsant drugs diphenylhydantoin and carbamazepine. *Mol Pharmacol* 22:627-635, 1982.
30. Willow M, Kuenzel EA, Catterall WA: Inhibition of voltage-sensitive sodium channels in neuroblastoma cells and synaptosomes by the anticonvulsant drugs diphenylhydantoin and carbamazepine. *Mol Pharmacol* 25:228-234, 1984.
31. Weigele JB, Barchi RL: Ultraviolet irradiation produces loss of saxitoxin binding to sodium channels in rat synaptosomes. *J Neurochem* 35:430-435, 1980.
32. Wixon HN, Hunt WA: Ionizing radiation decreases veratridine-stimulated uptake of sodium in rat brain synaptosomes. *Science* 220:1073-1074, 1983.



Immune Regulation by Characterized Polypeptides, pages 429-441  
© 1987 Alan R. Liss, Inc.

## RADIOPROTECTION BY INTERLEUKIN - 1

Ruth Neta\*, Susan D. Douches\*  
and Joost J. Oppenheim\*\*

\*Department of Experimental Hematology  
Armed Forces Radiobiology Research Institute  
Bethesda, MD 20814

\*\*Laboratory of Molecular Immunoregulation  
BRMP, NCI, Frederick, MD 21701

**ABSTRACT:** Protection from lethal effects of ionizing radiation has been achieved by administration prior to irradiation of immunomodulatory substances. The mechanism of radioprotection by immunomodulators is unknown. Since immunomodulatory substances induce the release of cytokines we studied two of the cytokines, IL-1 and IL-2 for their radioprotective effect. Administration of IL-1 protects mice in a dose dependent manner from lethal effect of ionizing radiation. The IL-1 conferred radioprotection is time dependent with administration 20 hrs prior to radiation yielding optimal effect. Administration of IL-2 did not have a significant radioprotective effect.

## INTRODUCTION

Rapid increases in industrial and medical applications of ionizing radiation make it essential to address the question of protection from damaging and often lethal effects of radiation. Studies of radiation induced damage to the living animal date back to the classical work of Heinecke in 1905 (1) and have been pursued extensively since 1945 (2). Studies of protection against

ionizing radiation have been conducted primarily on the cellular level and were concerned with the mechanism of DNA repair and the chemical radioprotection afforded by thiol compounds (3). It is also well established that transplantation of bone marrow cells into animals or patients irradiated with a lethal dose (below the dose inducing a gastrointestinal syndrome) protects them from death. Therefore, despite radiation induced damage to many cell types and tissues, a supply of undamaged, hematopoietic and lymphoid cells can protect an animal or a patient from death. Furthermore, radioprotection has been conferred by immunomodulatory substances. Immunomodulatory bacterial components such as bacterial lipopolysaccharide (LPS), *Mycobacterium bovis* strain BCG, muramyl dipeptide (MDP) or glucan have radioprotective effect when administered prior to irradiation. The immunomodulatory substances are known to induce the release of cytokines. It is therefore possible that these exogenous agents exert their effect via endogenously produced cytokines.

The availability at present of purified cytokines, obtained by recombinant DNA technology provides an opportunity to assess the role of such purified mediators of immune function as effectors of radioprotection. Presently, we chose to study two of the cytokines, IL-1 and IL-2. These two particular cytokines were selected because of their a) recognized effect in inducing entry of lymphoid cells into the cell cycle resulting in cells reaching a relatively radioresistant S phase and b) differences in cellular targets of these agents with IL-2 affecting lymphocytes and IL-1 implicated as a maturation and differentiation inducing agent for a variety of cells (5).

#### MATERIALS AND METHODS

Mice - Inbred strains of female C57BL/6 and DBA/1 mice, were obtained from Jackson Laboratories, Bar Harbor, Maine. All mice were quarantined and acclimated for at least 2 weeks to the conditions of the Veterinary Medicine Department Facility at the Armed Forces Radiobiology Research Institute. Mice were kept in cages, nine mice per cage, with filter lids. Standard lab chow and HCl acidified water, pH2.4, were given ad libitum. All cage cleaning procedures were carried out in a microisolator.



Irradiation - Mice were placed in Plexiglas containers and given whole body irradiation at 0.40 Gy/min by bilaterally positioned  $^{60}\text{Co}$  elements.

Interleukin-1, Interleukin-2 - Recombinant IL-1 (Lot No. 11319-159-46, 11430-110-48 and 14430-200) was a generous gift from Drs. W. Benjamin and P. Lomedico of Hoffman La-Roche. The preparations had a specific activity from  $4\text{--}6 \times 10^6$  u/mg and were supplied in 5M Guanidine Hydrochloride. As a control, a preparation of similarly purified and solubilized protein from *E. coli* (Lot No. 11319-177-46 and 13146-120-43) containing the plasmid without IL-1 cDNA was used. The LPS content of all preparations was established by chromogenic LAL assay. The highest concentration of LPS was observed in a lot 14430-200 of IL-1 that contained 71 pg LPS in 2500 ng IL-1, while the control protein contained 131 pg LPS in 2500 ng of protein.

Recombinant IL-2 lot 3646 with a sp. activity of  $5.3 \times 10^6$  u/mg was a gift from Dr. John Schindler of Biogen.

The lymphokines and control protein extract were diluted in pyrogen-free saline immediately before intraperitoneal administration.

## RESULTS

### DOSE DEPENDENCE OF RADIOPROTECTIVE EFFECT OF IL-1

IL-1 in doses ranging from 58 ng to 333 ng was administered intraperitoneally into 2-4 month old C57BL/6 mice, 20 hrs prior to irradiation. This particular time interval was chosen because of earlier demonstrations of radioprotective effect of LPS being optimal when administered 24 hrs prior to irradiation (6). The time lag for *in vitro* induction of IL-1 with LPS has been estimated at about 4 hrs (7). Control mice received injections of control protein in concentrations of 166 ng or 333 ng per mouse. An additional control group received irradiation only. The amount of contaminant LPS injected with the highest dose of IL-1 was less than 4 pg per mouse and for the control protein less than 20 pg per mouse. Administration of IL-1, but not of control protein, protected C57BL/6 mice from lethal effects of irradiation in a dose dependent manner (Table 1). Similar radioprotection by IL-1 was also demonstrated in DBA/1 mice which are more radioresistant than C57BL/6 mice,

TABLE 1

| Dose Dependence of Radioprotective Effect of IL-1<br>in C57BL/6 Mice |        |          |         |        |         |
|--|--------|----------|---------|--------|---------|
|  | 58 ng  | 83 ng    | 166 ng  | 250 ng | 333 ng  |
| IL-1   | 0*(8)  | 33 (9**) | 75 (16) | 75 (8) | 82 (42) |
| Control<br>Protein<br>Extract  |        |          | 7 (14)  |        | 0 (14)  |
| Radiation<br>Control   | 0 (36) |          |         |        |         |

1 unit of IL-1 is equivalent to 0.16 ng protein

\* Percent survival

\*\* Number of mice administered a given dose

TABLE 1 - C57BL/6 mice 2-4 months old were placed in plexiglass restrainers and given whole body irradiation at 40 rads/min by bilaterally positioned  $^{60}\text{Co}$  elements. The total dose was 950 rads. Recombinant IL-1 or a protein from *E. coli* extract containing the plasmid without IL-1 cDNA were diluted in pyrogen free saline and administered intraperitoneally 20 hours prior to irradiation. The lethal dose for radiation controls was LD<sub>100/16+1</sub> (dose of radiation that killed 100% of mice in 16+1 days).

since 950 rads, an LD<sub>100/17</sub> dose for C57BL/6 mice (dose of radiation that kills 100% of mice in 17 days), yielded only LD<sub>50/30</sub> for DBA/1 mice (Table 2). Doses of IL-1 ranging from 58ng to 333ng were administered ip without any obvious deleterious effects. A maximal dose of 333 ng was used since a twofold increase in concentration appeared to be toxic. The toxicity was due to the Guanidine Hydrochloride as the injection of the vehicle by itself had toxic effects.

#### TIME DEPENDENCE OF RADIOPROTECTIVE EFFECT OF IL-1

The critical time interval necessary for optimal protection with IL-1 was determined.

C57BL/6 mice received 500 ng of IL-1 (Lot 14430 200)

TABLE 2

| Radioprotective Effect of IL-1 in DBA/1 Mice |         |          |
|--|---------|----------|
|  | 83 ng   | 166 ng   |
| IL-1   | 80 (10) | 100 (27) |
| Bacterial Protein Extract                    | ND      | 30 (19)  |
| Radiation Control                            | 50 (26) |          |

TABLE 2 - DBA/1 were irradiated with 950 rads, an LD<sub>50/30</sub> dose for this strain. IL-1 or control protein extract was administered ip 20 hrs prior to irradiation.

equivalent to 2000 units. This preparation in LAL assay contained 14 pg of LPS contamination per inoculum. The equivalent amount of control protein contained 24 pg of LPS. The mice were injected either at 45 hrs, 20 hrs and 4 hrs before or 1 hr after irradiation with 950 rads. Results in Table 3 indicate that optimal protection was conferred by IL-1 when administered 20 hrs prior to radiation.

TABLE 3

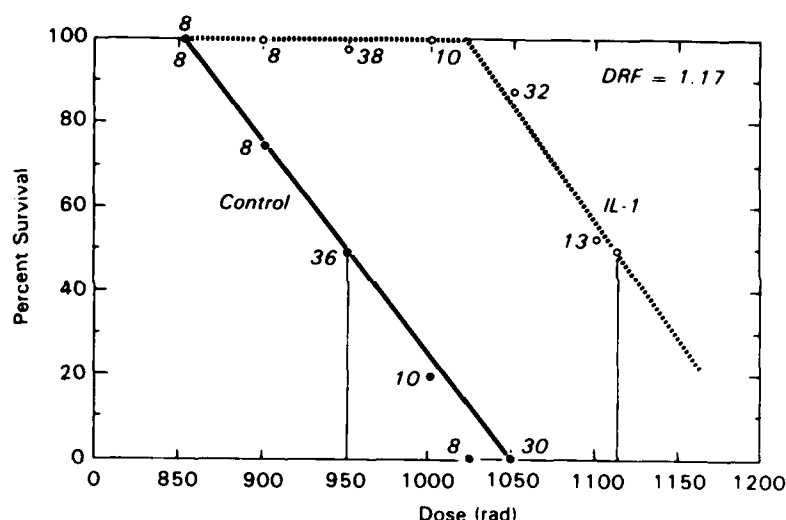
| Time Dependence of Radioprotective Effect of IL-1 in C57BL/6 Mice |          |         |         |        |
|---|----------|---------|---------|--------|
|   | -45 hrs  | -20 hrs | -4 hrs  | +1 hr  |
| IL-1  | 12.5 (8) | 85 (33) | 28 (39) | 0 (16) |
| Control Protein Extract   | 0 (8)    | 0 (35)  | 0 (12)  | 0 (12) |
| Radiation Control   |          |         | 0 (40)  |        |

TABLE 3 - C57BL/6 mice received 500 ng of IL-1 or control protein extract intraperitoneally at various times before or after 950 rads irradiation as indicated. The radiation dose resulted in LD<sub>100/16+1</sub>.

## DETERMINATION OF DOSE REDUCTION FACTOR (DRF)

The radioprotective effect of IL-1 was examined further in mice exposed to gradually increasing doses of radiation to determine the dose reduction factor (defined as the ratio of the dose of radiation yielding LD 50/30 with IL-1 vs the control LD 50/30 dose). DBA/1 mice were exposed to radiation doses ranging from 850 to 1100 rads (Fig. 1). The dose reduction factor for 160 ng of IL-1 in this strain was 1.17.

**Radioprotective Effect of IL-1 on DBA/1 Mice  
Exposed to Various Doses of Radiation**



The numbers are the numbers of experimental animals used for each point.

FIGURE 1 - DBA/1 mice 2-3 months old were administered 166 ng of recombinant IL-1 or control protein 20 hrs prior to irradiation. The numbers represent the numbers of experimental mice used for each point. DRF was calculated from the ratio of LD<sub>50/30</sub> of IL-1 treated to control mice.

**COMPARISON OF THE NUMBER OF NUCLEATED BONE MARROW  
CELLS IN LETHALLY IRRADIATED CONTROL AND  
IL-1 TREATED MICE**

Doses of irradiation sufficient to result in a lethal

FIGURE 2  
**Progressive Recovery of  
 Nucleated Bone Marrow Cells with Time  
 After Lethal Irradiation of C57BL/6 Mice**

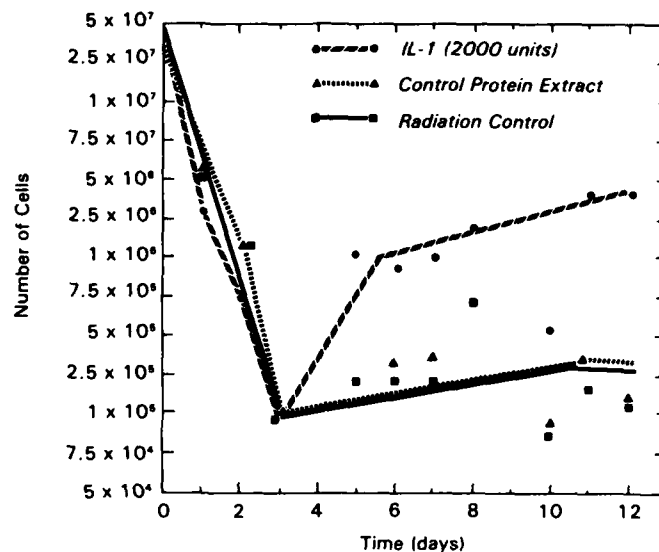


FIGURE 2 - C57BL/6 mice 2-4 months old received ip injections of IL-1 or control protein 20 hrs prior to whole body irradiation with 950 rads ( $LD_{100/16}$ ). The bone marrow cells were obtained from femurs of 3-5 mice/group. Viable cell counts were performed in hemacytometer using trypan blue exclusion method.

hematopoietic syndrome with depletion of hematopoietic progenitor cells and lymphoid cells were used (2). The numbers, by viability counts of these cells in bone marrow of control and IL-1 treated mice, were compared with time after irradiation (Fig.2). On day 1 and 2 after irradiation a similar decline in recoverable bone marrow cells was observed in IL-1 treated and the two control groups: control protein treated or irradiated only mice. By day 3 after irradiation the numbers of bone marrow cells in all 3 groups were equally reduced, and amounted to only 0.2 - 0.3% of the original cell numbers. While in

the two control groups only slight changes in cell numbers were observed for the remaining 12 days of the experiment, in IL-1 treated group a gradual rise in cell numbers was observed from day 5 until day 12. On the twelfth day of the experiment 50% of the control animals were dead, while IL-1 treated animals had 20% of the number of bone marrow cells of normal controls.

Using a Coulter channelizer, these bone marrow cells were determined to be primarily large in size consistent with the size of hematopoietic progenitor cells. These observations were confirmed by light microscopy of cytopsin preparations showing a high percentage of erythroid precursor cells.

#### COMPARISON OF RADIOPROTECTIVE EFFECT OF IL-1 WITH IL-2

Although the reasons for the radioprotective effect of IL-1 and exogenous immunomodulatory substances are not clear, this activity may be based on their shared effect

TABLE 4

| The Effect of IP Administration of IL-2 on<br>Survival of Lethally Irradiated C57BL/6 Mice |         |           |        |        |
|--|---------|-----------|--------|--------|
| IL-2 Dose  | -45 hrs | -20 hrs   | -4 hrs | + 1 hr |
| 20000 u<br>or 4 $\mu$ g  | 0* (8)  | 11.8 (17) | ND     | 0 (8)  |
| 6500 u<br>or 1.2 $\mu$ g   | 0 (8)   | 8.0 (36)  | 0 (12) | 0 (20) |
| 2000 u<br>or 400 ng  | 0 (8)   | 0 (8)     | ND     | ND     |
| Radiation<br>Control   | 0 (36)  |           |        |        |

(Numbers in parenthesis are numbers of mice)

\* Percent survival

TABLE 4 - Mice were administered IL-2 before or after irradiation as indicated. The survival of mice treated with IL-1 in the same experiments (4 experiments in all) was 78.5%, n = 28 mice.

on cell cycle induction, since late S phase cells become more resistant to ionizing radiation. We have therefore initiated experiments to compare the radioprotective activity of cell cycle inducing cytokines. IL-2 was administered in doses ranging from 2000 - 20000 units or 400 ng - 4 ug at 45, 20 or 4 hrs before and 1 hr after irradiation (Table 4). It is clear that even 10 fold higher doses of IL-2 than IL-1 did not induce significant radioprotection.

#### DISCUSSION

The data presented above demonstrates that IL-1, a cytokine released endogenously following administration of immunomodulatory bacterial components or other inflammation inducing agents, has a radioprotective effect.

The extent of radioprotection conferred with IL-1 (Table 1, 2, 3, Fig. 1) equals that produced with the most potent biological radioprotector-LPS (4). Historically, LPS was also the agent used to study the induction of IL-1 at the systemic and cellular level (7). Because exogenous inflammatory agents that confer radioprotection also induce IL-1 release, we propose that IL-1 mediates their radioprotective activity.

The mechanism of action of biological (as opposed to chemical thiol agents) radioprotectors is hypothetical at present. The very broad spectrum of effects induced by the inflammatory / immunomodulatory agents makes it difficult to determine which processes may account for radioprotection. A comparison of physiological effects induced by the systemic administration of IL-1 and LPS narrows the means by which they may contribute to radioprotection. The observation that, unlike LPS, IL-1 does not induce systemic mast cell degranulation (Donlon and Neta, unpublished results) in vivo interferon release (Vogel and Neta, unpublished results) or activates the complement cascade suggest that these may not play an important role in radioprotection. However, many shared effects of IL-1 and LPS remain to be considered. For example, LPS and IL-1 both are active in vivo in fever induction (8), acute phase proteins induction (9, 10) and colony stimulating factor (CSF) induction (11, Vogel and Neta, unpublished results).

The time interval necessary for optimal radioprotection (20 hours rather than 45 or 4 hrs before irradiation - Table 3) favors the hypothesis that the effects of IL-1 are indirect in inducing the radioprotective state. Induction of the cells into late S phase by IL-1 may contribute to systemic radioprotection. CSF induction by IL-1 as well as IL-1 itself promote proliferation of many cell types (5) and result in cycling of these cells. The cell cycle time for hematopoietic progenitor cells has been reported to last from 6 to 20 hrs (12-14) and would therefore account for the time lag necessary for radioprotection with IL-1. Ongoing studies using GM-CSF as a potential radioprotector should further determine the validity of this hypothesis.

The finding that recombinant IL-2 does not confer significant radioprotection (Table 4) indicates that survival of cells other than lymphocytes is of primary importance in the survival of an animal following radiation injury.

The enhanced recovery of bone marrow hematopoietic progenitor cells in IL-1 treated animals beginning at 5 days after irradiation (Fig. 2) indicates that these cells are protected from radiation damage, either physically by clot formation or chemically by scavengers or that their repair mechanisms are more effective. These 3 postulated mechanisms may coexist and may be mediated by acute phase reactive proteins induced with IL-1.

Induction of circulating fibrinogen by IL-1 (15) and of procoagulant formation by IL-1 stimulated endothelial cells (16) may promote formation of microthrombi. The hypoxic conditions created in such a milieu would protect the cells from radiation damage. The subsequent release of these cells would contribute to the increased cell numbers seen in IL-1 treated mice with time after irradiation.

Two other acute phase reactive proteins, metallothionins (MT) and ceruloplasmin may act as chemical radioprotectors. Ceruloplasmin is recognized as a copper transporting protein as well as ferrous ion oxidizing protein (17). In addition, ceruloplasmin has been implicated in inhibiting autooxidation of lipids and in inhibiting degradation of deoxyribonucleic acid (DNA) (20). Metallothioneins are proteins characterized by unusually high cysteine content (30 mole %) which (18)



selectively bind heavy metal ions Zn, Cd and Cu. These two types of metalloproteins, ceruloplasmin and MT, are recognized scavengers of superoxide radicals and free radicals respectively, the formation of which is known to cause extensive damage following irradiation. MTs have been shown to be the most effective scavengers of free radicals *in vitro* (20). The effect of MT as a radioprotector has been demonstrated since mammalian cells expressing high levels of MT were resistant to X-irradiation damage (21). As for ceruloplasmin, a two fold mechanism can be postulated for MT; a) as a scavenger of free radicals and b) as a source of Zn for DNA repair enzymes. Both MT and ceruloplasmin have been shown to be induced by IL-1 (22, 23).

Our data thus identifies IL-1 as a key endogenous signal which modulates a variety of subsequent physiological events resulting in radioprotection. IL-1 also provides a new means of radioprotection free of some of the harmful side effects of radioprotective drugs and immunomodulatory agents.

#### ACKNOWLEDGMENTS

We thank Mrs. Sonia Jones for her excellent assistance in typing the manuscript. This work was supported by the Armed Forces Radiobiology Research Institute, Defense Nuclear Agency, under Research Work Unit MJ 00148. The views presented in this paper are those of the authors; no endorsement by the Defense Nuclear Agency has been given or should be inferred. Research was conducted according to principles enunciated in the "Guide for the Care and Use of Laboratory Animals" prepared by the Institute of Laboratory Animals resources, National Research Council.

#### REFERENCES

1. Heinecke, H, (1905). Experimentelle Untersuchungen uber die Einwirkung der Roentgenstrahlen auf das Knochenmark nebst einigen Bemerkungen uber die Roentgentherapie der Leukaemie und Pseudoleukaemie und des Sarkoms. Deutch Z Chir 78, 196.

2. Bond, VP, Fliedner TM, Archambeau JO (1965). "Mammalian Radiation Lethality - a disturbance in cellular kinetics." Acad. Press, New York and London.
3. Radioprotectors and anticarcinogens" (1983). Nygard OF and Simic MG (eds): Acad. Press, New York and London.
4. Behling UH (1983). The radioprotective effect of bacterial endotoxin. In Nowotny A, ed. "Beneficial effects of endotoxins" Plenum Press New York p.127.
5. Kluger MJ, Oppenheim JJ, Powanda MC, eds (1985). "The Physiologic, metabolic and immunologic action of IL-1. Alan R. Liss, New York.
6. Ainsworth EJ, Chase HB, (1959). Effect of microbial agents on irradiation mortality in mice. Proc. Soc. Exp. Biol. Med. 102, 483.
7. Wood DD, (1984). Antigen - nonspecific factors elaborated by macrophages which stimulate lymphocytes. Interleukin 1. In Bellanti JA, Herscowitz HB, eds, "The reticuloendothelial system, a comprehensive treatise" Plenum Press, New York and London p. 201.
8. Dinarello CA, Goldin NP, Wolff SM, (1974). Demonstration and characterization of two distinct human leukocytic pyrogens. J Exp Med 139:1369.
9. Sipe JD, Vogel SN, Ryan JL, McAdam KPWJ, Rosenstreich DL, (1979). Detection of a mediator derived from endotoxin-stimulated macrophages that induces the acute phase SAA response in mice. J Exp Med 150: 597.
10. McAdam KPWJ, Dinarello CA, (1980) Induction of serum amyloid A synthesis by human leukocytic pyrogen. In Agarwal MK, ed. "Bacterial Endotoxins and Host Response" Elsevier / North Holland Biomedical Press, Amsterdam p. 167.
11. Kampschmidt RF, Pulliam LA, Upchurch HF, (1980). The activity of partially purified leukocytic endogenous mediator in endotoxin resistant C<sub>3</sub>H/HeJ mice. J Lab Clin Med 95: 616.
12. Boggs SS, Chervenick PA, Boggs DR. (1972). The effect of postirradiation bleeding or endotoxin on proliferation and differentiation of hematopoietic stem cells. Blood 40: 375.
13. Soren L, (1973). Variability of the time in which PHA-stimulated lymphocytes initiate DNA synthesis. Exp Cell Res 78: 201.

14. Darzynkiewicz Z, Traganos F, Sharpless T, Melamed MR, (1976). Lymphocyte stimulation: a rapid multiparameter analysis. *Proc Natl Acad Sci USA* 73: 2881.
15. Kampschmidt RF, Upchurch HF, Pulliam LA, (1982). Characterization of a leukocyte-derived endogenous mediator responsible for increased plasma fibrinogen. *Ann. NY Acad Sci* 389: 338.
16. Bevilacqua MP, Pober JS, Majeau GR, Cotran RS, Gimbrone MA, (1984). Interleukin 1 (IL-1) induces biosynthesis and cell surface expression of procoagulant activity in human vascular endothelial cells. *J Exp Med* 160: 618.
17. Goldstein IM, Charo IF, (1983) Ceruloplasmin: An acute phase reactant and antioxidant. In Pick E, ed. "Lymphokines" Academic Press. New York 8: 373.
18. Karin M, (1985). Metallothioneins: Proteins in search of function. *Cell* 41: 9.
19. Guttenridge JM, Stocks J, (1981). Ceruloplasmin: Physiological and pathological perspective. *CRC Crit Rev Clin Lab Sci* 14: 257.
20. Thornalley PJ, Vajak M, (1985). Possible role for metallothionein in protection against radiation induced oxidative stress. Kinetics and mechanism of its reaction with superoxide and hydroxyl radicals. *Bioch Biophys Acta* 827: 36.
21. Bakka A, Johnson AS, Enderssen L, Rugstad HE, (1982) Radioresistance in cells with high content metallothionein. *Experientia* 38: 381.
22. Karin M, Imbra RJ, Heguy A, Wong G, (1985) Interleukin 1 regulates human metallothionein gene expression. *Mol Cell Biol.* 5: 2866.
23. Pekarek RS, Powanda MC, Wannemacher PW, (1972) The effect of leukocytic endogenous mediator (LEM) on serum copper and ceruloplasmin concentrations in the rat. *Proc Soc Exp Biol Med* 141: 1029

## Cytokines in Radioprotection. Comparison of the Radioprotective Effects of IL-1 to IL-2, GM-CSF and IFN $\gamma$

RUTH NETA,<sup>1</sup> STEFANIE N. VOGEL,<sup>2</sup> JOOST J. OPPENHEIM,<sup>3</sup>  
and SUSAN D. DOUCHES<sup>1</sup>

<sup>1</sup>Department of Experimental Hematology, Armed Forces Radiobiology Research Institute, Bethesda, MD 20814

<sup>2</sup>Department of Microbiology, Uniformed Services University of Health Sciences, Bethesda, MD 20814

<sup>3</sup>Laboratory of Molecular Immunoregulation, National Cancer Institute, Frederick Cancer Research Facility, Frederick, MD 21701

### ABSTRACT

Immunomodulatory agents are radioprotective when administered to animals prior to irradiation. The mechanisms for this radioprotection have as yet not been determined, but may involve endogenously released cytokines. We have recently demonstrated that murine IL-1 is radioprotective in mice (Neta et al. *J. Immunol.*, 136, 2483, 1986). In this study we have further explored this effect and investigated whether the radioprotective effect of IL-1 is mediated by other cytokines. Optimal radioprotection with IL-1 was obtained with administration 20 hr prior to irradiation and was greatly reduced with administration 45 or 4 hr before or 1 hr after irradiation with 950 cGy, an LD100/30 dose. The dose reduction factor (DRF) measured by LD50/30 was 1.25 for C57Bl/6 mice. The presence of a lag period in IL-1 induced radioprotection suggests that the effect of IL-1 may be indirect. The hypothesis that IL-1 may act by inducing the release of other cytokines was tested in part by two approaches: (a) Assays for circulating IFN and CSF. High titers of CSF were present at 3 and 6 hrs and declined at 24 hrs after administration of 0.1  $\mu$ g of IL-1, a dose radioprotective in mice. Assays for IFN in the same sera were negative. (b) Direct administration of recombinant IFN- $\gamma$ , GM-CSF, or IL-2 prior to LD100/30 irradiation. Using a wide range of doses of these cytokines delivered 20 or 3 hr prior to irradiation, no significant radioprotective effect was observed.

### INTRODUCTION

Radioprotectors are either chemical or biological agents, the administration of which before or during irradiation diminishes radiation-induced damage. The chemical agents are primarily thiol compounds which are known to act by scavenging free radicals (1). The biological agents are immunomodulatory and/or inflammatory substances (2). The mechanisms by which they induce radioprotection are not known.

Many of the immunomodulatory substances (e.g., LPS or BCG) which are radioprotective also induce the release of cytokines (3). It could, therefore, be hypothesized that these exogenous agents exert their radioprotective effects via induction of cytokines. The recent availability of purified cytokines

obtained by recombinant DNA technology provides an opportunity to assess the role of such purified mediators as radioprotectors.

Our previous work demonstrated recombinant murine IL-1 to be radioprotective in mice (4). However, IL-1 is only one of a number of cytokines released following LPS or BCG administration. Other cytokines present in the circulation in high titers following challenge with LPS or BCG are IFN (5) and CSF (6). These two cytokines were suggested by others to be important in radioprotection (7,8). We have, therefore, initiated experiments to test the recombinant cytokines IFN- $\gamma$  and GM-CSF for their effect on survival of lethally irradiated mice. Recombinant IL-2 was also included since this activator of lymphoproliferation is induced *in vitro* by IL-1 (9).

In this work we demonstrate that using comparable conditions in LD100/30 irradiated C57BL/6 mice, the radioprotective effect of IFN- $\gamma$ , GM-CSF, and IL-2 is much less than that of IL-1.

#### MATERIALS AND METHODS

Mice - Inbred strains of female C57BL/6 and C<sub>3</sub>H/HeJ mice were obtained from Jackson Laboratories, Bar Harbor, Maine. All mice were quarantined and acclimated for at least 2 weeks to the conditions of the Veterinary Medicine Department Facility at the Armed Forces Radiobiology Research Institute. Mice were housed, nine mice per cage, under filter lids. Standard lab chow and HCl acidified water, pH 2.4, were given *ad libitum*. All mice-handling procedures were carried out in a microisolator.

Irradiation - Mice were placed in Plexiglas containers and given whole-body irradiation at 40 cGy/min by bilaterally positioned <sup>60</sup>Co elements.

Recombinant Cytokines - Recombinant murine IL-1 (Lot Nos. 11319-159-46, 11430-110-48, and 14430-200) was a generous gift from Drs. W. Benjamin and P. Lomedigo of Hoffman La-Roche. The preparations had a specific activity of 4-6x10<sup>6</sup> u/mg and were supplied in 5M Guanidine Hydrochloride. As a control, a preparation of similarly purified and solubilized protein from *E. coli* (Lot Nos. 11319-177-46 and 13146-120-43) containing the plasmid without IL-1 cDNA was used. Recombinant human IL-1 $\alpha$  and IL-1 $\beta$  were both kindly provided by Dr. Steven Gillis of Immunex. The preparations were supplied in PBS pH 7.2 and as suggested used on weight basis. Recombinant murine IFN $\gamma$  Lot No. 3209-24 with specific activity 5.2x10<sup>6</sup> u/mg was a gift from Dr. Michael Shepard of Genetech. Recombinant murine GM-CSF was provided by Dr. Steven Gillis of Immunex as a lyophilized powder with sucrose as a stabilizing agent. Recombinant IL-2 Lot 3646 with a sp. activity of 5.3x10<sup>6</sup> u/mg was a gift from Dr. John Schindler of Biogen. The LPS content of all preparations was established by chromogenic LAL assay and was less than 1 unit (0.1 ng) in each inoculum. The lymphokines and control protein extract were diluted in pyrogen-free saline immediately before intraperitoneal administration.

Measurements of colony stimulating factor activity and of interferon in the sera were performed as previously described (10,11).

Statistical analysis of the data was performed using z - statistics with = 0.05 type I error allocated to the tests for an effect. This was done using the Bonferroni inequality (12).

#### RESULTS

Time Dependence of Radioprotective Effect of IL-1 - The critical time interval necessary for optimal protection with IL-1 was determined.

C57BL/6 mice received 500 ng of IL-1 (Lot 14430-200) equivalent to 2000 units of IL-1 activity. This preparation in LAL assay contained 14 pg of LPS contamination per inoculum. The equivalent amount of control protein contained 24 pg of LPS. The mice were injected either at 45 hr, 20 hr and 4 hr before or 1 hr after irradiation with 950 cGy. Results in Figure 1 indicate that optimal protection was conferred by IL-1 when administered 20 hr prior to radiation.

### Time Dependence of Radioprotective Effect of IL-1

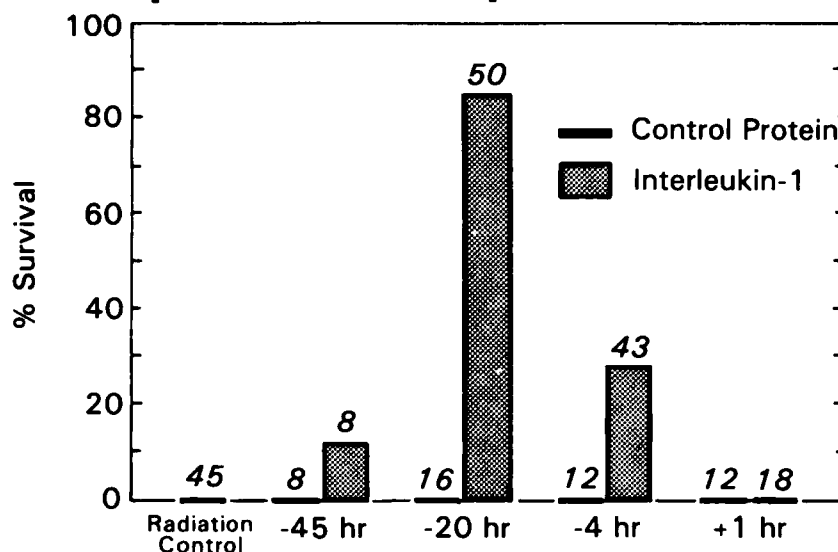


FIGURE 1 - C57BL/6 mice 2-4 months old were placed in Plexiglas restrainers and given whole-body irradiation at 40 cGy/min by bilaterally positioned  $^{60}\text{Co}$  elements. The total dose was 950 cGy. Recombinant IL-1 or a protein from *E. coli* extract containing the plasmid without IL-1 cDNA were diluted in pyrogen free saline and administered intraperitoneally at various times before or after irradiation as indicated. The radiation dose killed 100% of control mice in 16+1 days. The numbers represent total numbers of mice used in the experiments. IL-1 had a significant ( $p < 0.001$ ) radioprotective effect compared to controls at -20 hr and -4 hr prior to irradiation.

**Determination of Dose Reduction Factor (DRF)** - The radioprotective effect of IL-1 was examined further in mice exposed to gradually increasing doses of radiation to determine the dose reduction factor (defined as a ratio of the dose of radiation yielding LD50/30 with IL-1 to the control LD50/30 dose). C57BL/6 mice received 100 ng of human IL-1 $\alpha$  and 20 hr later were exposed to radiation doses ranging from 750 to 1000 cGy. The dose reduction factor for this dose of IL-1 was 1.25 (Fig. 2).

**Induction of Cytokines in Circulation Following IL-1 Administration** - Although the reasons for the radioprotective effect of IL-1 and exogenous immunomodulatory substances are not clear, this activity may be mediated by the induction of other cytokines. We have, therefore, assayed for the appearance in the circulation of two cytokines, CSF and IFN. These two cytokines are known to be present in the circulation following LPS administration. Administration of 100 ng of human IL-1, a dose which is radioprotective in mice, resulted in the appearance of high serum titers of CSF at 3 and 6 which declined by 24 hr following injection of IL-1 (Table 1). Assays for IFN in the same sera were negative. However, following challenge with 10  $\mu\text{g}$  of LPS, C57BL/6 but not C3H/HeJ mice release IFN and CSF, indicating that when appropriately stimulated, responsive mice have both cytokines in circulation. These results suggest that CSF but not IFN may be implicated in IL-1 induced radioprotection.

**Comparison of the Radioprotective Effects of IL-1 $\alpha$  with IL-1 $\beta$ , IL-2, GM-CSF, and IFN $\gamma$ .** - Radioprotective immunomodulatory substances induce the release of a variety of cytokines. We therefore compared the radioprotective effect of IL-1 measured by survival of lethally irradiated mice, with IL-1, IL-2, GM-CSF, and IFN $\gamma$ . Figure 3 summarizes the results of these experiments. The radioprotective effects of human IL-1 $\beta$  were comparable to those of human IL-1 $\alpha$  (significant ( $p < 0.001$ )) and also comparable to the protection offered to mice using murine IL-1 (see Fig. 1). However, using comparable conditions (i.e.,

**Radioprotective Effect of IL-1 on C57BL/6 Mice Exposed  
to Various Doses of Radiation  
Determination of Dose Reduction Factor**

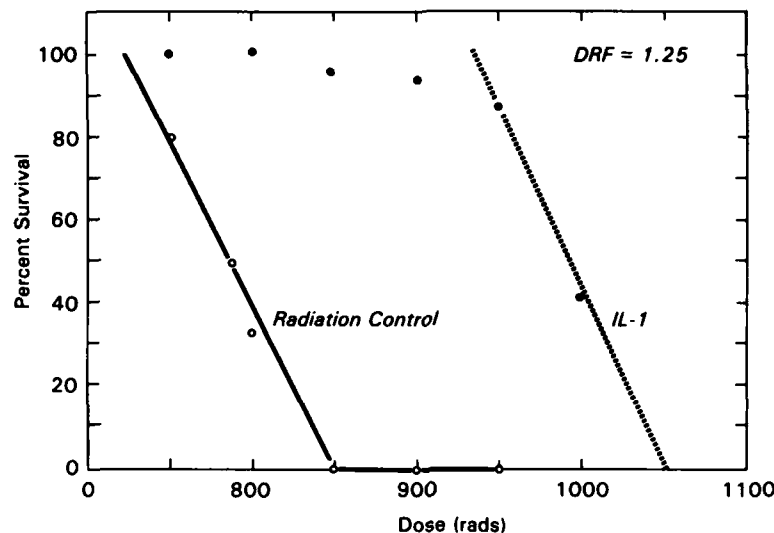


FIGURE 2 - C57BL/6 mice, 10-12 weeks old, received ip 0.1 ug of human IL-1 or control saline, 20 hr prior to irradiation. Each point represents groups of 12-16 mice. DRF was calculated from the ratio of LD50/30 of IL-1 treated to control mice.

administration at 20 hr prior to irradiation and a wide range of doses of GM-CSF, IL-2, or IFN- $\gamma$ , no significant effect on survival of LD100/30 irradiated mice was observed (Fig. 3). Similarly, administration of GM-CSF, IL-2, or IFN- $\gamma$  3 hr prior to irradiation had no effect whatsoever on survival of mice (data not shown). These results provide additional evidence against the possibility that CSF or IL-2 produced in response to IL-1 mediate its radioprotection.

TABLE 1  
**Comparison of the Effect of LPS and IL-1  
in In Vivo Induction of CSF and IFN**

|                |       | C57BL/6 |       | C <sub>3</sub> H/HeJ |       |
|----------------|-------|---------|-------|----------------------|-------|
|                |       | CSF     | IFN   | CSF                  | IFN   |
| LPS 10 $\mu$ g | 6 hr  | 3150    | 50    | .....                | ..... |
| IL-1 100 ng    | 3 hr  | 1740    | <3    | 1817                 | <3    |
|                | 6 hr  | .....   | ..... | 845                  | <3    |
|                | 24 hr | .....   | ..... | 110                  | <3    |
| Control        |       | 0       | <3    | 10                   | <3    |

TABLE 1 - Groups of C57BL/6 and C3H/HeJ mice received 100 ng IL-1 intraperitoneally. Additional group of C57BL/6 mice received ip administration of 10 ug LPS. Treated and control mice were bled at designated times, and the pools of the sera (at least 5 mice per group) were assayed for CSF and IFN.

### The Effect of Administration of Four Recombinant Cytokines IL-1, IL-2, GM-CSF, and IFN- $\gamma$ on Survival of LD<sub>100/30</sub> Irradiated Mice

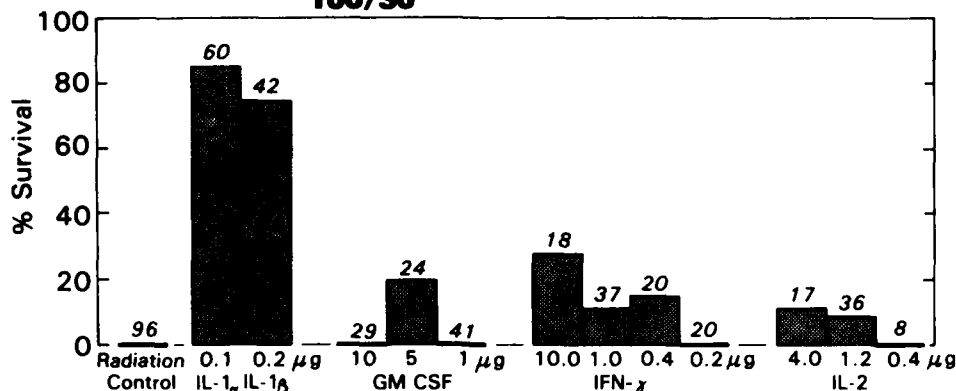


FIGURE 3 - C57BL/6 mice, 10-12 weeks old, received ip injections of cytokines, in doses as specified, 20 hours prior to irradiation. The radiation dose, 950 cGy killed 100% of control mice in 16 $\pm$ 1 days. The percent of surviving mice was calculated from 2-6 experiments each with groups of 8-10 mice. The numbers at the top of the bars indicate the total numbers of mice used for a given dose of cytokine.

#### DISCUSSION

Administration of IL-1 at 20 hr or 4 hr prior to irradiation had a significant radioprotective effect (Figs. 1,2 ). The extent of radioprotection conferred with IL-1 was similar to the radioprotection produced by inflammatory agents - LPS (2). Historically, LPS has also been a potent agent used for the induction of IL-1 *in vivo* and *in vitro*. We therefore propose that IL-1 may mediate the radioprotective activity.

Our findings permit studies of radioprotection using physiological agents, cytokines, rather than the exogenous immunomodulatory microbial agents. The lag period necessary for radioprotection with IL-1 suggests that IL-1 may only initiate the radioprotective events and not be directly radioprotective.

Administration of IL-1 initiates several systemic responses which could conceivably contribute to its radioprotective effects. These include the production of acute-phase proteins by the liver (13) of which ceruloplasmin and metallothioneins have scavenging capabilities.

IL-1 also enhances the production of a number of lymphokines, such as CSF or IL-2 and in this paper we have investigated whether this process could contribute to the radioprotective effect of IL-1. Although GM-CSF, IFN- $\gamma$  or IL-2 did not induce significant radioprotection, our experimental conditions may have not mimicked their physiological concentrations following IL-1 administration. However, the particular choice of the site of cytokine delivery (ip) and of the range of doses was justified on the basis of their documented *in vivo* effects as follows: Administration of 2 µg or 10,000 units of IL-2 ip into mice was followed for at least 4 hr by detectable IL-2 titers in circulation (14). Administration ip of radiolabeled GM-CSF was followed by detectable serum levels of radioisotope within 10 minutes. In addition, enhanced numbers of CFU-C in the marrow of mice administered 5 µg of GM-CSF provided evidence that this cytokine has systemic activity following ip administration (P. Morrisay, personal communications). Extensive experiments with *in vivo* delivery of IFN- $\gamma$  showed it to be biologically effective in ng to µg doses (15,16). Thus, at the range of doses and site of delivery used in our study, these cytokines induce systemic effects.

IFN has previously been reported to lengthen the survival of lethally irradiated mice (7). However, crude virally induced IFN was used in these studies, and the results could not be reproduced using purified IFN (17).



Similarly, we failed to observe recombinant IFN- $\gamma$  to have any significant radioprotective effect. While our experiments with IFN- $\gamma$ , GM-CSF, and IL-2 did not indicate that administration of any one of these agents alone protects significantly from radiation-induced mortality it is still possible that these agents work in concert or may be more effective at different times, in different doses, or against lower doses of irradiation.

Radioprotection by IL-1 was only effective for radiation doses causing a hematopoietic syndrome. Our previous studies have revealed that the number of nucleated cells in the bone marrow of IL-1 treated mice recovers considerably more rapidly than in irradiated control mice (18). This observation suggests that effects on bone marrow stem cells and progenitor cells should be investigated in greater detail.

#### ACKNOWLEDGEMENTS

We are grateful to Drs. W. D. Hankins, T. J. MacVittie, and J. J. Conklin for constructive reviews of this manuscript, to Mr. W. E. Jackson for statistical analysis, and to Mrs. Sonia Jones for typing the manuscript. This work was supported by the Armed Forces Radiobiology Research Institute, Defense Nuclear Agency, under Research Work Unit MJ B3148 and USUHS Protocol No. R07338 and R07364. The opinions or assertions contained herein are the private views of the authors and should not be construed as official or necessarily reflecting the views of DNA, USUHS or DoD; no endorsement by the Defense Nuclear Agency has been given or should be inferred. There is no objection to presentation or publication of this information. Research was conducted according to principles enunciated in the "Guide for the Care and Use of Laboratory Animals" prepared by the Institute of Laboratory Animal Resources, National Research Council.

#### REFERENCES

- 1.) "Radioprotectors and anticarcinogens" (1983) Nygard O. F., Simic M. G., eds. Acad. Press, New York
- 2.) BEHLING U. H., (1983) in "Beneficial effects of endotoxins" Nowotny, A. ed. Plenum Press, New York, p. 127
- 3.) ADELMAN, N. E., HAMMOND, E. M., COHEN, S., and DVORAK, M. F. (1979) IN "Biology of the Lymphokines" eds. Cohen, S. Pick, E. and Oppenheim J. J. Academic Press N.Y., p. 13
- 4.) NETA, R., DOUCHES, S. D. and OPPENHEIM, J. J. 9 (1986) J. Immunol. 136, 2483
- 5.) NETA, R., and SALVIN, S. B. (1981) Inf. Immun. 34,160
- 6.) METCALF, D., (1971) Immunology 21, 427
- 7.) KHALTOVICH, A. G., LVOVSKY, E. A., and KISELLOV, P. N. (1974) Radiobiologia 14, 356
- 8.) URBASCHEK, R., and URBASCHEK B., (1983) Inf. Immun. 35, 1488
- 9.) SMITH, K. A., LACHMAN, L. B., OPPENHEIM, J. J. and FAVOTA, M. P., (1980) J. Exp. Med. 151, 1551
- 10.) VOGEL, S. N., ENGLISH, K. E. and O'BRIEN, A. D. (1982) Inf. Immun. 38, 681
- 11.) MADONNA, G. S., and VOGEL, S. N. (1985) J. Immunol. 135, 3763
- 12.) SNEDECOR, G. W. and COCHRAN, W. G. (1980) "Statistical Methods" 7th Edition. The Iowa State University Press p. 124.
- 13.) KAMPSCHMIDT, R. F., (1984) J. Leuk. Biol. 36, 341
- 14.) CHANG, A. E., HYATT, C. L., and ROSENBERG, S. A., (1984) J. Biol. Res. Mod. 3,561
- 15.) VARELIO, L., BLASI, E., THURMAN, G. B., TALMADGE, J. E., WILTROUT, R. M. and HERBERMAN, R. B. (1984) Cancer Res. 44, 4465
- 16.) TALMADGE, J. E., HERBERMAN, R. B., CHIRIGOS, M. A. et al. (1985). J. Immunol. 135, 2483
- 17.) LVOVSKY, E., BAZE, W. B., HILMAS D. E., and LEVY, H. B. (1977). Texas Reports on Biology and Medicine 35, 388
- 18.) NETA, R., DOUCHES, S. D., and OPPENHEIM, J. J., (1986) in "Immunoregulation by Characterized Polypeptides" Proceedings of the UCLA Symposia on Molecular and Cellular Biology (in press)

## Dithiothreitol elicits epileptiform activity in CA<sub>1</sub> of the guinea pig hippocampal slice

James M. Tolliver and Terry C. Pellmar

*Department of Physiology, Armed Forces Radiobiology Research Institute, Bethesda, MD 20814-5145 (U.S.A.)*

(Accepted 27 July 1986)

**Key words:** Dithiothreitol; Epileptiform activity; Hippocampus; Sulfhydryl reagent; Radioprotectant

Dithiothreitol (DTT) is a sulfhydryl reducing agent used as a radioprotectant. Exposure of hippocampal slices for 30 min to 0.5 mM DTT irreversibly increased the orthodromic population spike amplitude, promoted repetitive firing and induced spontaneous epileptiform activity in the CA<sub>1</sub> subfield. The same concentration of the oxidized form of DTT did not increase hippocampal excitability. Although the slope of the population synaptic response to afferent stimulation (popPSP) was unchanged by DTT, the duration of the popPSP was prolonged. Recurrent inhibition was unaffected. DTT probably exerts its effects through an irreversible chemical reaction with cellular components. Possible mechanisms of DTT-induced epileptiform activity are discussed.

### INTRODUCTION

Dithiothreitol (DTT) is a sulfhydryl-reducing agent that maintains SH groups and reduces disulfide bonds<sup>10</sup>. It is frequently studied at concentrations of 0.3–2.0 mM as a radioprotectant in cellular and in enzyme systems. The predominant protective mechanism is probably the scavenging of free radicals produced by ionizing radiation<sup>15,26</sup>. DTT and other sulfhydryl-containing radioprotectants, however, have an additional protective action<sup>15,26</sup> thought to be afforded by their ability to donate hydrogen and thereby promote the repair of damaged macromolecules.

Previous studies have demonstrated several effects of DTT on the nervous system. DTT alters the response of nicotinic acetylcholine (ACh) receptors to cholinergic agonists and antagonists presumably by disrupting disulfide bonds in the ACh receptor<sup>19,21,25</sup>. The conductance and open lifetimes of channels regulated by ACh are decreased by DTT<sup>19,21</sup>. DTT, as well as other sulfhydryl-reducing agents, diminish binding of agonists to  $\beta$  adrenergic, muscarinic, dopaminergic and opiate recep-

tors<sup>14,20,22,30</sup>. DTT-induced attenuation in opiate receptor binding may account for the ability of DTT to antagonize morphine-induced analgesia<sup>22</sup>. These observations suggest that disulfide bonds play an important role in neurotransmitter receptor binding.

The present study examines the effects of the radioprotectant, DTT, on neuronal activity in the guinea pig hippocampal slice. This preparation was selected for two reasons. First, the hippocampus provides an integrated neuronal network that incorporates many of the transmitter systems, including the cholinergic, adrenergic, dopaminergic and opiate systems, known to be sensitive to sulfhydryl reducing agents (for review see ref. 11). Secondly, the hippocampus appears to be sensitive to ionizing radiation and to oxidizing agents. Exposure of animals to low doses (4–8 Gy) of ionizing radiation alters the pattern of spike activity recorded from the hippocampus *in vivo*<sup>6,12</sup>. Exposure of hippocampal slices to high doses (75–100 Gy) of ionizing radiation or to the oxidizing agent, hydrogen peroxide, decreases neuronal excitability<sup>23,24</sup>. The results of this study will allow fu-

ture investigations of the interactions of radioprotectants with the effects of ionizing radiation and with oxidizing agents.

#### MATERIALS AND METHODS

Hippocampal slices were obtained from adult, male Hartley guinea pigs (250–400 g). Under halothane anesthesia, guinea pigs were decapitated and the hippocampus was dissected free. Transverse slices (400–450  $\mu$ m thick) of the hippocampus were made using a McIlwain tissue chopper. Slices were incubated at room temperature for at least 2 h in a standard bathing medium having the following composition (mM): NaCl, 124.0; KCl, 3.0;  $\text{CaCl}_2$ , 2.4;  $\text{MgSO}_4$ , 1.3;  $\text{KH}_2\text{PO}_4$ , 1.24; glucose, 10.0 and  $\text{NaHCO}_3$ , 26.0. This solution was continuously bubbled with 95%  $\text{O}_2$  and 5%  $\text{CO}_2$ . For electrophysiological recordings, slices were placed in a submerged slice chamber<sup>33</sup>. Once in the chamber, slices were continuously superfused with standard medium equilibrated with 95%  $\text{O}_2$ –5%  $\text{CO}_2$  and maintained at  $30 \pm 1^\circ\text{C}$ . Slices were allowed an equilibration period of 40–60 min before exposure to drug. Drugs were applied to the hippocampal slice via superfusion in the standard medium for 30 min. After drug exposure, slices were again superfused with normal medium for the remainder of the experiment. Data were always collected prior to and at 60 min after initial exposure to the drugs, since at the 60-min time point, DTT-induced epileptiform activity was always evident. Both D,L-dithiothreitol (Lot 123F-0143) and *trans*-4,5 dihydroxy-1,2 dithiane (Lot 53f-5012) were obtained from the Sigma Chemical Company. Immediately prior to use, each drug was dissolved in the bathing medium to give a final appropriate concentration.

Concentric, bipolar stainless-steel electrodes were used to provide constant-current stimuli (0.0–0.5 mA, 200  $\mu$ s duration) at 0.1–2.0 Hz to hippocampal pathways. In time-response and inhibition experiments the stimulus strength (less than 0.25 mA) was initially adjusted to give a half maximum response. Antidromic potentials were elicited by stimulation of the alveus. Afferent fibers (including the Schaffer collaterals) in the stratum radiatum were stimulated to elicit the orthodromic population spike, the population postsynaptic potential (popPSP) and the af-

ferent volley.

Field potentials were recorded using micropipettes (borosilicate capillary tubing) filled with 2 M NaCl and having resistances of less than 10 M $\Omega$ . Orthodromic and antidromic field potentials were recorded through an electrode in the CA<sub>1</sub> cell body layer. In some experiments, spontaneous single-unit discharges and spontaneous synchronized field potential fluctuations were continuously monitored on a storage oscilloscope or chart recorder. A second electrode in the stratum radiatum recorded the popPSP and afferent volley. All potentials were referenced to system ground potential. The bathing solution was grounded through a chlorided silver wire in a 3 M KCl agar bridge.

All field potentials were recorded using a high-gain differential preamplifier. The potentials were digitized, stored and analyzed on a LSI 11-03 mini-computer. Amplitudes of the orthodromic and antidromic population spikes were determined as the potential difference between the peak negativity and the average of the early and late positive deflections<sup>3</sup>. The afferent volley amplitude was measured peak-to-peak. Using the computer, the slope of the popPSP was computed at the initial negative deflection. Statistical analysis of the data involved using either the analysis of variance or the Student's *t*-test. Differences were considered significant at  $P < 0.05$ . Data are expressed as the mean  $\pm$  S.E.M.

To determine possible sites of action of DTT, the following relationships were considered: afferent volley amplitude vs stimulus strength; popPSP slope vs afferent volley amplitude; orthodromic population spike amplitude vs popPSP slope; and the orthodromic population spike vs the afferent volley amplitude. To generate these 4 input-output curves, the orthodromic population spike, popPSP and afferent volley were recorded in response to stimuli of steadily increasing stimulus strength (0.0–0.5 mA) applied to the stratum radiatum at a rate of 0.2 Hz. At each stimulus strength, potentials were elicited 4 times and the signal-averaged waveforms stored on the computer. Data for the graph of the stimulus strength vs the afferent volley amplitude were computer fitted by a straight line. Data for the other 3 curves were computer fitted by an equation for a sigmoid curve. The magnitude of the afferent volley was considered to be a measure of the number of presynaptic nerve

fibers activated by the stimulus pulse. The slope of the popPSP was used to quantify the postsynaptic dendritic response to orthodromic stimulation. The size of the orthodromic population spike reflected the number of postsynaptic fibers firing in response to presynaptic stimulation.

Recurrent inhibition was examined by measuring the reduction in orthodromic population spike amplitude at selected intervals after maximal antidromic stimulation. Such stimulation activates recurrent collaterals involved in evoking recurrent inhibition. In all experiments, the stimulus strength applied to the stratum radiatum to elicit the orthodromic population spike was sufficient to evoke a population spike 40–50% of maximum amplitude. The interpulse intervals were decreased from 21 to 7 ms in increments of 2 ms. The frequency of stimulation was 0.2 Hz. At each interpulse interval, a single orthodromic population spike was evoked and stored on the computer. Recurrent inhibition was expressed as the percentage decrease in the population spike amplitude relative to the population spike amplitude evoked at an interpulse interval of 21 ms. Inhibition at an interpulse interval of 21 ms was defined as 0%. When multiple spikes appeared in the orthodromic response, only the amplitude of the first spike was used to calculate percent inhibition.

## RESULTS

DTT altered electrical activity in the CA<sub>1</sub> region of guinea pig hippocampus. DTT increased the amplitude of the orthodromic population spike and induced multiple spiking in the orthodromic field potential (Fig. 1B<sub>1</sub>). In addition, the duration of the dendritic field potential recorded in the stratum radiatum was prolonged (Fig. 1B<sub>2</sub>). An increase in spontaneously occurring synchronous and asynchronous activity was also clearly evident after DTT exposure (Fig. 2). This effect along with the alterations occurring in the orthodromic field potential indicate that DTT induces epileptiform activity in the hippocampal slice. In contrast to the effects of DTT on synaptically evoked responses, no significant effect on the antidromic response was observed.

A period of approximately 60 min after initial exposure to 0.5 mM DTT was required to fully express the epileptiform activity and the increased population spike amplitude (Fig. 3). In 3 out of 7 slices, DTT (0.5 mM) produced a transient 20–30% depression in the orthodromic spike amplitude at approximately 25–35 min after starting superfusion. At approximately 35–45 min, the baseline noise level and the orthodromic population spike began to increase in amplitude in all slices. The appearance of spontaneous

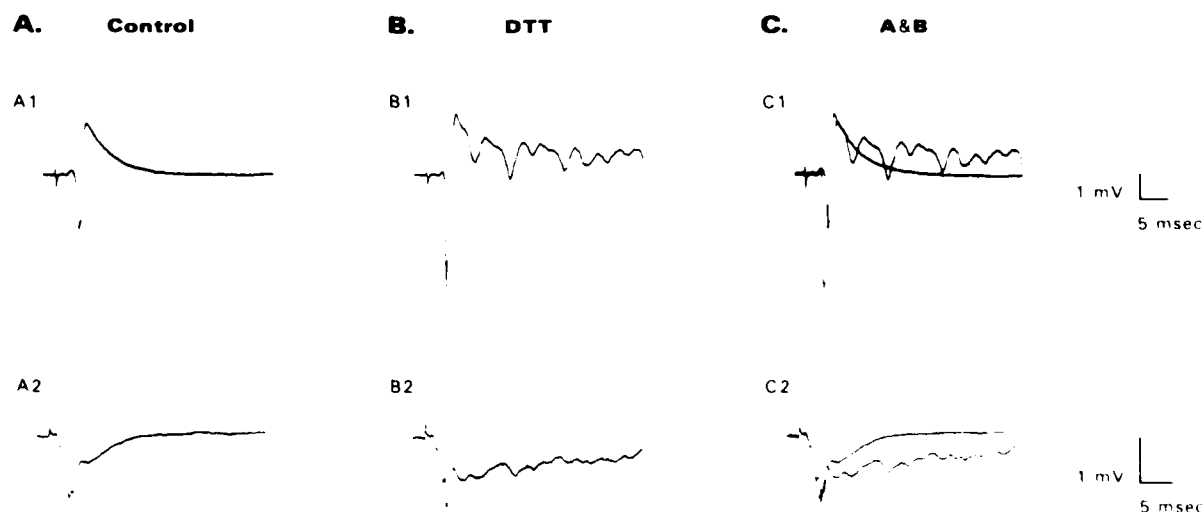


Fig. 1. Effect of DTT on the orthodromic field potential and on the popPSP. The orthodromic field potential and popPSP were recorded from the CA<sub>1</sub> cell body layer and stratum radiatum, respectively, in response to stimulation of the stratum radiatum. A: orthodromic field potential (A<sub>1</sub>) and popPSP (A<sub>2</sub>) obtained prior to starting DTT superfusion. B: orthodromic field potential (B<sub>1</sub>) and popPSP (B<sub>2</sub>) obtained at 60 min after starting a 30-min superfusion with 0.5 mM DTT. C: superimposition of A and B to accentuate the effects of DTT. DTT increased the amplitude of the orthodromic population spike and caused multiple spiking in the orthodromic field potential. In addition, DTT prolonged the popPSP without affecting the initial slope.

**A. Orthodromic Field Potential****B. Spontaneous Field Potential**

1 mV  
20 msec

Fig. 2. Effect of DTT on spontaneous electrical activity in CA<sub>1</sub>. Traces were obtained at 60 min after starting a 30-min superfusion with 0.5 mM DTT. A: DTT induced synchronized multiple spiking in the orthodromic response evoked by stimulation of the stratum radiatum. B: DTT also evoked spontaneous synchronized field potentials. The appearance of these spontaneous potentials coincided with the appearance of multiple spiking in the evoked response.

single-unit discharges (asynchronous activity) coincided with the elevation in baseline noise level. By 45–50 min, multiple spiking (4–10 spikes) was evident in the orthodromic field potential. Spontaneous synchronized fluctuations in the extracellular field potentials first appeared with the onset of synaptically evoked multiple spiking. By 60 min after beginning the 30-min exposure to 0.5 mM DTT, epileptiform activity was established and the orthodromic spike amplitude was significantly elevated (Fig. 3). Extending the observation period by an additional hour did not reveal any further alterations in the recorded electrical activity of the hippocampus. The effects of DTT were not reversed by continued washing with normal solution. Considering that the effects of DTT were fully established at 60 min, all subsequent experiments on DTT effects on input–output relationships and on recurrent inhibition were done at 1 h after beginning DTT superfusion.

Exposure of slices for 30 min to higher concentrations (0.8 mM  $n = 3$  slices and 1.0 mM  $n = 4$  slices) of DTT produced similar effects to those observed with 0.5 mM DTT. As the concentration of DTT was increased, there was a corresponding reduction in the time of onset of the elevated orthodromic spike amplitude and in the appearance of epileptiform activity. DTT at a concentration of 2 mM ( $n = 2$ ) caused only a transient period of epileptiform activity accompanied by elevated orthodromic spike amplitudes. These effects were followed, within 45–60 min after starting DTT superfusion, by the irreversible

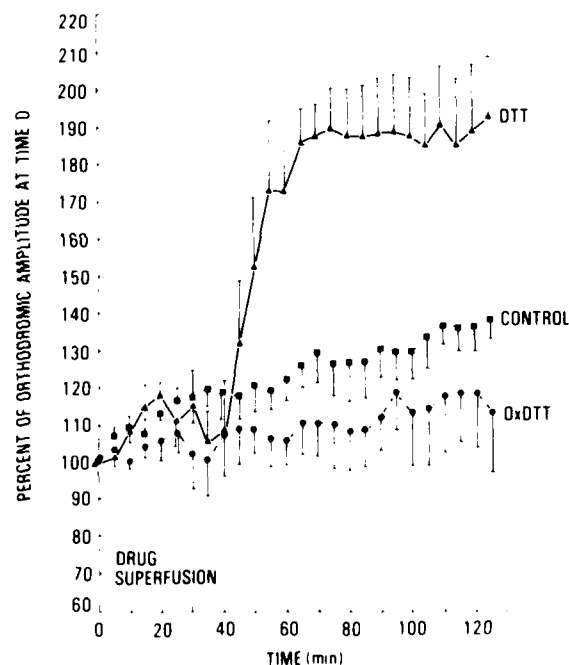


Fig. 3. Time course for the effects of 0.5 mM DTT and 0.5 mM OxDTT on the amplitude of the orthodromic population spike recorded from CA<sub>1</sub>. Slices were exposed to either drug solution for 30 min (bar in lower left corner) and then washed with normal bathing medium for the remainder of the 2-h period. For control recordings, drug solution was replaced by the normal bathing medium. Data are expressed as a percentage of the amplitude of the orthodromic population spike elicited just prior (time 0) to start of drug superfusion. Each point is the mean  $\pm$  S.E.M. for  $n = 7$  (DTT), 4 (OxDTT) and 4 (CONTROL) determinations. DTT superfusion significantly increased the orthodromic response starting at approximately 50 min. OxDTT was either without effect or slightly but insignificantly reduced the orthodromic population spike amplitude.

loss of orthodromic and antidromic population spikes. A 30-min exposure of slices to a lower concentration (0.1 mM) of DTT did not noticeably alter electrical activity in the hippocampal slice. These observations clearly show that DTT, at concentrations (0.5–2.0 mM) known to provide radiation protection and to alter the function of several receptor systems, disrupts the normal electrical activity on the hippocampus. In all subsequent experiments on input–output relationships and recurrent inhibition, the concentration of DTT used was 0.5 mM.

To determine whether DTT induces epileptiform activity by acting as a reducing agent, the effect of the oxidized form of DTT (OxDTT) on the orthodromic response was examined. No slice treated with 0.5 mM OxDTT for 30 min ( $n = 4$ ) showed enhancement of the orthodromic response during the 2-h observation period (Figs. 3 and 4). OxDTT did tend to suppress the gradual time-dependent increase in the orthodromic amplitude observed under control conditions (Fig. 3). In one slice, the orthodromic response was reduced to 10% of the control amplitude observed between 20 and 30 min after starting OxDTT superfusion; by 40 min, however, the orthodromic amplitude had returned to control levels. In contrast to DTT, OxDTT never induced multiple spiking in the orthodromic field potential (Fig. 4).

To elucidate possible sites of action of DTT, input–output curves were generated. The average input–output curves obtained from 8 slices are shown in Fig. 5. Representative examples of popPSPs with the corresponding orthodromic population spikes obtained in control and following DTT exposure are shown in Fig. 1B. Input–output curves were obtained prior to and at 1 h after beginning a 30-min superfusion with 0.5 mM DTT. At 1 h, epileptiform activity was well established. DTT superfusion caused a small but insignificant increase in the afferent volley amplitude for a given stimulus strength (Fig. 5A). DTT did significantly increase the population spike amplitude elicited for a given afferent volley amplitude or popPSP slope (Fig. 5C, D). On the average, DTT did not significantly alter the popPSP slope evoked by a given afferent volley (Fig. 5B). A more consistent effect of DTT on the popPSP is illustrated in Fig. 1B. DTT always prolonged the duration of the synaptic response. The increase in duration of the popPSP resulted from a prolongation of the decay

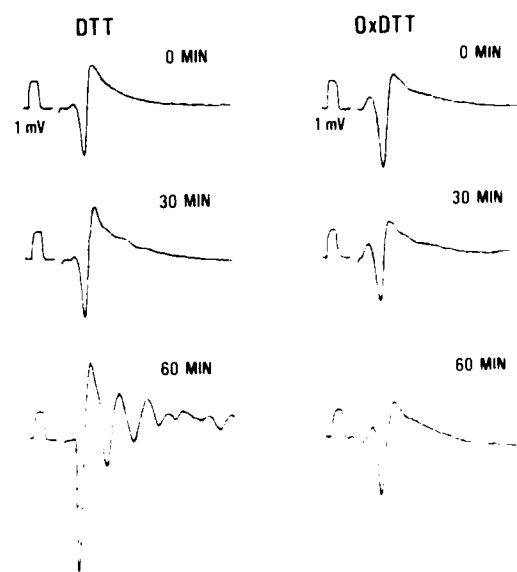


Fig. 4. Effect of OxDTT on the orthodromic field potential recorded from CA<sub>1</sub> in response to stimulation of the stratum radiatum. Potentials were recorded at the designated times (0, 30 and 60 min) after beginning a 30-min superfusion with either 0.5 mM DTT or 0.5 mM OxDTT. Each trace is the signal-averaged waveform of 4 orthodromic responses. A 1-mV calibration pulse with a 2-ms duration is present at the beginning of each trace. DTT increased the amplitude of the orthodromic spike and caused multiple spiking. In contrast, OxDTT did not alter the orthodromic response.

phase of the popPSP and not from an increase in the time to reach the maximum popPSP amplitude (Fig. 1B, C). Superfusion of control slices for 60 min with normal bathing medium did not significantly alter input–output curves or prolong the duration of the popPSP.

To test whether DTT induced an increase in activity by blocking inhibition, recurrent inhibition was examined 1 h after beginning a 30-min superfusion with 0.5 mM DTT. In all slices used to study recurrent inhibition, epileptiform activity was evident at 1 h following the start of exposure to DTT. As shown in Fig. 6, exposure to DTT did not reduce recurrent inhibition elicited at interpulse intervals of from 5 to 19 ms ( $n = 7$  slices). Superfusion of slices with normal bathing medium in the absence of drug for 1 h did not alter recurrent inhibition (data not shown).

## DISCUSSION

This study reveals that DTT increases the ortho-

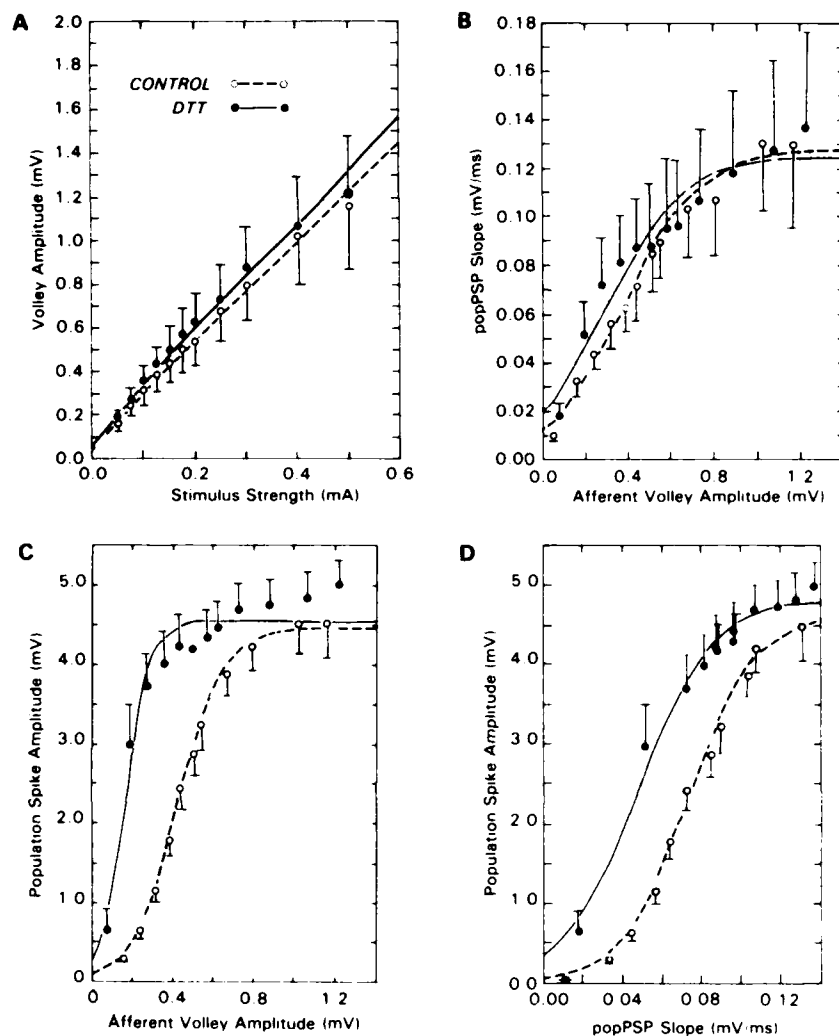


Fig. 5. Effects of DTT on input-output relationships recorded from CA<sub>1</sub>. Recordings were made prior to (CONTROL) and at 60 min after starting a 30-min superfusion with 0.5 mM DTT. Each point is the mean  $\pm$  S.E.M. for 8 slices. For graphs A-D, open circles represent control and filled circles represent DTT. A: afferent volley amplitude plotted against the stimulus strength. DTT did not significantly affect the afferent volley. B: slope of the popPSP is plotted against the afferent volley amplitude. DTT did not significantly alter the popPSP slope for a given afferent volley amplitude. C: graph of the population spike amplitude versus the afferent volley amplitude. D: graph of population spike amplitude versus the popPSP slope. DTT significantly increased the population spike amplitude evoked by a given popPSP slope or afferent volley amplitude.

dromic population spike, prolongs the popPSP and induces epileptiform activity in CA<sub>1</sub> of guinea pig hippocampal slices. These effects are produced by concentrations (0.5–1.0 mM) of DTT similar to that previously found to have radioprotective activity in cellular or enzymatic systems and to alter the function of several neurotransmitter receptors<sup>14,15,19,20,22,26,27</sup>. The effect of DTT probably results from an irreversible chemical reaction between DTT and unknown chemical components of

neurons in the hippocampus. This hypothesis is supported by 3 observations. First, the onset of the effects of DTT is slow. Secondly, the effects of DTT appear to be permanent considering that the amplitude of the orthodromic spike and the degree of epileptiform activity is not attenuated by subsequent washing of slices after DTT exposure. Third, the oxidized form of DTT does not induce epileptiform activity or increase the orthodromic spike amplitude.

DTT consistently increased the amplitude of the

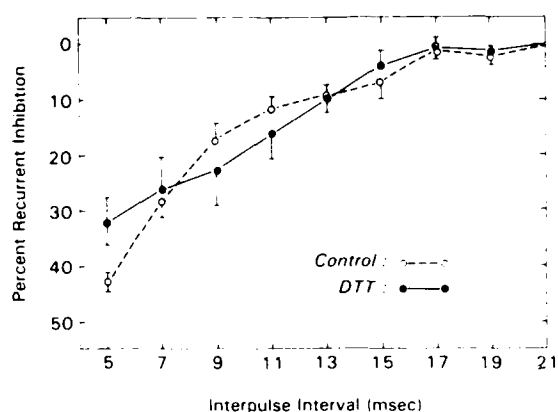


Fig. 6. DTT did not significantly reduce recurrent inhibition. Recurrent inhibition was examined by measuring the reduction in orthodromic spike amplitude at selected intervals after maximal antidromic stimulation. At interpulse intervals of 21 ms and above, recurrent inhibition was either small or undetectable; therefore, at an interpulse interval of 21 ms, the amount of recurrent inhibition was set at zero. Recurrent inhibition was measured just prior to (Control) and at 60 min after starting DTT superfusion. Open circles represent control and filled circles represent DTT, respectively. Each point is the mean  $\pm$  S.E.M. ( $n = 7$  slices).

orthodromic population spike. Previous studies indicate that the amplitude of the population spike is a function of the number of neurons firing and the degree of synchronization of neuronal firing<sup>4</sup>. The increased orthodromic population spike observed after DTT treatment suggests that DTT either increases the number of neurons activated by a given stimulus or increases the synchronization or both.

DTT induced epileptiform activity in CA<sub>1</sub> as revealed by multiple spiking in the evoked orthodromic field potential and by the appearance of spontaneous synchronized activity. Just prior to the onset of epileptiform activity, an increase in the baseline noise level was evident. This probably resulted from an increase in asynchronous single-unit discharges. Preliminary intracellular experiments have correlated the period of increased baseline noise level with an increase in the frequency of spontaneous action potentials recorded from CA<sub>1</sub> pyramidal cells (unpublished observations). In addition, the appearance of DTT-induced epileptiform activity as revealed by extracellular recordings coincides with the appearance of evoked and spontaneous bursting recorded intracellularly from CA<sub>1</sub> pyramidal cells (unpublished observations). There are at least two possible sites of origin for the spontaneous field potentials recorded

from CA<sub>1</sub>. One possibility is that the synchronized firing originates in CA<sub>1</sub>. The second possibility is that CA<sub>1</sub> pyramidal cells fire synchronously in response to synchronized input from CA<sub>2</sub> and/or CA<sub>3</sub> via the Schaffer collaterals. The latter possibility is more likely since studies have shown that CA<sub>2</sub> and CA<sub>3</sub>, but not CA<sub>1</sub>, endogenously generate synchronized field potentials<sup>28,32</sup>.

A consistent observation made in this study was that the dendritic response (popPSP) evoked a larger population spike after DTT exposure. This indicates that the intracellular excitatory postsynaptic potential (EPSP) was more efficient at eliciting an action potential. Several mechanisms that could account for this effect include the following: (1) a membrane depolarization; (2) an increase in membrane input resistance; (3) a reduction in the threshold for action potential generation; and (4) a decrease in potassium currents. Preliminary intracellular experiments demonstrate that a 30-min superfusion with 0.5 mM DTT causes a depolarization of 1–6 mV but little change in membrane resistance in CA<sub>1</sub> pyramidal cells (unpublished observation). A small membrane depolarization would bring the membrane potential closer to threshold; this effect, in turn, would result in more fibers being activated for a given stimulus. Similar results have been obtained in the frog cutaneous pectoris muscle where a 20–30-min exposure to 1.0 mM DTT also caused a small depolarization<sup>31</sup>.

DTT consistently increased the duration of the evoked popPSP. This observation suggests a prolonged period of increased dendritic excitability which could lead to evoked multiple firing of pyramidal cells and epileptiform activity. Several mechanisms can be proposed for the prolongation of the popPSP. One possible mechanism would be a blockade of the reuptake of the intrinsic excitatory neurotransmitter acting on the dendrites of CA<sub>1</sub> pyramidal cells. Although the exact identity of this transmitter is not known, evidence exists that it is an amino acid, possibly glutamate<sup>13</sup>. Since DTT causes a small blockade of  $\gamma$ -aminobutyric acid (GABA) reuptake<sup>16</sup>, it is feasible that through a similar mechanism DTT could block reuptake of the excitatory amino acids.

A second mechanism leading to a prolonged popPSP would be a loss of inhibition. This effect would unmask the EPSP and prolong the excitability



of the membrane<sup>2</sup>. In the present study, DTT did not alter recurrent inhibition evoked by antidromic stimulation. In the hippocampus, recurrent inhibition is believed to be mediated through GABAergic synapses<sup>5,8,30</sup>. The lack of effect on antidromically evoked inhibition is not surprising considering that previous studies have failed to show an effect of DTT on the GABAergic system. In *Aplysia* neurons and crab muscle, DTT has no effect on responses to GABA<sup>7,27</sup>. If anything, enhanced inhibition may be expected since DTT at a concentration of 0.5 mM slightly blocks GABA reuptake into rat synaptosomes<sup>16</sup>. The present study failed to detect any effect of DTT on recurrent inhibition; considering, however, the importance of disinhibition in the generation of epileptiform activity, future intracellular studies will further address the possible effects of DTT on inhibition in the hippocampal slice.

The increase in population spike amplitude induced by DTT was not accompanied by an increase in the slope of the popPSP. The lack of a change in the popPSP slope would indicate that DTT is not altering the initial synaptic current flow through the pyramidal cell dendrites. This, in turn, would suggest that DTT is not altering the transmitter release or dendritic membrane sensitivity to the excitatory amino

acid. To date, no effects of DTT on glutamate or other amino acid receptors in mammalian preparations have been reported. DTT does not alter the response of GH cells of the *Onchidium* oesophageal ganglia to applied L-glutamate<sup>18</sup>. Additionally, DTT at concentrations around 0.5–2.0 mM tends to decrease, not increase, the affinity of various receptors<sup>14,20,22,30</sup>.

The mechanisms by which DTT induces epileptiform activity require further investigation. We are currently pursuing this with intracellular techniques. Epileptiform activity may limit the usefulness of DTT as a radioprotective agent in the nervous system. In limited concentrations, however, DTT may reverse the decreased neuronal excitability in the hippocampus resulting from ionizing radiation and oxidizing agents such as peroxide<sup>23,24</sup>.

#### ACKNOWLEDGEMENTS

This work was supported by the Armed Forces Radiobiology Research Institute, Defense Nuclear Agency, under Research Work Unit MJ 00105. The views presented in this paper are those of the authors; no endorsement by the Defense Nuclear Agency has been given or should be inferred.

#### REFERENCES

- 1 Albuquerque, E.X., Sokoll, M.D., Sonesson, B. and Thesleff, S., Studies on the nature of the cholinergic receptor, *Eur. J. Pharmacol.*, 4 (1968) 40–46.
- 2 Alger, B.E. and Nicoll, R.A., Feedforward inhibition in rat hippocampal pyramidal cells studied in vitro, *J. Physiol. (London)*, 328 (1982) 105–123.
- 3 Alger, B.E. and Tyler, T.J., Long-term and short-term plasticity in the CA1, CA3 and dentate regions of the hippocampal slice, *Brain Research*, 110 (1976) 463–480.
- 4 Andersen, P., Bliss, T.V.P. and Skrede, K.K., Unit analysis of hippocampal population spikes, *Exp. Brain Res.*, 33 (1971) 208–221.
- 5 Andersen, P., Dingledine, R., Gjerstad, L., Langmoen, I.A. and Mosfeldt-Laursen, A., Two different responses of hippocampal pyramidal cells to application of Gamma-aminobutyric acid, *J. Physiol. (London)*, 305 (1980) 279–296.
- 6 Bassant, M.H. and Court, I., Effects of whole body gamma irradiation on the activity of rabbit hippocampal neurons, *Radiat. Res.*, 75 (1973) 109–117.
- 7 Ben-Haim, D., Landau, E.M. and Silman, I., The role of a reactive disulphide bond in the function of the acetylcholine receptor at the frog neuromuscular junction, *J. Physiol. (London)*, 234 (1973) 305–325.
- 8 Ben-Ari, Y., Krnjevic, K., Reiffenstein, R.J. and Reinhart, W., Inhibitory conductance changes and actions of GABA in the rat hippocampus, *Neuroscience*, 6 (1981) 2445–2463.
- 9 Brown, D.A. and Kwiatkowski, D., A note on the effect of dithiothreitol (DTT) on the depolarization of isolated sympathetic ganglia by carbachol and bromo-acetylcholine, *Br. J. Pharmacol.*, 56 (1976) 128–130.
- 10 Cleland, W.W., Dithiothreitol, A new protective reagent for SH groups, *Biochemistry*, 3 (1964) 480–482.
- 11 Dingledine, R., Hippocampus synaptic pharmacology, In R. Dingledine (Ed.), *Brain Slices*, Plenum Press, New York, 1984, pp. 87–112.
- 12 Gangloff, H., Hippocampal spike activity following low doses of radiation, In *Responses of the Nervous System to Ionizing Radiation*, Little, Brown and Co., Boston, 1964, pp. 374–374.
- 13 Hablitz, J.J. and Langmoen, I.A., Excitation of hippocampal pyramidal cells by glutamate in the guinea pig and rat, *J. Physiol. (London)*, 325 (1982) 317–331.
- 14 Hedlund, B. and Bartlett, L., The importance of thiol and disulfide groups in agonist and antagonist binding to the muscarinic receptor, *Mol. Pharmacol.*, 15 (1979) 531–544.
- 15 Held, K.D., Harrop, H.A. and Michael, B.D., Effects of oxygen and sulphhydryl-containing compounds on irradiated transforming DNA. I. Actions of dithiothreitol, *Int. J. Radiat. Biol.*, 40 (1981) 613–622.
- 16 Iversen, L.L. and Johnston, G.A., GABA uptake in rat central nervous system: comparison of uptake in slices and homogenates and the effects of some inhibitors, *J. Neuro-*

- chem.*, 18 (1971) 1939–1952.
- 17 Karlin, A. and Bartels, E., Effects of blocking sulphhydryl groups and of reducing disulphide bonds on the acetylcholine-activated permeability system of the electroplax. *Biochim. Biophys. Acta*, 126 (1966) 525–535.
  - 18 Kato, M., Oomura, Y. and Maruhashi, J., Effects of chemical modification on the L-glutamate receptors on the *Onchidium* neurons. *Jap. J. Physiol.*, 33 (1983) 535–546.
  - 19 Landau, E.M. and Ben-Haim, D., Acetylcholine noise: analysis after chemical modification of receptor. *Science*, 185 (1974) 944–946.
  - 20 Lucas, M., Hanoune, J. and Bockaert, J., Chemical modification of the beta adrenergic receptors coupled with adenylate cyclase by disulfide bridge-reducing agents. *Mol. Pharmacol.*, 14 (1978) 227–236.
  - 21 Lukas, R.J. and Bennett, E.L., Chemical modification and reactivity of sulfhydryls and disulfides of rat brain nicotinic-like acetylcholine receptors. *J. Biol. Chem.*, 255 (1980) 5573–5577.
  - 22 Marzullo, G. and Hine, B., Opiate receptor function may be modulated through an oxidation-reduction mechanism. *Nature (London)*, 208 (1980) 1171–1173.
  - 23 Pellmar, T.C., Electrophysiological correlates of peroxide damage in guinea pig hippocampus in vitro. *Brain Research*, 364 (1986) 377–381.
  - 24 Pellmar, T.C. and Tolliver, J.M., Effects of ionizing radiation on hippocampal excitability. *Proceedings of the Conference on Brain Slice, Fundamentals, Applications and Implications*, in press.
  - 25 Rang, H.P. and Ritter, J.M., The effects of disulphide bond reduction on the properties of cholinergic receptors in chick muscle. *Mol. Pharmacol.*, 7 (1971) 620–631.
  - 26 Redpath, J.L., Radioprotection of enzyme and bacterial systems by dithiothreitol. *Radiation Res.*, 55 (1973) 109–117.
  - 27 Sato, T., Makoto, S. and Sawada, M., Effects of disulfide bond reduction on the excitatory and inhibitory postsynaptic responses of *Aplysia* ganglion cells. *Jap. J. Physiol.*, 26 (1976) 471–485.
  - 28 Schwartzkroin, P.A. and Prince, D.A., Cellular and field potential properties of epileptogenic hippocampal slices. *Brain Research*, 147 (1978) 117–130.
  - 29 Storm-Matthesen, J. and Fonnum, F., Quantitative histochemistry of glutamate decarboxylase in the rat hippocampus region. *J. Neurochem.*, 18 (1971) 1105–1111.
  - 30 Suen, E.T., Stefanini, E. and Clement-Cormier, Y.C., Evidence for essential thiol groups and disulfide bonds in agonist and antagonist binding to the dopamine receptor. *Biochem. Biophys. Res. Commun.*, 96 (1980) 953–960.
  - 31 Terrar, D.A., Effects of dithiothreitol on end-plate currents. *J. Physiol. (London)*, 276 (1978) 403–417.
  - 32 Wong, R.K.S. and Traub, R.D., Synchronized burst discharge in disinhibited hippocampal slice. I. Initiation in CA2–CA3 region. *J. Neurophysiol.*, 49 (1983) 442–458.
  - 33 Zbicz, K.L. and Weight, F.F., Transient voltage and calcium dependent outward currents in hippocampal CA3 pyramidal neurons. *J. Neurophysiol.*, 40 (1985) 1038–1058.

NSL 04188

## Resistance of afterhyperpolarizations in hippocampal pyramidal cells to prostaglandins and vasoactive intestinal polypeptide (VIP)

Jordan E. Warnick<sup>2</sup> and Terry C. Pellmar<sup>1</sup>

<sup>1</sup>*Physiology Department, Armed Forces Radiobiology Research Institute, Bethesda, MD 20814-5145, and*

<sup>2</sup>*Department of Pharmacology and Experimental Therapeutics, University of Maryland School of Medicine, Baltimore, MD 21201 (U.S.A.)*

(Received 13 March 1986; Revised version received 19 June 1986; Accepted 30 June 1986)

**Key words:** Prostaglandin — Vasoactive intestinal polypeptide — Forskolin — Hippocampus — Histamine — 8-Bromo-cyclic adenosine monophosphate

The afterhyperpolarization (AHP) that follows repetitive stimulation was recorded intracellularly from CA<sub>1</sub> pyramidal neurons in the guinea pig hippocampal slice preparation. Although the late AHP could be blocked by histamine (1–10  $\mu$ M), forskolin (10  $\mu$ M) and 8-bromo-cyclic AMP (100 and 500  $\mu$ M), neither prostaglandins D<sub>2</sub>, E<sub>1</sub> and F<sub>2a</sub> (0.5  $\mu$ M) nor vasoactive intestinal polypeptide (0.5  $\mu$ M) had any effect on the AHP, membrane potential, membrane resistance or action potential properties.

A train of action potentials in hippocampal pyramidal cells is normally followed by an afterhyperpolarization (AHP). The duration and magnitude of the AHP is dependent upon the membrane potential and the number and frequency of action potentials in a train. The resultant AHP consists of two components: an initial fast conductance dependent upon potassium and blocked by tetraethylammonium [19]; and a late calcium-mediated potassium conductance [6, 10, 20]. The late AHP is sensitive to neurotransmitters. Both histamine and norepinephrine block the AHP by directly decreasing the calcium-mediated potassium conductance [8, 12]. The actions of histamine are specific to the calcium-mediated potassium current [15] while norepinephrine blocks both this current and the fast transient current (A-current) [17]. By decreasing the AHP, these neurotransmitters reduce spike frequency adaptation (i.e. accommodation) and increase neuronal excitability.

The activation of cyclic adenosine monophosphate (cyclic AMP) has been postulated to mediate the actions of histamine and norepinephrine on the AHP [7, 12]. Both histamine and norepinephrine increase the cyclic AMP content of the hippocampus of the rat and guinea pig [3, 4, 18, 22]. In addition, forskolin, which stimu-

*Correspondence:* T.C. Pellmar, Physiology Department, Armed Forces Radiobiology Research Institute, Bethesda, MD 20814-5145, U.S.A.

lates adenylate cyclase activity [21], and 8-bromo-cyclic AMP mimic the ability of these neurotransmitters to reduce the AHP in CA<sub>1</sub> cells of rat hippocampus [7, 12].

Among other agents that activate cyclic AMP in the hippocampal brain slice preparation are vasoactive intestinal polypeptide (VIP) and prostaglandins (PGs). VIP produces a highly significant increase in cyclic AMP levels while PGs increase cyclic AMP to a lesser, but still significant extent [4]. We hypothesized that VIP and the PGs should decrease the AHP. We found, however, that neither of these agents had a direct effect on the electrophysiological properties of hippocampal pyramidal cells of the guinea pig.

Male Hartley guinea pigs (250–500 g) were anesthetized with halothane and decapitated. The brains were removed and transverse slices of the hippocampus (350–400  $\mu$ m thick) were cut. After incubating the slices at room temperature (24–25°C) for 1 h or more, a single slice was transferred to the recording chamber. The slice was submerged in solution that flowed through the 0.5-ml chamber at a rate of 1–2 ml/min at a temperature of  $30 \pm 1^\circ\text{C}$ . The normal solution contained (mM): NaCl 124.0, KCl 3.0, CaCl<sub>2</sub> 2.4, MgSO<sub>4</sub> 1.3, KH<sub>2</sub>PO<sub>4</sub> 1.24, NaHCO<sub>3</sub> 26.0, glucose 10.0, when bubbled with 95% O<sub>2</sub>–5% CO<sub>2</sub> it had a pH of 7.4.

All intracellular recordings were made with a Dagan 8100 single electrode clamp system using the switch clamp in current clamp mode. The headstage output and unsampled (continuous) current were continually monitored to ensure appropriate adjustment of capacitance. Data were recorded on a Gould 2400 chart recorder and Ampex PR2200 tape recorder.

Intracellular electrodes (Omega Dot, Frederick Haer) were pulled from microfilament glass (1.2 mm o.d., 0.9 mm i.d.) on a Brown-Flaming micropipette puller and filled with 2 M KCl. These electrodes had resistances of 25–35 M $\Omega$  and were capable of passing  $\pm 3$  nA of current without developing offset potentials. Aided by a transient increase in capacitance feedback or a large depolarizing current pulse, neurons were impaled in the CA<sub>1</sub> area of the hippocampus. Stable recordings were made from 26 hippocampal CA<sub>1</sub> neurons. The impaled cells had membrane potentials more negative than  $-60$  mV, action potential amplitudes greater than 75 mV and membrane resistance of 25–50 M $\Omega$ .

Solutions containing PGs and forskolin were prepared by dilution from a concentrated stock solution ( $10^{-2}$  M) in DMSO that was kept frozen. In the PG and forskolin experiments, a solution containing an equivalent percentage of DMSO (up to 0.25%) was used as the control. At this concentration, DMSO had little, if any, influence on the membrane properties of CA<sub>1</sub> pyramidal cells. Solutions of VIP and 8-bromo-cyclic AMP were prepared from frozen stock solutions in distilled water. Histamine was prepared daily by adding the chemical to the normal solution. All compounds were tested in at least 3 different cells from different animals. After changing to a new solution, an equilibration period of at least 10 min was allowed before data were collected. If more than one concentration of drug was used, the lowest was applied first.

The AHP was evoked with a train of 3–6 current pulses (4 ms duration) every 8–10 ms. The amplitude of the current pulses was adjusted to consistently produce an ac-

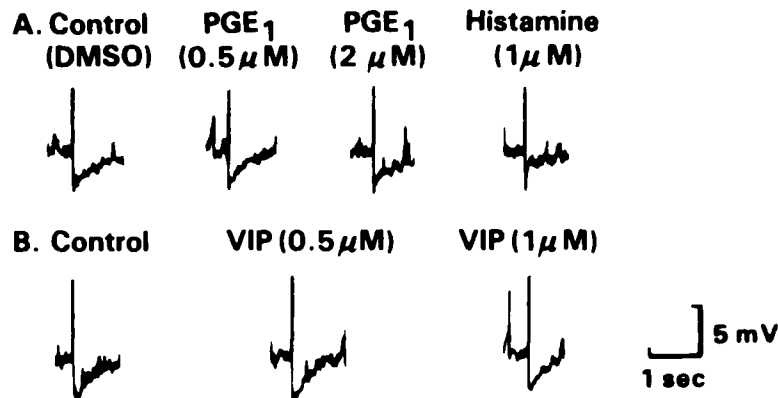


Fig. 1. Examples of the AHP at a membrane potential of  $-65$  mV evoked by 6 suprathreshold current pulses in two different hippocampal CA<sub>1</sub> neurons. A: application of  $0.5$  and  $2$   $\mu$ M PGE<sub>1</sub> for 30 min each had no effect on the AHP. DMSO was present throughout the experiment. In the same cell,  $1$   $\mu$ M histamine reduced the late phase of the AHP more than 70% after 20 min. B: the AHP was unaffected by 20 min application of  $0.5$   $\mu$ M VIP or subsequent 13 min exposure to  $1.0$   $\mu$ M VIP. Subsequent exposure of this cell to histamine (not shown) did block the late AHP. Action potentials are truncated. On this time scale, individual action potentials cannot be resolved.

tion potential from membrane potentials of  $-65$  to  $-70$  mV. Trains were evoked with a frequency of  $0.05$ – $0.1$  Hz. As reported elsewhere [6], CA<sub>1</sub> neurons displayed a characteristic initial, fast component followed by a slower, prolonged component as seen in Fig. 1. Exposure to  $0.5$   $\mu$ M PGE<sub>1</sub> produced no obvious effects on the AHP (Fig. 1), membrane potential, membrane resistance or action potential. Raising the concentration of PGE<sub>1</sub> to  $2$   $\mu$ M for 30 min was without effect (Fig. 1) but washing and subsequent exposure of the same cell to histamine ( $1$   $\mu$ M) significantly and reversibly reduced the late phase of the AHP (Fig. 1). A similar lack of effect was observed in 3 other cells exposed to  $0.5$   $\mu$ M PGE<sub>1</sub>. Likewise, neither PGD<sub>2</sub> ( $n = 5$ ), nor PGF<sub>2 $\alpha$</sub>  ( $n = 3$ ) ( $0.5$   $\mu$ M) had any direct effects on CA<sub>1</sub> cells.

While the ability of PGs to enhance cyclic AMP content of hippocampal cells is limited, this is not the case with VIP [4]. We therefore superfused VIP onto hippocampal slices during impalement of CA<sub>1</sub> neurons. In 3 cells exposed to VIP ( $0.5$   $\mu$ M), there was no apparent effect of this peptide. The results from one such cell are shown in Fig. 1B exposed to  $0.5$   $\mu$ M VIP for 20 min, followed by  $1.0$   $\mu$ M VIP for 15 min. Although VIP was ineffective at these concentrations, subsequent exposure of these cells to histamine did result in blockade of the slow AHP.

Since the previous electrophysiological studies on cyclic AMP were on rat hippocampus, we considered the possibility that a species difference might account for the negative results. Therefore, we examined the effects of forskolin ( $10$   $\mu$ M,  $n = 3$ ) and 8-bromo-cyclic AMP ( $100$   $\mu$ M,  $n = 4$ ;  $500$   $\mu$ M,  $n = 3$ ) on hippocampal pyramidal cells of the guinea pig. As found in the rat [12], forskolin and 8-bromo-cyclic AMP both blocked the AHP in guinea pig CA<sub>1</sub> pyramidal cells\*. Pyramidal cells of the guinea

\*These results contrast with those of Benardo and Prince [2] who reported that in the guinea pig, 8-bromo-cyclic AMP enhanced the AHP. We can offer no explanation for the discrepancy.

pig and rat hippocampus also respond similarly to histamine [15] and norepinephrine (T. Pellmar, unpublished observations). Likewise, PGs had no effect on the AHP on either the rat hippocampus (PGD<sub>2</sub>, R.W. Greene and H. Haas, personal communication) or, as reported here, on the guinea pig hippocampus. Species differences may occur, however, in the distribution of VIP receptors; they have been localized in the hippocampus of the rat [16] but not the cat [14].

Although VIP causes a much more significant increase in cyclic AMP levels than either histamine or norepinephrine [4], the peptide had no effect on the AHP in the present study. Similarly, the PGs increase cyclic AMP levels in hippocampal slices [4] but did not block the AHP. These results with VIP and PGs are inconsistent with the cyclic AMP-mediated mechanism postulated for norepinephrine and histamine. Although cyclic AMP may block the AHP, not all agents that increase cyclic AMP are effective. It is possible that VIP and PGs do not actually increase the cyclic nucleotide in CA<sub>1</sub> pyramidal cells but rather have their effect in other neurons or glia of the hippocampus. Alternatively, compartmentalization may occur within the neuron. Under these conditions, the cyclic AMP produced by VIP and PGs might not be at the proper location to affect the AHP.

Our results in the hippocampus differ from those reported for the nodose ganglion [5] and the superior cervical ganglion [13] of the rabbit where PGE<sub>1</sub> blocked the calcium-dependent AHP. The mechanism underlying this effect is uncertain. Because PGE<sub>1</sub> also blocked other calcium-dependent responses including the calcium action potential, Mo et al. [13] suggested a direct effect on calcium influx. On the other hand, Fowler et al. [5] found a selective effect on one of two calcium-mediated events indicating that the PG is blocking a transduction mechanism rather than calcium influx.

Effects of PGs on synaptic responses have also been reported. Some investigators [1, 9, 23] found a decrease in presynaptic release but not postsynaptic sensitivity to neurotransmitter [1], perhaps as a consequence of decreased presynaptic calcium conductance [13]. In contrast, others [11] have observed potentiation of the response of cerebellar Purkinje cells to iontophoretic application of GABA and glutamate, suggesting postsynaptic modulation of the transmitter responses. The absence of direct effects in the present experiments do not rule out the potential for other PG effects in the hippocampus. This possibility deserves further investigation.

- 1 Belluzzi, O., Biondi, C., Borasio, P.G., Capuzzo, A., Ferretti, M.E., Trevisani, A. and Perri, V., Electrophysiological evidence for a PGE-mediated presynaptic control of acetylcholine output in the guinea-pig superior cervical ganglion, *Brain Res.*, 236 (1982) 383-391.
- 2 Benardo, L.S. and Prince, D.A., Dopamine action on hippocampal pyramidal cells, *J. Neurosci.*, 2 (1982) 415-423.
- 3 Chasin, M., Mamrak, F., Samaniego, S.G. and Hess, S.M., Characteristics of the catecholamine and histamine receptor sites mediating accumulation of cyclic adenosine 3':5'-monophosphate in guinea-pig brain, *J. Neurochem.*, 21 (1973) 1415-1427.
- 4 Etgen, A.M. and Browning, E.T., Activities of adenosine 3':5'-monophosphate accumulation in rat hippocampal slices: action of vasoactive intestinal polypeptide (VIP), *J. Neurosci.*, 3 (1983) 2487-2493.
- 5 Fowler, J.C., Greene, R.W. and Weinreich, D., Two calcium-sensitive spike after-hyperpolarizations in visceral sensory neurones of the rabbit, *J. Physiol. (London)*, 365 (1985) 59-75.

- 6 Gustafsson, B. and Wigstrom, H., Evidence for two types of afterhyperpolarization in CA1 pyramidal cells in the hippocampus, *Brain Res.*, 206 (1981) 462-468.
- 7 Haas, H.L., Histamine may act through cyclic AMP on hippocampal neurones, *Agents Actions*, 16 (1985) 234-235.
- 8 Haas, H.L. and Konnerth, A., Histamine and noradrenaline decrease calcium-activated potassium conductance in hippocampal pyramidal cells, *Nature (London)*, 302 (1983) 432-434.
- 9 Hedqvist, P., Autonomic neurotransmission. In P.W. Ramwell (Ed.), Vol. I, *The Prostaglandins*, Plenum Press, New York, 1973, pp. 101-131.
- 10 Hotson, J.R. and Prince, D.R., A calcium-activated hyperpolarization follows repetitive firing in hippocampal neurons, *J. Neurophysiol.*, 43 (1980) 409-419.
- 11 Kimura, H., Okamoto, K. and Sakai, Y., Modulatory effects of Prostaglandin D<sub>2</sub>, E<sub>2</sub>, and F<sub>2</sub> on the postsynaptic actions of inhibitory and excitatory amino acids in cerebellar Purkinje cell dendrites in vitro, *Brain Res.*, 330 (1985) 235-244.
- 12 Madison, D.V. and Nicoll, R.A., Noradrenaline blocks accommodation of pyramidal cell discharge in the hippocampus, *Nature (London)*, 299 (1982) 636-638.
- 13 Mo, N., Ammari, R. and Dun, N.J., Prostaglandin E<sub>1</sub> inhibits calcium-dependent potentials in mammalian sympathetic neurons, *Brain Res.*, 334 (1985) 325-329.
- 14 Obata-Tsuto, H.L., Okamura, H., Tsuto, T., Terubayashi, H., Fukui, K., Yanaihara, N. and Ibata, Y., *Distribution of the VIP-like immunoreactive neurons in the cat central nervous system*, *Brain Res. Bull.*, 10 (1983) 653-660.
- 15 Pellmar, T.C., Histamine decreases calcium-mediated potassium current in guinea pig hippocampal CA1 pyramidal cells, *J. Neurophysiol.*, 55 (1986) 727-738.
- 16 Roberts, G.W., Woodhams, P.L., Polak, J.M. and Crow, T.J., Distribution of neuropeptides in the limbic system of the rat: the hippocampus, *Neuroscience*, 11 (1984) 35-77.
- 17 Sah, P., French, C.R. and Gage, P.W., Effects of noradrenaline on some potassium currents in CA1 neurones in rat hippocampal slices, *Neurosci. Lett.*, 60 (1985) 295-300.
- 18 Schwartz, J.C., Histaminergic mechanisms in brain, *Annu. Rev. Pharmacol. Toxicol.*, 17 (1977) 325-339.
- 19 Schwartzkroin, P.A. and Prince, D.A., Effects of TEA on hippocampal neurons, *Brain Res.*, 185 (1980) 169-181.
- 20 Schwartzkroin, P.A. and Stafstrom, C.E., Effects of EGTA on the calcium activated afterhyperpolarization in hippocampal CA3 pyramidal cells, *Science*, 210 (1980) 1125-1126.
- 21 Seamon, K.B., Padgett, W. and Daly, J.W., Forskolin: unique diterpene activator of adenylate cyclase in membrane and intact cells, *Proc. Natl. Acad. Sci. USA*, 78 (1981) 3363-3367.
- 22 Segal, M., Greenberger, V. and Hofstein, R., Cyclic AMP-generating systems in rat hippocampal slices, *Brain Res.*, 213 (1981) 351-364.
- 23 Starke, K., Regulation of noradrenaline release by presynaptic receptor systems, *Rev. Physiol. Biochem. Pharmacol.*, 7 (1977) 1-124.

# Kinetic Flow Dichroism Study of Conformational Changes in Supercoiled DNA Induced by Ethidium Bromide and Noncovalent and Covalent Binding of Benzo[a]pyrene Diol Epoxide<sup>†</sup>

Hiroko Yoshida and Charles E. Swenberg\*

Department of Radiation Sciences, Division of Physical Radiobiology, Armed Forces Radiobiology Research Institute, Bethesda, Maryland 20814

Nicholas E. Geacintov

Chemistry Department, New York University, New York, New York 10003

Received August 7, 1986; Revised Manuscript Received November 14, 1986

ARMED FORCES RADIOBIOLOGY  
RESEARCH INSTITUTE  
SCIENTIFIC REPORT  
**SR87-9**

**ABSTRACT:** The dynamic conformational changes due to the noncovalent intercalative binding of ethidium bromide and racemic *trans*-7,8-dihydroxy-*anti*-9,10-epoxy-7,8,9,10-tetrahydrobenzo[a]pyrene (BPDE), and the covalent binding of BPDE to supercoiled  $\phi$ X174 DNA, have been studied by gel electrophoresis and a novel application of a kinetic flow linear dichroism technique. The magnitude of the linear dichroism ( $\Delta A$ ) of the DNA oriented in the flow gradient is sensitive to the hydrodynamic shape of the DNA molecule which is affected by the binding of the drug or the carcinogen BPDE. While the linear dichroism of ethidium bromide supercoiled DNA is time independent, the  $\Delta A$  spectra of BPDE-DNA reaction mixtures vary on time scales of minutes, which correspond to the reaction rate constant of BPDE to form 7,8,9,10-tetrahydroxytetrahydrobenzo[a]pyrene hydrolysis products and covalent DNA adducts. The rapid noncovalent intercalation of BPDE causes an initial large increase in  $\Delta A$  (up to 250%, corresponding to the dichroism observed with relaxed circular DNA), followed by a slower decrease in the linear dichroism signal. This decrease in  $\Delta A$  is attributed to the removal of intercalated diol epoxide molecules and the resulting reversible increase in the number of superhelical turns. The kinetic flow dichroism spectra indicate that the noncovalent BPDE-DNA complexes are intercalative in nature, while the covalent adducts are characterized by a very different conformation in which the long axes of the pyrenyl residues are oriented at a large angle with respect to the average orientation of the planes of the DNA bases. These results suggest that conformations of carcinogen-DNA adducts, other than intercalative ones, can cause the unwinding of superhelical DNA. The flow dichroism method is capable of following kinetically changes not only in the shapes, and thus conformations of supercoiled DNA molecules, but also in the conformations of drugs or carcinogens causing these changes.

The polycyclic aromatic hydrocarbon benzo[a]pyrene, a known environmental pollutant, is metabolically converted in living cells to a variety of oxygenated derivatives (Gelboin, 1978; Singer & Grunberger, 1983; Conney, 1982; Harvey, 1981). The diol epoxide *trans*-7,8-dihydroxy-*anti*-9,10-epoxy-7,8,9,10-tetrahydrobenzo[a]pyrene (BPDE)<sup>1</sup> is known to be the ultimate mutagenic and tumorigenic metabolite of benzo[a]pyrene. It is widely believed that the covalent binding of BPDE to DNA plays an important role in the initiation of the carcinogenic process and in mutagenesis (Singer & Grunberger, 1983; Brookes & Osborne, 1982). The primary covalent adduct formed involves the 10-position of BPDE and the exocyclic amino group of guanine (Osborne et al., 1976; Weinstein et al., 1976; Meehan et al., 1977; Koreeda et al., 1978). Other minor adducts have also been identified (King et al., 1976; Jeffrey et al., 1977; Osborne et al., 1981).

There are striking differences in the biological activities of the different stereoisomers of BPDE (Conney, 1982) which have been, at least in part, attributed to differences in the spatial orientation of the covalently bound pyrenyl aromatic

ring system (Brookes & Osborne, 1982). Such differences have indeed been found experimentally by utilizing linear dichroism techniques (Geacintov et al., 1984a,b; Jernstrom et al., 1984; Undeman et al., 1983; Shahbaz et al., 1986). Generally, two types of conformations have been identified; type I involves an intercalative binding mode in which the aromatic pyrene residue tends to be oriented parallel to the planes of the bases, while in type II binding the plane of the aromatic residue tends to be tilted away from the planes of the bases (Geacintov et al., 1982a, 1985). The reaction mechanism of the tumorigenic (+) isomer of BPDE with double-stranded DNA in aqueous solution involves first a rapid noncovalent intercalation (site I binding) followed by a slower covalent binding step in which the pyrene residue undergoes reorientation to a type II binding site (Geacintov et al., 1984a). However, covalent binding constitutes a minor reaction pathway since, typically, about 90% of the BPDE molecules are hydrolyzed to tetraols.

On the basis of the effect of BPDE on the superhelicity of supercoiled DNA, other models describing the conformations of covalent BPDE-DNA adducts have been proposed. Drinkwater et al. (1978) and Kakefuda and Yamamoto (1978)

<sup>†</sup>H.Y. is a National Research Council Research Associate. The portion of this work performed at New York University was supported by Grant CA-20851, awarded by the National Cancer Institute, Department of Health and Human Services, and by Grant DE-FG02-86ER60405 and Contract DE-AC02-78EV04959 from the U.S. Department of Energy.

<sup>1</sup> Abbreviations: BPDE, *trans*-7,8-dihydroxy-*anti*-9,10-epoxy-7,8,9,10-tetrahydrobenzo[a]pyrene; tetraol, 7,8,9,10-tetrahydroxytetrahydrobenzo[a]pyrene; EDTA, ethylenediaminetetraacetic acid; Tris, tris(hydroxymethyl)aminomethane; THF, tetrahydrofuran.



found that the covalent binding of BPDE to SV40 DNA causes an unwinding of supercoiled DNA. Since these changes are similar to those produced by the intercalating agent ethidium bromide, a model of covalent intercalative binding for the BPDE-DNA adducts was suggested (Drinkwater et al., 1978). A similar conclusion was reached by Agarwal et al. (1983) based on their observations that BPDE causes a rapid positive supercoiling of relaxed circular pBR322 DNA; however, it is not totally clear whether the observed effects in the work of Agarwal et al. (1983) were due to the noncovalent intercalation or to the covalent binding of BPDE. Meehan et al. (1982) observed that the noncovalent intercalation of BPDE causes an unwinding of SV40 DNA, but not as effectively as in the case of ethidium bromide. The results of Gamper et al. (1980), also obtained with SV40 DNA, are consistent with the formation of a noncovalent intercalative BPDE-DNA complex prior to the formation of the covalent adducts (Meehan & Straub, 1979; Geacintov et al., 1981; MacLeod & Selkirk, 1982). However, Gamper et al. (1980) concluded that the unwinding associated with the covalent alkylation of DNA is also consistent with an external binding mode, as suggested by the linear dichroism experiments of Geacintov et al. (1978). The increased mobility of covalent BPDE-nicked circular DNA adducts on agarose gels was attributed to the existence of flexible "hinges" at the covalent alkylation sites (Gamper et al., 1980). On the basis of linear dichroism and other data, a wedge-shaped covalent intercalation model was proposed for linear DNA covalently modified with BPDE (Hogan et al., 1981; Taylor et al., 1983); however, alternate interpretations of these and other experimental data have been discussed (Geacintov et al., 1985; MacLeod & Tang, 1985).

In order to help resolve these discrepancies, we introduce here a new application of flow dichroism techniques which constitutes a first attempt to measure changes in the conformational states of supercoiled DNA kinetically, on the time scale of seconds, produced by the interaction of the carcinogen BPDE with RF I  $\phi$ X174 DNA. Utilizing the intercalator ethidium bromide, we have found that the linear dichroism signal within the DNA absorption band is remarkably sensitive to the extent of supercoiling and parallels the well-known behavior of the sedimentation coefficient (Waring, 1970). Because the linear dichroism technique is especially useful for following the kinetics of the changes in the supercoiled state of DNA qualitatively, the effects of the rapid noncovalent intercalation of BPDE can be distinguished from the slower effects produced by the covalent binding of this diol epoxide to DNA.

#### MATERIALS AND METHODS

The  $\phi$ X174 DNA dissolved in 5 mM Tris buffer at pH 7.4, and containing 1 mM EDTA, was obtained from Bethesda Research Laboratories (Bethesda, MD); utilizing agarose gel electrophoresis, it was determined that the initial content of supercoiled RF I DNA was at least 65–70%. Racemic BPDE was obtained from the National Cancer Institute Chemical Carcinogen Reference Standard Repository, and stock solutions (3%) were prepared in THF. Nicked circular  $\phi$ X174 DNA was prepared by exposing the supercoiled DNA solutions to  $^{60}\text{Co}$   $\gamma$  irradiation (total dose of 400 Gy); agarose gel electrophoresis indicated that the concentration of supercoiled DNA in these irradiated solutions was negligible, while approximately 20% of the DNA was in the linear form. Calf thymus DNA (type I, Sigma Chemical Co., St. Louis, MO), dissolved in 5 mM Tris, 3 mM EDTA, and 0.1 M NaCl solution, was sonicated with a Heat Systems-Ultrasonics, Inc. (Plainview, NY) sonicator for a total time of 30 min (5-min

periods interspersed with 5-min rest periods) under an atmosphere of nitrogen at 0 °C. After extensive dialysis against a 5 mM Tris and 1 mM EDTA solution, the sonicated DNA was subjected to polyacrylamide gel electrophoresis, and the chain length was found to be  $800 \pm 300$  base pairs.

Small aliquots of the BPDE-THF stock solutions were added to the aqueous DNA solutions, and the concentration of THF was always less than 1%. The concentration of BPDE was determined by utilizing an extinction coefficient of  $29\,000\text{ M}^{-1}\text{ cm}^{-1}$  at 344 nm. Only samples of BPDE containing less than 10% of the hydrolysis products (tetraols) were utilized. The concentration of the ethidium bromide (Sigma Chemical Co.) was determined by absorption spectrophotometry using an extinction coefficient of  $5800\text{ M}^{-1}\text{ cm}^{-1}$  at 480 nm in buffer solution and  $4800\text{ M}^{-1}\text{ cm}^{-1}$  for the DNA complexes (absorption maximum at 520 nm).

Electrophoresis on agarose gels (1% by weight) was performed by utilizing vertical slabs and TEA electrophoresis buffer (40 mM Tris, 1 mM EDTA, and 5 mM sodium acetate solution, pH 8.2) at 17 °C. Mixtures representing 20  $\mu\text{L}$  of the DNA sample and 5  $\mu\text{L}$  of a bromophenol-ficol solution were loaded onto the gels, and electrophoresis was performed at 40 V for 12 h in the absence of light. The gels were then placed in TEA buffer containing ethidium bromide (1  $\mu\text{g}/\text{mL}$ ) for staining for 1 h. After being stained, the gels were photographed in UV light. The negatives were then analyzed, and the relative optical densities as a function of migration distance were determined by utilizing a P1000 photoscanner (Optronics International, Inc., Chelmsford, MA) and a digitizer interfaced to a computer.

The flow linear dichroism experiments were performed as described previously (Geacintov et al., 1984a) utilizing a Couette cell. The latter consists of two concentric quartz cylinders, a stationary outer cylinder, and a rotating inner cylinder (400–600 rpm). The diameter of the outer cylinder is about 26 mm, and the aqueous DNA solution is contained in the 0.6-mm annular space. As the inner cylinder is rotated, the DNA molecules tend to align along the flow lines so that the planes of the bases are tilted partially in a vertical direction with respect to the flow lines. The linear dichroism is defined by

$$\Delta A = A_{\parallel} - A_{\perp} \quad (1)$$

where  $A_{\parallel}$  and  $A_{\perp}$  are the absorbances of the solutions measured with the polarization vector of the light beam oriented either parallel or perpendicular to the direction of the flow. This flow linear dichroism system requires a sample volume of 1 mL and is capable of following changes in the linear dichroism signals with a time resolution of about 100 ms with a reasonable signal/noise ratio, as long as the DNA concentration is at least 10  $\mu\text{g}/\text{mL}$ . In this work, DNA concentrations of 30  $\mu\text{g}/\text{mL}$  were utilized. In general,  $\Delta A$  is determined as a function of wavelength. Thus, the orientations of non-covalently or covalently bound carcinogen and drug molecules relative to those of the DNA bases can be determined. Because the planes of the bases in linear DNA tend to be tilted perpendicular to the flow lines, the  $\Delta A$  signal within the DNA absorption band (below 300 nm) is negative in sign. Intercalated planar molecules also display negative  $\Delta A$  values within their absorption bands, while molecules whose planes tend to be oriented vertically with respect to the planes of the DNA bases are characterized by positive  $\Delta A$  values.

#### RESULTS

*Incubation with BPDE and Levels of Covalent Binding.* In all experiments, the DNA concentration was  $7.6 \times 10^{-5}\text{ M}$

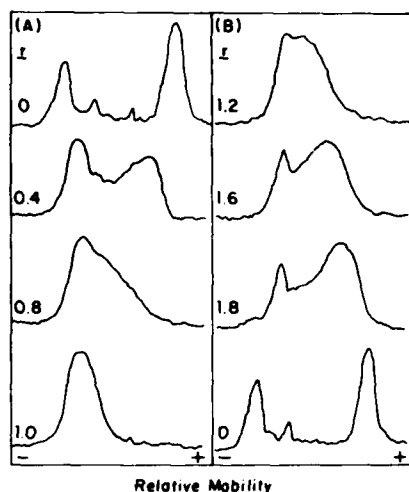


FIGURE 1: Microdensitometry traces of agarose gels of covalent BPDE- $\phi$ X174 adducts prepared at different reaction ratios,  $r$  (initial moles of BPDE per mole of nucleotides). The reaction mixtures ( $7.6 \times 10^{-5}$  M DNA, 5 mM Tris buffer, and 1 mM EDTA, pH 7.8) were incubated for 2 h at the indicated values of  $r$  and then electrophoresed for 12 h at 40 V, 17 °C, in the absence of light.

(expressed in terms of the concentration of nucleotides). The incubations were carried out at 25 °C and at different molar reaction ratios,  $r$  (initial moles of BPDE per mole of DNA). The reactions reached completion after about 10 min, and the level of covalent binding of the diol epoxide was determined spectrophotometrically after the tetraol hydrolysis products were extracted with ether (Geacintov et al., 1980; Yoshida, 1984). At molar ratios of  $r = 0.1, 0.2, 0.6$ , and  $1.8$ , the level of covalent binding corresponded to molar binding ratios,  $r_b$  (generally defined as moles of drug or carcinogens bound to the DNA per mole of nucleotides), of  $0.005, 0.007, 0.01$ , and  $0.015$ , respectively. These ratios translate to  $28, 38, 52$ , and  $82$  BPDE molecules per molecule to  $\phi$ X174 DNA, respectively.

**Gel Electrophoresis.** Some typical densitomer traces of  $\phi$ X174 DNA incubated with various amounts of BPDE are shown in Figure 1. The top trace in Figure 1A (and the bottom trace in Figure 1B) represents the electrophoretic gel patterns of DNA samples without addition of BPDE. The high-mobility band is due to the supercoiled RF I form, while the low mobility band is attributed to relaxed closed circular RF II DNA, which was present in varying amounts in the original DNA samples, depending on the batch furnished by the supplier.

The  $r = 0.4$  and other traces show the effects of covalent binding of BPDE to DNA and are consistent with the results of Drinkwater et al. (1978) and Gamper et al. (1980). The  $r = 0.4$  trace shows that the mobility of RF II DNA is increased, probably because of increased flexibility of the DNA at the alkylation sites as proposed by Gamper et al. (1980). The mobility of the RF I DNA decreases upon modification with BPDE which is attributed to a loss in superhelicity resulting from a local unwinding of the DNA superhelix as discussed by Drinkwater et al. (1978). The broadening of the RF I band for  $r = 0.4$  is presumably due to the heterogeneity in the number and spatial location of covalently bound BPDE molecules per DNA molecule, and the resulting heterogeneity in the superhelicity of the DNA. At  $r = 1.0$ , only one peak is apparent which suggests that the BPDE-modified RF I and RF II forms have equivalent mobilities and thus comigrate. Another possible interpretation is that the supercoiled DNA is converted to the RF II form by the introduction of at least

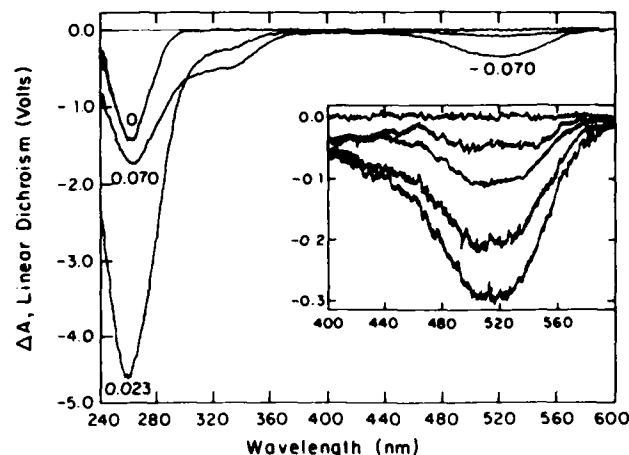


FIGURE 2: Flow linear dichroism spectra of supercoiled DNA and of ethidium bromide- $\phi$ X174 complexes at different ratios,  $r_b$  (moles of drug bound per mole of DNA nucleotides). The inset represents expanded dichroism spectra in the region of the visible absorption band of ethidium bromide; the  $r_b$  values are (from the top to the bottom trace)  $0.00, 0.010, 0.023, 0.050$ , and  $0.070$ . The vertical  $\Delta A$  signal is expressed in volts (output of the lock-in amplifier).

one single-strand break due to the binding of BPDE. However, this interpretation seems unlikely since at higher initial BPDE concentrations ( $r > 1.2$ ) a broadened, higher mobility band reappears, while the low-mobility peak attributed to the relaxed circular form appears to remain nearly stationary (Figure 1B). At the molar reaction ratio  $r = 1.8$ , the leading edge of the fastest band has a mobility which is almost comparable to that of the unmodified RF I form. Such an effect was also observed by Drinkwater et al. (1978). The increased electrophoretic mobility at high  $r$  values is attributed to a rewinding (in the opposite sense) of the modified supercoiled DNA at high concentrations of the covalently bound carcinogen. This effect appears to be analogous to the unwinding and rewinding effects induced by increasing concentrations of ethidium bromide (Waring, 1970).

**Flow Linear Dichroism.** (A) *Ethidium Bromide-DNA Complexes.* We first investigated whether the flow dichroism technique was capable of revealing changes in the superhelicity of  $\phi$ X174 DNA induced by the well-known intercalator ethidium bromide. Some typical linear dichroism spectra obtained at different  $r_b$  (=moles of ethidium bromide bound per mole of DNA) values are shown in Figure 2. The linear dichroism at  $500\text{--}520$  nm due to the drug molecule is negative in sign, as expected for an intercalative mode of binding, and increases with increasing ethidium concentration. However, within the absorption band of DNA below  $300$  nm, the dependence of  $\Delta A$  on  $r_b$  is quite different. The negative dichroism increases in magnitude as the drug concentration is increased from zero to  $r_b \approx 0.023$  and remains constant up to  $r_b = 0.04$ . At these values of  $r_b$ , the magnitude of the dichroism at  $260$  nm is higher by the remarkably large factor of  $3.5$ . Above this concentration of ethidium, the magnitude of the dichroism decreases with increasing  $r_b$  until a constant value, approximately equal to the original  $r_b = 0$  value, is reached (Figure 3). In contrast to the behavior of supercoiled DNA, the linear dichroism signal of linear DNA at  $260$  nm increases monotonically as the ethidium bromide concentration is increased (Figure 3).

These results suggest that the changes in superhelicity are accompanied by changes in the hydrodynamic shapes of the DNA molecules which are detectable by the flow linear dichroism technique. The more compact, highly supercoiled RF I DNA is characterized by a lower overall dichroism; this

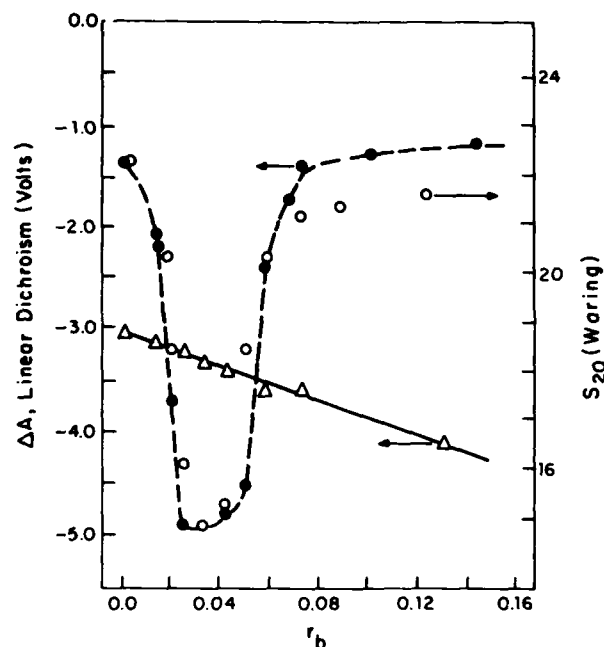


FIGURE 3: Flow linear dichroism signals measured within the DNA absorption band at 260 nm at different ethidium bromide concentrations expressed in terms of the molar binding ratio  $r_b$ , and constant  $\phi$ X174 DNA ( $\bullet$ ) or linear calf thymus DNA ( $\Delta$ ) concentration ( $7.6 \times 10^{-5}$  M). The open circles (O) represent the sedimentation coefficients,  $s_{20}$ , determined by Waring (1970) and superimposed on the  $\Delta A$  data.

indicates either (1) an average lower degree of orientation of the DNA molecule in the flow gradient or (2) a lower average degree of orientation of the bases perpendicular to the flow lines, or both.

There is a remarkable correlation between the magnitude of the linear dichroism signal at 260 nm, and the sedimentation coefficient ( $s_{20}$ ) determined by Waring (1970), as a function of increasing ethidium bromide concentration. These data are compared to one another in Figure 3. It is evident that the flow linear dichroism results provide data which are similar to those obtained by the sedimentation method, except with the following advantages: the relative orientations of the polycyclic molecules and the DNA bases can be determined simultaneously, and changes in the superhelicity of the DNA molecule can be followed kinetically with a time resolution as high as 100 ms at a particular fixed wavelength.

As in the case of the sedimentation data (Waring, 1970), the ethidium bromide concentration-dependent changes in the linear dichroism are interpreted in terms of the following: (1) as the drug concentration is increased from  $r_b = 0$  to  $r_b = 0.023$ , the negatively supercoiled DNA unwinds and reaches a minimum (closed circular DNA) and the magnitude of the dichroism increases; (2) as  $r_b$  is increased still further, the formation of a positively supercoiled helix results in a more compact and twisted DNA molecule characterized by a lower dichroism.

**(B) BPDE-DNA Reaction Mixtures.** The flow linear dichroism spectra of a RF I DNA solution taken just prior to the addition of BPDE, and at two different time intervals after the addition of BPDE ( $r \approx 0.1$ ), are depicted in Figure 4. Before addition of BPDE, the highest linear dichroism signal is observed at 258 nm, as expected, since the magnitude of the dichroism is proportional to the absorption spectrum within a homogeneous absorption band (Frederick & Houssier, 1972).

When BPDE is added to a DNA solution, the BPDE binds noncovalently to the DNA by an intercalation mechanism

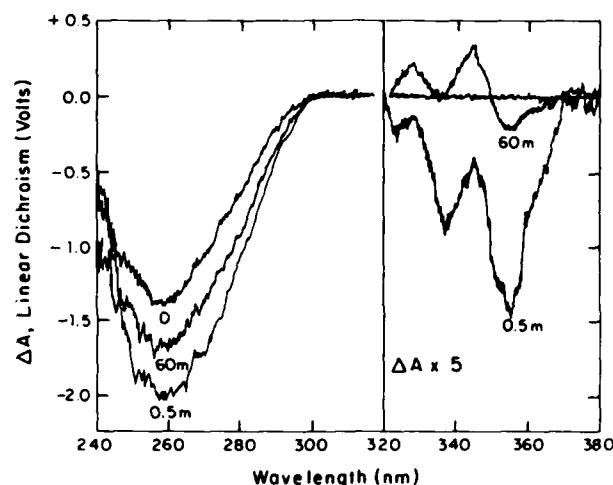


FIGURE 4: Linear dichroism spectra of reaction mixtures containing BPDE ( $8.3 \times 10^{-6}$  M) and  $\phi$ X174 DNA ( $7.6 \times 10^{-5}$  M) measured 0.5 and 60 min after mixing. The initial spectrum is characteristic of noncovalently intercalated BPDE molecules, while the final spectrum is characteristic of mostly covalent adducts (see text). The linear dichroism of the DNA sample before addition of BPDE is also shown.

within several milliseconds (Geacintov et al., 1981). The negative linear dichroism spectrum in the 320–370-nm region is attributed to the intercalated pyrenyl chromophore of BPDE (Geacintov et al., 1984a). On the time scale of minutes, over 90% of the BPDE molecules are converted to tetraols, while less than 10% are converted to adducts bound covalently to DNA (Yoshida, 1984). After a 10-min reaction time, the linear dichroism spectrum can be attributed solely to covalent adducts and intercalated tetraol molecules. The noncovalent association constant  $K$  of the tetraols is lower than that of BPDE by a factor of 3–4 (Geacintov et al., 1981, 1982; Yoshida, 1984); therefore, the linear dichroism signal due to intercalated tetraols is lower than that of BPDE and gives rise to the negative  $\Delta A$  signal at about 353 nm in the equilibrated reaction mixture (Figure 4). This negative band disappears upon extraction of the tetraols with ether, and only the positive  $\Delta A$  bands at about 328 and 345 nm due to the covalently bound (+) enantiomer of BPDE remain (Geacintov et al., 1984a; Yoshida, 1984).

The kinetics of the changes in the  $\Delta A$  signals at 260 nm taken from successive spectral linear dichroism scans are depicted in Figure 5 for  $r = 0.1$ . Immediately after addition of BPDE to RF I  $\phi$ X174, the magnitude of the  $\Delta A$  signal increases by about 30%. This change is attributed to two factors: (1) an unwinding of DNA induced by the noncovalent intercalation of BPDE, and (2) a contribution of intercalated BPDE to the linear dichroism signal at 260 nm; the  $\Delta A$  signals of the DNA and intercalated carcinogen are expected to be additive, since the planes of the bases and BPDE are parallel to one another. The latter effect produces an increase in the  $\Delta A_{260}$  signal upon addition of BPDE in the cases of nicked circular RF II and linear DNA (Figure 5).

In all three cases, using supercoiled, relaxed circular, and linear DNA, the magnitude of the  $\Delta A$  signal decreases as the reaction of BPDE progresses and reaches an equilibrium value after approximately 8 min. In contrast, when ethidium bromide is added to supercoiled DNA, the absolute value of  $\Delta A$  increases immediately by a factor of 3.5 ( $r_b = 0.03$ ) and remains constant as a function of time. The decrease in  $\Delta A$  in the case of linear DNA modified covalently with BPDE is attributed to the formation of a kink or bend at the alkylation site (Hogan et al., 1981). An increase in the electrophoretic mobility of RF II DNA upon covalent binding of BPDE has

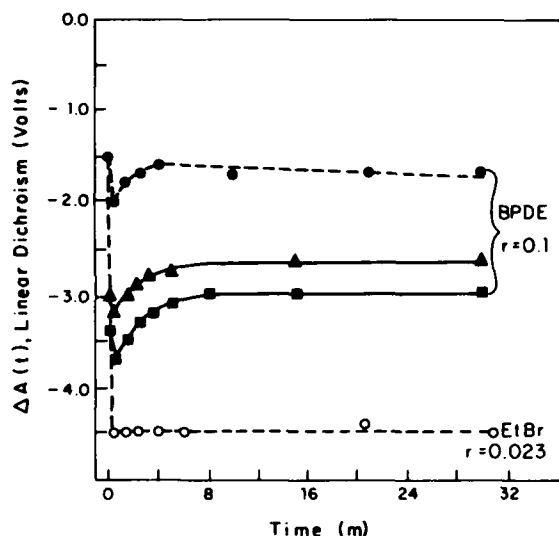


FIGURE 5: Time dependence of the linear dichroism measured within the DNA absorption band at 260 nm at a BPDE molar reaction ratio of  $r = 0.1$ , and in the presence of ethidium bromide [(O)  $r_0 = 0.023$ ]. All DNA concentrations were  $7.6 \times 10^{-5}$  M. Supercoiled RF I DNA (●); calf thymus linear DNA (▲); nicked circular  $\phi$ X174 DNA (■).

been observed (Drinkwater et al., 1978; Gamper et al., 1980), which has been attributed by Gamper et al. to the formation of "flexible hinges" at the BPDE covalent binding sites. This effect also gives rise to a diminished overall degree of alignment of the DNA bases in relaxed circular DNA in the flow gradient, thus causing a decrease in the magnitude of  $\Delta A$  as the covalent binding reaction progresses.

The decrease in the magnitude of  $\Delta A$  after addition of BPDE in the case of supercoiled DNA can, in principle, be due to the kinking effect, or due to a rewinding of the DNA as the BPDE molecules are hydrolyzed and leave the intercalation sites. It is not possible to distinguish between these two effects on the basis of the experimental data alone depicted in Figure 5. However, at higher values of the reaction ratio  $r$ , the effect of rewinding can be observed more easily. In order to accentuate the differences in behavior between supercoiled and relaxed circular DNA, we have plotted the ratios  $\Delta A(t)/\Delta A(0)$  as a function of time in Figure 6, where  $\Delta A(0)$  is the initial dichroism (before the addition of BPDE) while  $\Delta A(t)$  is the dichroism at 260 nm measured at different times after the addition of BPDE. The immediate sharp rise is due to the unwinding of supercoiled DNA produced by the intercalation of BPDE, while the subsequent rapid drop is attributable to the rewinding of the DNA as the BPDE molecules are hydrolyzed to tetraols and the number of intercalated diol epoxide molecules decreases. We mention in passing that the addition of equivalent amounts of tetraols produces only a negligibly small unwinding of RF I DNA (data not shown). The sharp decreases in the quantity  $\Delta A(t)/\Delta A(0)$  as the reaction progresses are too large to be explained in terms of the kinking effect. The changes in the dichroism of relaxed DNA attributable to kink formation are significantly smaller than the effects observed in the case of supercoiled DNA (Figure 6).

In the  $r = 1.8$  case, a positive dichroism signal is observed in the 280–300-nm region (data not shown), which also disappears with increasing time of reaction. This effect, observed only at relatively high concentrations of BPDE, is attributed to the aggregation of BPDE molecules on the surface of the DNA and has not been further investigated. However, this phenomenon accounts for the fact that immediately after addition of such a high quantity of BPDE, the  $\Delta A(t)/\Delta A(0)$

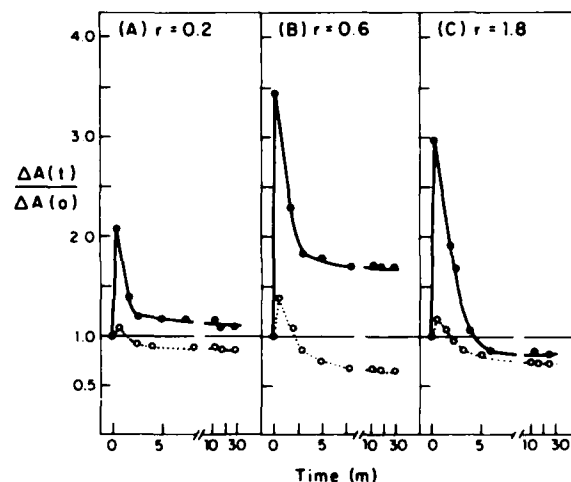


FIGURE 6: Kinetics of the ratio  $\Delta A(t)/\Delta A(0)$  at different initial concentrations of BPDE expressed in terms of the molar reaction ratios  $r$ , where  $\Delta A(0)$  is the linear dichroism signal measured at 260 nm just after the addition of BPDE, while  $\Delta A(t)$  is the dichroism measured at time  $t$  after the addition of BPDE. Supercoiled  $\phi$ X174 DNA (●); nicked circular  $\phi$ X174 DNA (linear DNA exhibits analogous behavior; data not shown) (○). All DNA concentrations were  $7.6 \times 10^{-5}$  M.

signal is lower in the  $r = 1.8$  case than in the  $r = 0.6$  experiment.

The limiting, constant values of  $\Delta A(\infty)/\Delta A(0)$  at long reaction times are due to the covalent adducts. We have found that the level of covalent binding of BPDE to linear and supercoiled DNA is approximately the same [see also MacLeod & Tang (1985)]. Thus, the differences in the limiting dichroism values observed with supercoiled and relaxed or linear DNA cannot be attributed to differences in the number of covalently bound BPDE residues. In the  $r = 0.2$  and  $0.6$  cases,  $\Delta A(\infty)/\Delta A(0) > 1.0$ , indicating that the modified supercoiled DNA orients better than the unmodified RF I DNA. This correlates with the apparent larger hydrodynamic volume of the modified DNA and its decreased electrophoretic mobility at these values of  $r$  (Figure 1). At still higher degrees of modification at  $r = 1.8$  (about 80 covalently bound BPDE molecules per genome),  $\Delta A(\infty)/\Delta A(0) < 1.0$ , and the modified DNA orients less well in the flow gradient than unmodified supercoiled DNA. This may be due to the induction of the more compact positive supercoiled form at these high levels of modification (Figure 1B), or to the kinking effect, or to a combination of these two effects.

**(C) Kinetics of Relaxation of Linear Dichroism.** The minimum elapsed time between the addition of either ethidium bromide or BPDE to the DNA-containing solutions and the first linear dichroism measurement is about 20 s. This is the time required to achieve adequate mixing and the full rotational speed of the inner cylinder in the Couette cell. In the case of ethidium bromide, the maximum magnitude of the linear dichroism signal is achieved within less than 20 s, since there is no change in  $\Delta A$  from the very first measurement to the last (after 2 days; data not shown). Thus, the intercalation of this drug and its effect on the conformational state of superhelical DNA occur on time scales faster than 20 s. In the case of BPDE, the initial effects of noncovalent intercalation and unwinding also occur on time scales which are too rapid to be resolved (less than 20 s); however, the subsequent effects of the chemical reactions of BPDE occur on time scales of minutes, and the accompanying changes in the dichroism spectra can be easily followed as a function of time.

The kinetics of the relaxation of the linear dichroism signals within the DNA absorption band (260 nm) and the absorption

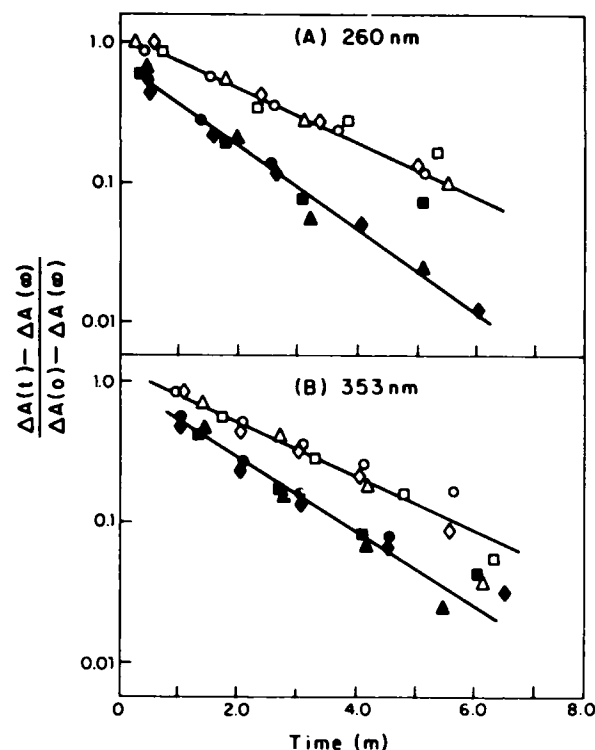


FIGURE 7. Semilogarithmic plots of eq 2. The linear dichroism data were obtained from  $\Delta A$  spectra measured for reaction mixtures with different initial BPDE concentrations at 260 nm (DNA absorption) and 353 nm (absorption band of noncovalently intercalated BPDE):  $r = 0.10$ ; (○, ●);  $r = 0.20$  (□, ■);  $r = 0.60$  (△, ▲);  $r = 1.8$  (◇, ◆). Supercoiled  $\phi$ X174 DNA (●, ■, ▲, ◆); nicked circular  $\phi$ X174 DNA (○, □, △); linear calf thymus DNA (◇). All DNA concentrations were  $7.6 \times 10^{-5}$  M. The data points obtained at different  $r$  values were shifted vertically to fall on the same straight line plots for supercoiled, relaxed circular, or linear DNA. These two different sets of lines were further offset from one another along the vertical axis for clarity.

band of intercalated BPDE molecules (353 nm) are compared in the semilogarithmic plots of the time-dependent normalized linear dichroism

$$\frac{\Delta A(t) - \Delta A(\infty)}{\Delta A(0) - \Delta A(\infty)} = \exp(-kt) \quad (2)$$

as a function of time (Geacintov et al., 1984a) in Figure 7;  $\Delta A(0)$ ,  $\Delta A(t)$ , and  $\Delta A(\infty)$  are the linear dichroism signals measured just after the addition of BPDE, at a time  $t$  after addition, and for equilibrated reaction mixture (all BPDE molecules reacted), respectively. The pseudo-first-order reaction rate constant of BPDE is defined by  $k$ . In Figure 7, the data points obtained from dichroism spectra of reaction mixtures with different  $r$  values have been combined. The data points obtained with relaxed circular and linear DNA fall on lines with the same slopes with constants  $k = 0.29 \pm 0.02 \text{ min}^{-1}$  (260 nm) and  $0.30 \pm 0.02 \text{ min}^{-1}$  (353 nm). In the case of supercoiled DNA, the data points fall on lines with different slopes ( $k = 0.44 \pm 0.02 \text{ min}^{-1}$  at 260 nm and  $k = 0.40 \pm 0.02 \text{ min}^{-1}$  at 353 nm). Within experimental error, the relaxation kinetics are approximately the same at 260 and 353 nm for both the supercoiled and the circular and linear DNA samples. The kinetics of this rewinding parallel the decay of BPDE and are the same for all reaction ratios  $r$  (Figure 7). At the different reaction ratios used ( $r = 0.1$ – $1.8$ ), the levels of covalent binding vary from  $r_0 = 0.005$  to  $0.015$  and give rise to large differences in the final values of the linear dichroism (time points beyond 10 min in Figures 5 and 6). The covalent

adducts are produced during the time intervals of 0–6 min, however, when the large changes in  $\Delta A$ , attributed to the rewinding of the DNA, are occurring.

It has been shown previously (Geacintov et al., 1984a; Yoshida, 1984) that  $k$  obtained from plots of eq 2 using linear dichroism data at 353 nm (due mostly to physically intercalated BPDE molecules) indeed represents the decay constant of BPDE. The fact that at 260 nm the kinetics are similar to those at 353 nm suggests that the conformational changes of the DNA (rewinding in the case of supercoiled DNA, kink or bend formation in the case of relaxed circular and linear DNA) occur as soon as the BPDE molecules are hydrolyzed or converted to covalently bound moieties. There is no measurable time lag between these events and the conformational changes of the DNA molecules.

In the case of supercoiled DNA, the reaction rate constant  $k$  is about 1.3–1.5 times faster than in the cases of relaxed circular and linear DNA. This difference is consistent with the results of MacLeod and Tang (1985), who, utilizing different methods of analysis, found a ratio of 1.21; since the reaction rate constant of BPDE in DNA solution depends on the intercalative association constant  $K$  (Geacintov et al., 1982b), the higher reactivity of BPDE in the presence of supercoiled DNA can probably be attributed to a somewhat higher value of  $K$  in RF I DNA than in RF II DNA (MacLeod & Tang, 1985).

## DISCUSSION

**Flow Linear Dichroism as a Technique for Monitoring Changes in Shape of Supercoiled DNA.** The linear dichroism signal of supercoiled DNA oriented in a flow gradient is sensitive to the changes in shape of the macromolecule induced by the intercalative binding of ethidium bromide, or the noncovalent and covalent binding of BPDE. The more compact supercoiled DNA molecules are characterized by faster mobilities on electrophoretic gels and higher sedimentation coefficients, but lower linear dichroism signals than nicked circular, relaxed DNA. The lower dichroism measured within the DNA absorption band at 260 nm is associated with a lower average degree of alignment of the nucleic acid bases with respect to the flow lines. Such a lower average alignment may be due either to a greater rotational mobility of the compact supercoiled molecules and/or to a lower degree of orientation of the bases with respect to the axis of alignment of the macromolecule in the flow field. The noncovalent intercalation of drug or carcinogen molecules causes a partial unwinding of the supercoiled DNA leading to an apparent hydrodynamically larger molecule with reduced electrophoretic mobility and lower sedimentation coefficient, but higher linear dichroism. The magnitude of the linear dichroism of relaxed circular DNA is 3.5 times higher than that of the supercoiled DNA sample. It is interesting to note that the magnitude of the dichroism signal closely parallels the changes in the sedimentation coefficient,  $s_{20}$ , measured by Waring (1970) at different ethidium bromide concentrations. The linear dichroism method is therefore suitable for following the kinetics of unwinding (or rewinding) on the time scale of seconds. The limiting factor in measuring the kinetics is the 20-s time period required to add the drug to the DNA sample and to subsequently bring the Couette cell to its full rotational speed. Thus, the flow dichroism technique can provide information similar to that obtained by the sedimentation technique, but with the additional advantage that the kinetics of the changes in the shape of the DNA can also be followed.

**Effect of Noncovalent Binding.** The effect of the noncovalent binding of ethidium bromide and BPDE on the su-

perhelicity of supercoiled  $\phi$ X174 DNA can be compared by considering the magnitudes of the dichroism induced by these two molecules at the same value of  $r_b$ . The first value of  $\Delta A$ , measured within less than 1 min of mixing (Figures 5 and 6), is an indication of the effect of noncovalent intercalative binding of BPDE on the shape of supercoiled DNA. The value of  $r_b$  can be estimated from the reaction ratio  $r$ , the DNA concentration, the known association constant for linear DNA ( $K = 12\,000\text{ M}^{-1}$ ; Geacintov et al., 1982b; Yoshida, 1984), and the finding that  $K$  is only slightly larger (about 40% in the case of the tetraol derived from the hydrolysis of BPDE; MacLeod & Tang, 1985) for supercoiled than for linear DNA. At relatively low molar reaction ratios, e.g., when  $r = 0.1$ , the fraction of physically bound BPDE molecules can be estimated from the expression (Geacintov et al., 1982)

$$K[\text{DNA}]/(1 + K[\text{DNA}]) \quad (3)$$

At a DNA concentration of  $7.6 \times 10^{-5}\text{ M}$ , the fraction of bound molecules is about 0.48 and  $r_b = 0.048$ . Under these conditions, the magnitude of the linear dichroism is increased by 30% immediately after the addition of BPDE, and before any substantial decomposition of BPDE has occurred (Figure 5). At a similar value of  $r_b$ , ethidium bromide causes a 250% increase in the magnitude of  $\Delta A$  and complete unwinding (Figure 3). It is thus concluded that ethidium bromide is much more effective, per molecule bound, in inducing unwinding of supercoiled DNA than the noncovalent binding of BPDE. Meehan et al. (1982) reported an unwinding angle of  $13^\circ$  for the physical binding of BPDE to SV40 DNA as compared to a value of  $30^\circ$  for ethidium bromide, which is consistent with our conclusions based on kinetic flow dichroism data. This difference may be due to a larger distortion of the local structure of the DNA by the more tightly and electrostatically bound drug molecule than the distortion caused by the more weakly bound electrically neutral diol epoxide molecule.

**Effect of Covalent Binding of BPDE.** The linear dichroism signal of the fully equilibrated BPDE-DNA reaction mixtures reflects the effects of the covalently bound 7,8,9-trihydroxy-7,8,9,10-tetrahydrobenzo[a]pyrene residues. Since the effects of the noncovalently bound tetraols on the unwinding and on the linear dichroism changes of supercoiled DNA are negligible, the variations in  $\Delta A(\infty)$  are due to the covalently bound BPDE residues. In the experiments described here, the covalent binding ratio varied from  $r_b = 0.005$  (at an initial reaction ratio of  $r = 0.1$ ) to  $r_b = 0.015$  at  $r = 1.8$ . While a detailed quantitative study of the effect of covalent binding on the linear dichroism of superhelical DNA was not the focus of this study, a rough comparison between the effects produced by ethidium bromide and by the covalent binding produced by BPDE is nevertheless possible. For example, at  $r = 0.6$ , the covalent BPDE binding ratio is  $r_b = 0.010$ , and at equilibrium, this level of covalent binding leads to a 70% increase in  $\Delta A$  (Figure 6). In the case of ethidium bromide, a similar increase in  $\Delta A$  is produced at  $r_b = 0.010$ – $0.015$ . This result is consistent with the findings of Drinkwater et al. (1978), who reported that the unwinding produced by the noncovalent binding of ethidium bromide is about the same as the effect produced by the covalent binding of BPDE to supercoiled SV40 DNA. It is thus evident that the noncovalent intercalative binding of BPDE, which precedes the covalent binding reaction, causes much less of a perturbation of the local structure of supercoiled DNA, and thus less unwinding, than the covalently bound benzo[a]pyrene triol residues.

**Orientation of Pyrenyl Chromophores and Unwinding.** The linear dichroism spectra of BPDE-DNA noncovalent complexes and covalent adducts provide information on the relative

orientations of the pyrenyl chromophores and the planes of the DNA bases. As in the case of linear DNA, the  $\Delta A$  spectra of the noncovalent BPDE-DNA complexes, taken within 1 min of mixing, are negative in sign (Figure 4); the minima in  $\Delta A$  at 337 and 353 nm coincide with the absorption bands of physically bound BPDE and are consistent with a type I intercalative conformation of the BPDE chromophore (Geacintov et al., 1984a; Yoshida, 1984).

In the case of the equilibrated reaction mixtures (the 60-min spectrum in Figure 4), the positive maxima at 328 and 345 nm are due to the covalently bound (+) enantiomer of BPDE and are attributed to type II conformations in which the pyrenyl residue is located either in an external region or in a disordered region of the DNA (Geacintov et al., 1978, 1982a, 1984a). A wedge-shaped intercalative complex is unlikely for this structure since other diol epoxides, e.g., the (–) enantiomer of BPDE, display a red-shifted negative linear dichroism which is more consistent with such a quasi-intercalative conformation (Yoshida, 1984; Geacintov, 1985). Drinkwater et al. (1978) suggested that the covalently bound residue of BPDE is intercalated since the unwinding effect produced is similar to that generated by the intercalator ethidium bromide. However, the linear dichroism spectrum shown in Figure 4 is not consistent with such an assignment, since the positive  $\Delta A$  peaks at 328 and 345 nm are characteristic of type II, nonintercalated adducts.

In summary, the advantage of the kinetic flow dichroism technique is that changes in the conformation of the DNA can be monitored simultaneously with changes in the conformation of the drug or carcinogen causing the unwinding of superhelical DNA. We conclude that conformations of carcinogens, other than intercalative binding, can cause changes in the superhelicity of supercoiled DNA.

#### ACKNOWLEDGMENTS

We are grateful to Dr. Y. Mnyukh for performing the linear dichroism measurements.

Registry No. (±)-BPDE, 58917-67-2; ethidium bromide, 1239-45-8.

#### REFERENCES

- Agarwal, K. L., Hrinyo, T. P., & Yang, N.-C. (1983) *Biochem. Biophys. Res. Commun.* 114, 14–19.
- Brookes, P., & Osbornes, M. R. (1982) *Carcinogenesis (London)* 3, 1223–1226.
- Conney, A. H. (1982) *Cancer Res.* 42, 4875–4917.
- Drinkwater, N. R., Miller, J. A., Miller, E. C., & Yang, N.-C. (1978) *Cancer Res.* 38, 3247–3255.
- Fredericq, E., & Houssier, C. (1973) *Electric Dichroism and Electric Birefringence*, Clarendon Press, Oxford University, Oxford, England.
- Gamper, H. B., Straub, K., Calvin, M., & Bartholomew, J. C. (1980) *Proc. Natl. Acad. Sci. U.S.A.* 77, 2000–2004.
- Geacintov, N. E. (1985) *ACS Symp. Ser. No.* 283, 107–124.
- Geacintov, N. E., Gagliano, A. G., Ivanovic, V., & Weinstein, I. B. (1978) *Biochemistry* 17, 5256–5262.
- Geacintov, N. E., Yoshida, H., Ibanez, V., & Harvey, R. G. (1981) *Biochem. Biophys. Res. Commun.* 100, 1569–1577.
- Geacintov, N. E., Gagliano, A. G., Ibanez, V., & Harvey, R. G. (1982a) *Carcinogenesis (London)* 3, 247–253.
- Geacintov, N. E., Yoshida, H., Ibanez, V., & Harvey, R. G. (1982b) *Biochemistry* 21, 1864–1869.
- Geacintov, N. E., Yoshida, H., Ibanez, V., Jacobs, S. A., & Harvey, R. G. (1984a) *Biochem. Biophys. Res. Commun.* 122, 33–39.

- Geacintov, N. E., Ibanez, V., Gagliano, A. G., Jacobs, S. A., & Harvey, R. G. (1984b) *J. Biomol. Struct. Dyn.* 1, 1473-1484.
- Gelboin, H. V. (1980) *Physiol. Rev.* 60, 1107-1166.
- Harvey, R. G. (1981) *Acc. Chem. Res.* 14, 218-226.
- Hogan, M. E., Dattagupta, N., & Whitlock, J. P. (1981) *J. Biol. Chem.* 256, 4504-4513.
- Jeffrey, A. M., Weinstein, I. B., Jennette, K. W., Grezeskowiak, K., Harvey, R. G., Autrup, H., & Harris, C. (1977) *Nature (London)* 269, 348-350.
- Jernstrom, B., Lycksell, P. O., Graslund, A., & Norden, B. (1984) *Carcinogenesis (London)* 5, 1129-1135.
- Kakefuda, T., & Yamamoto, H. A. (1978) *Proc. Natl. Acad. Sci. U.S.A.* 75, 415-419.
- Koreeda, M., Moore, P. D., Wislocki, P. G., Levine, W., Cooney, A. H., Yagi, H., & Jerina, D. M. (1978) *Science (Washington, D.C.)* 199, 778-781.
- King, H. W. S., Osborne, M. R. M., Beland, F. A., Harvey, R. G., & Brookes, P. (1976) *Proc. Natl. Acad. Sci. U.S.A.* 73, 2679-2681.
- MacLeod, M. C., & Selkirk, J. K. (1982) *Carcinogenesis (London)* 3, 287-292.
- MacLeod, M. C., & Tang, M.-S. (1985) *Cancer Res.* 45, 51-56.
- Meehan, T., & Straub, K. (1979) *Nature (London)* 277, 410-442.
- Meehan, T., Straub, K., & Calvin, M. (1977) *Nature (London)* 269, 725-727.
- Meehan, T., Gamper, H., & Becker, J. F. (1982) *J. Biol. Chem.* 257, 10479-10485.
- Osborne, M. R., Beland, F. A., Harvey, R. G., & Brookes, P. (1976) *Int. J. Cancer* 18, 362-368.
- Shahbaz, M., Geacintov, N. E., & Harvey, R. G. (1986) *Biochemistry* 25, 3290-3296.
- Singer, D., & Grunberger, D. (1983) *Molecular Biology of Mutagens and Carcinogens*, Plenum Press, New York.
- Taylor, E. R., Miller, K. J., & Bleyer, A. J. (1983) *J. Biomol. Struct. Dyn.* 1, 883-904.
- Undeman, O., Lycksell, P. O., Graslund, A., Astlind, T., Ehrenberg, A., Jernstrom, B., Tjerneld, F., & Norden, B. (1983) *Cancer Res.* 43, 1851-1860.
- Waring, M. (1970) *J. Mol. Biol.* 54, 247-279.
- Weinstein, I. B., Jeffrey, A. M., Jennette, K. W., Blobstein, S. H., Harvey, R. G., Harris, C., Autrup, H., Kasai, H., & Nakanishi, K. (1976) *Science (Washington, D.C.)* 193, 592-595.
- Yoshida, H. (1984), Ph.D. Thesis, New York University, New York, NY.

# AFRRI — TECHNICAL REPORT



AFRRI TR86-4

## **Reference dosimetry for 1986 NATO battlefield dosimetry intercomparison at Army Pulsed Radiation Facility**

**M. Dooley  
D. M. Eagleson  
T. H. Mohaupt  
A. H. Kazi  
G. H. Zeman**

DEFENSE NUCLEAR AGENCY

**ARMED FORCES RADIOBIOLOGY RESEARCH INSTITUTE**

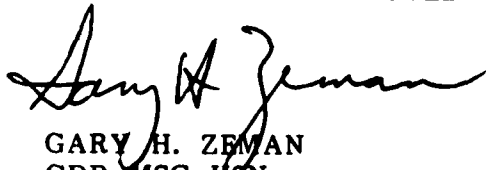
BETHESDA, MARYLAND 20814-5145

---

APPROVED FOR PUBLIC RELEASE DISTRIBUTION UNLIMITED

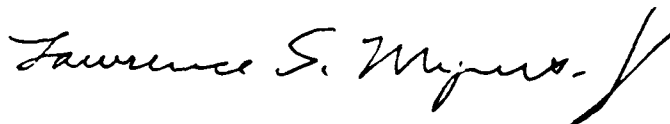


REVIEWED AND APPROVED

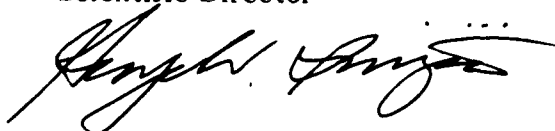


GARY H. ZEMAN  
CDR, MSC, USN

Chairman  
Radiation Sciences Department



LAWRENCE S. MYERS, Ph.D.  
Scientific Director



GEORGE W. IRVING, III  
Col, USAF, BSC  
Director

## CONTENTS

|                                     |    |
|-------------------------------------|----|
| INTRODUCTION                        | 1  |
| RADIATION FIELDS                    | 1  |
| MEASUREMENTS                        | 6  |
| RESULTS                             | 12 |
| DISCUSSION                          | 15 |
| CONCLUSIONS                         | 17 |
| APPENDIX A. CALCULATION OF $K_t$    | 19 |
| APPENDIX B. IONIZATION CHAMBER DATA | 21 |
| REFERENCES                          | 23 |

## INTRODUCTION

A NATO Dosimetry Study is scheduled for September 1986 at the Aberdeen Proving Grounds Pulsed Radiation Facility (APRF) in Aberdeen, Maryland. This study is designed to determine the accuracy of battlefield dosimeters in a simulated tactical environment, and to compare the different NATO dosimeters in simple, well-defined radiation fields. Dosimeters are to be irradiated in four radiation fields: free in air (FIA) and on the surface of polyethylene phantoms by the APRF reactor, FIA by the APRF flash X-ray machine, and FIA by a prompt X-ray spike followed by a delayed neutron and gamma-ray pulse from the reactor.

Reference dosimetry for the NATO Dosimetry Study reactor irradiations was performed by members of the Armed Forces Radiobiology Research Institute (AFRRI) at the APRF facility in April 1986. Kerma rates FIA and on the surface of the phantoms were measured using paired ionization chambers and the reactor in the steady-state mode. Monitor sulfur pellets and calcium fluoride thermoluminescent dosimeters (TLD's) were used to establish kerma in the pulsed environment. Contained in this report are a brief description of the radiation facilities and the measurement procedures, and a discussion of the results as they pertain to the intercomparison study.

## RADIATION FIELDS

### REACTOR

The APRF "fast-burst" reactor is a bare critical assembly that may be operated at steady-state power levels up to 10 kW and at super-prompt criticality to produce pulses with microsecond durations (1-3). For these studies, the reactor was operated inside the reactor silo with the center 200 cm above the floor. All dosimetry measurements were performed 166 cm from the core center and 200 cm above the floor. A converter shield was placed in front of the reactor core to better approximate the neutron spectrum 1 km downrange of a nuclear blast. The shield, 12.7 cm thick and 46 cm high, was constructed of polyethylene loaded with cadmium oxide (5% by weight).

Spectral data for the unshielded APRF configuration are shown in Table 1 and Figure 1 (3). Spectral data behind the converter shield were not available, but the qualitative effects of the shield were to reduce the neutron-to-gamma ratio from about 9:1 to less than 1:1, and to produce a harder (more energetic) neutron spectrum. (Neutrons are absorbed by the hydrogenous material, decreasing the fast neutron flux and increasing the gamma-ray flux from hydrogen and cadmium capture reactions.) Boron and cadmium were added to absorb the thermal and low-energy neutrons.

Table 1. APRF Neutron Spectrum at 15 Meters\*

| Group | Upper Bin<br>Energy (MeV) | Group<br>Fluence | Fluence Per<br>Unit Lethargy |
|-------|---------------------------|------------------|------------------------------|
| 1     | 19.600000                 | 0.0000           | 0.000000                     |
| 2     | 16.900000                 | 0.0000           | 0.000000                     |
| 3     | 14.900000                 | 0.0000           | 0.000000                     |
| 4     | 14.200000                 | 0.0000           | 0.000000                     |
| 5     | 13.800000                 | 0.0000           | 0.000000                     |
| 6     | 12.800000                 | 0.0000           | 0.000000                     |
| 7     | 12.200000                 | 0.0000           | 0.000000                     |
| 8     | 11.100000                 | 2.8305e-11       | 2.712246e+08                 |
| 9     | 10.000000                 | 6.0121e-11       | 6.022941e+08                 |
| 10    | 9.050000                  | 8.2983e-11       | 8.310683e+08                 |
| 11    | 8.190000                  | 1.58e-10         | 1.578737e+09                 |
| 12    | 7.410000                  | 3.11e-10         | 2.078044e+09                 |
| 13    | 6.380000                  | 1.0439e-09       | 4.17978e+09                  |
| 14    | 4.970000                  | 3.2581e-10       | 6.312802e+09                 |
| 15    | 4.720000                  | 1.1325e-09       | 7.643248e+09                 |
| 16    | 4.070000                  | 2.9465e-09       | 9.766324e+09                 |
| 17    | 3.010000                  | 2.9711e-09       | 1.288142e+10                 |
| 18    | 2.390000                  | 5.1056e-10       | 1.499618e+10                 |
| 19    | 2.310000                  | 3.4421e-09       | 1.47774e+10                  |
| 20    | 1.830000                  | 7.4068e-09       | 1.481479e+10                 |
| 21    | 1.110000                  | 1.0124e-08       | 1.441754e+10                 |
| 22    | 0.550000                  | 1.4855e-08       | 1.190973e+10                 |
| 23    | 0.158000                  | 3.4836e-09       | 9.866878e+09                 |
| 24    | 0.111000                  | 6.5104e-09       | 8.695373e+09                 |
| 25    | 0.052500                  | 5.4841e-09       | 7.312426e+09                 |
| 26    | 0.024800                  | 8.2094e-10       | 6.601319e+09                 |
| 27    | 0.021900                  | 4.5044e-09       | 5.971313e+09                 |
| 28    | 0.010300                  | 5.4068e-09       | 4.813746e+09                 |
| 29    | 0.003350                  | 3.7165e-09       | 3.709452e+09                 |
| 30    | 0.001230                  | 2.3617e-09       | 3.163358e+09                 |
| 31    | 0.000583                  | 4.0416e-09       | 2.305402e+09                 |
| 32    | 0.000101                  | 2.034e-09        | 1.630069e+09                 |
| 33    | 0.000029                  | 1.2523e-09       | 1.256005e+09                 |
| 34    | 0.000011                  | 1.2139e-09       | 9.697236e+08                 |
| 35    | 0.000003                  | 7.4402e-10       | 7.468581e+08                 |
| 36    | 0.000001                  | 5.9514e-10       | 5.927099e+08                 |
| 37    | 4.14e-07                  |                  |                              |

\*From reference 3

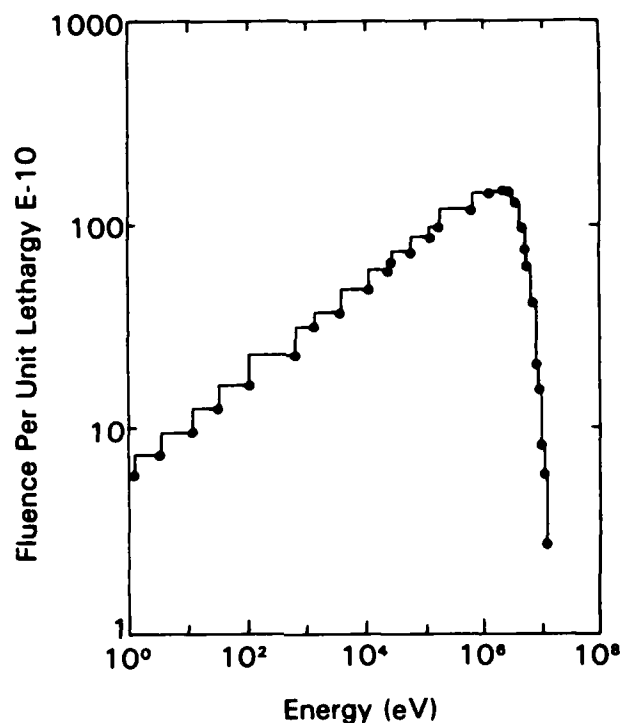


Figure 1. APRF neutron spectrum at 15 meters  
(from Table 1)

FIA irradiations were performed with the dosimeters mounted on thin aluminum screens, which were placed on a larger aluminum stand (Figure 2). The phantoms (polyethylene blocks 61 cm high by 30 cm wide by 10 cm thick) were placed on a large wooden stand so that the center of the front surface (facing the core) of each phantom was 166 cm from the core centerline (see Figure 3). The dosimeters were mounted directly on the front surface of the phantoms.



Figure 3. Phantom setup

## FLASH X-RAY MACHINE

As part of the intercomparison, dosimeters will be irradiated FIA with a 4-MV flash X-ray machine (FX). The dosimeters will be positioned 150 cm from the front of the faceplate, where the instantaneous exposure rate is approximately  $8 \times 10^8$  roentgens/second and a total exposure of about 73 roentgens is obtained with a pulse width of 87 nanoseconds (FWHM). Reference dosimetry for the FX will use calcium fluoride TLD's.

## COMBINED REACTOR AND X-RAY MACHINE

This irradiation will be performed to simulate the radiation field immediately following a nuclear detonation. Dosimeters will be positioned FIA 150 cm from the FX faceplate, and the reactor will be moved so that it is 200 cm from the dosimeters. The initial FX pulse will be followed 100 microseconds later by a reactor pulse of about  $6 \times 10^{16}$  fissions with a pulse width of about 90 microseconds (FWHM).

## MEASUREMENTS

The reactor reference dosimetry was based on measurements using paired ionization chambers with the reactor operated in the steady-state mode. These results were transferred to the pulsed environment through the use of sulfur monitor foils and calcium fluoride TLD's. Rhodium activation foils were also irradiated to test their effectiveness as kerma monitors. Table 2 lists the reactor runs and the dosimetry used for each run. Figures 4, 5, and 6a,b show the dosimetry setup FIA and on the phantoms, respectively. Note that the APRF staff also placed dosimeters in some of the reactor runs to compare with the AFRRI results. Each AFRRI dosimetry system is discussed separately below.

## IONIZATION CHAMBERS

Measurements were made using a pair of 0.5-cm<sup>3</sup> Exradin (Warrenville, IL) ionization chambers consisting of an A150 plastic tissue-equivalent (TE) chamber (Model T2) filled with methane-based TE gas (MTE) and a magnesium chamber (Model MG2) filled with argon gas. Both chambers had cobalt-60 calibrations directly traceable to the National Bureau of Standards (NBS). Gas flow rates were maintained at approximately 30 cm<sup>3</sup>/min, and collecting potentials of 400 volts (both + and -) were used for each measurement. Charge was collected through a Keithley (Cleveland, OH) 616 electrometer using the computer-controlled data acquisition system described previously (4).

Table 2. Summary of Irradiations at APRF, 31 March - 2 April 1986

| Date     | Run No.   | Array    | Power          | AFRRI Dosimeters   | APRF Dosimeters                         |
|----------|-----------|----------|----------------|--|---|
| 31 March | SS 86-99  | FIA      | 6 kW           | Paired chambers<br>Monitor chamber<br>S foils                          | Paired chambers<br>S foils              |
|          | SS 86-100 | FIA      | 6 kW           | Paired chambers<br>Monitor chamber<br>S foils                          | Paired chambers<br>S foils              |
|          | SS 86-101 | FIA      | 6 kW           | Paired chambers<br>Monitor chamber<br>S foils                          | Paired chambers                         |
|          | SS 86-102 | FIA      | 6 kW           | Paired chambers<br>Monitor chamber<br>S foils<br>CaF TLD's             | Paired chambers                         |
| 1 April  | SS 86-103 | FIA      | 6 kW           | Paired chambers<br>Monitor chamber<br>S foils<br>CaF TLD's<br>Rh foils | S foils<br>CaF TLD's                    |
|          | SS 86-104 | FIA      | 3 kW           | Paired chambers<br>Monitor chamber<br>S foils<br>CaF TLD's<br>Rh foils |   |
|          | SS 86-105 | Phantoms | 6 kW           | Paired chambers<br>Monitor chamber<br>S foils<br>CaF TLD's<br>Rh foils | Paired chambers<br>S foils<br>CaF TLD's |
| 2 April  | P 86-15   | Phantoms | 24.9<br>kW-min | S foils<br>CaF TLD's<br>Rh foils                                       |   |
|          | P 86-16   | FIA      | 39.5<br>kW-min | S foils<br>CaF TLD's<br>Rh foils                                       | S foils<br>CaF TLD's                    |

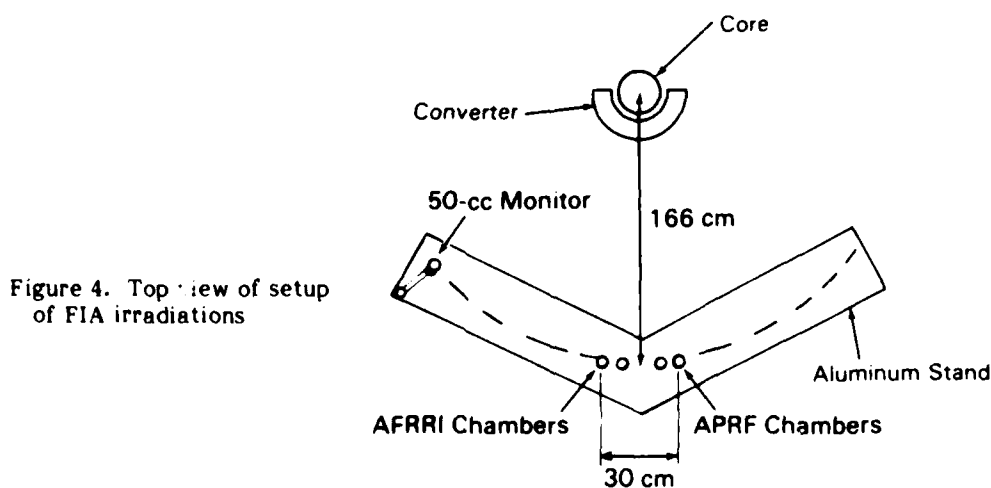


Figure 4. Top view of setup of FIA irradiations



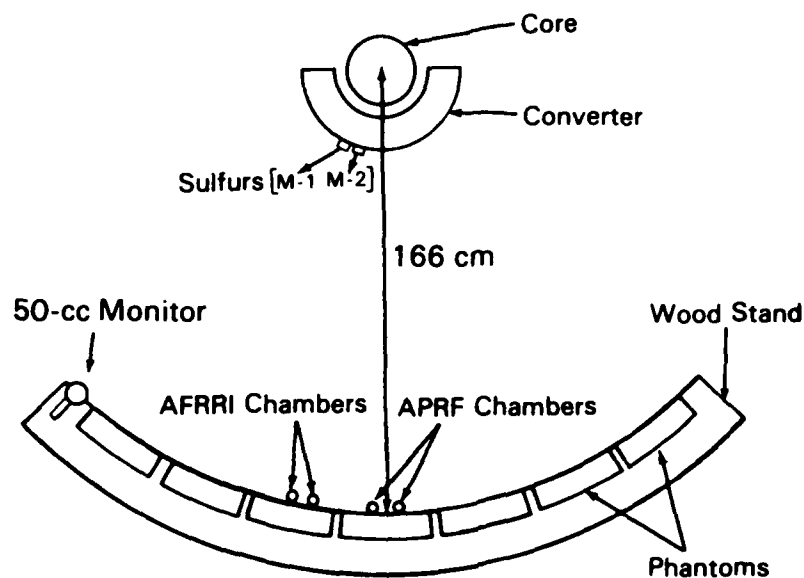


Figure 5. Top view of phantom setup

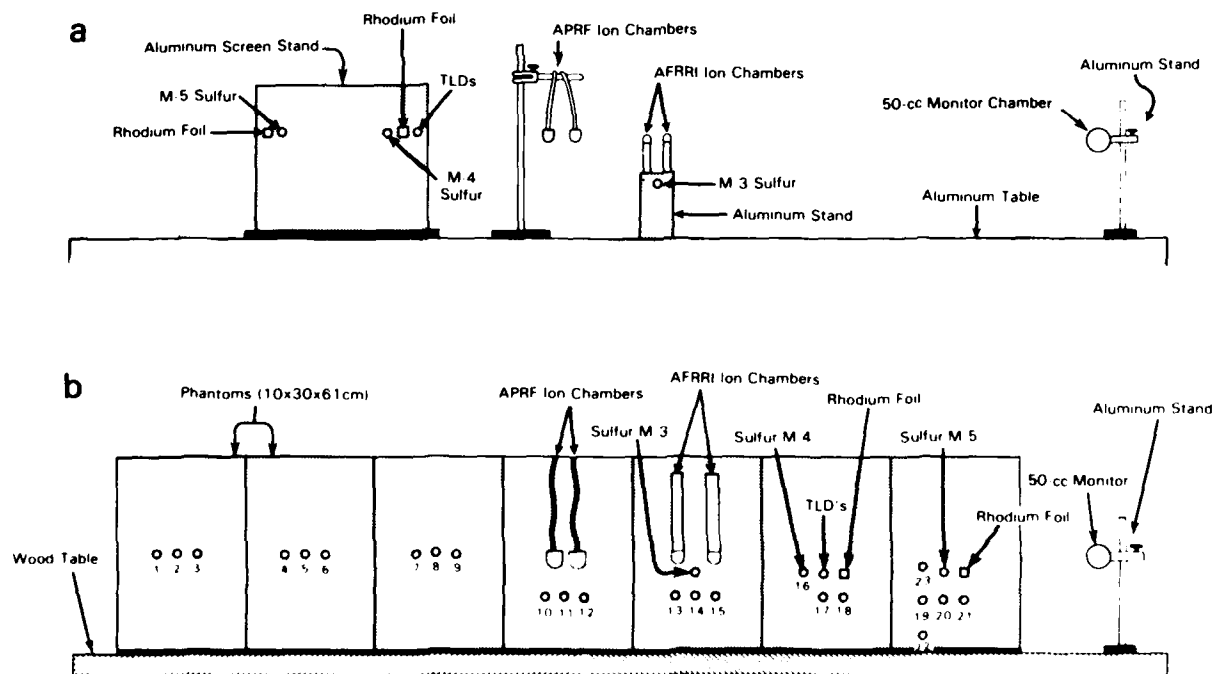


Figure 6a. FIA dosimetry setup viewed from reactor. Figure 6b. Phantom dosimetry setup with field uniformity sulfurs (numbers 1-23), viewed from reactor.

Neutron and gamma-ray tissue-kerma rates FIA and on the surface of the polyethylene phantoms were calculated from the measured chamber responses using the two-dosimeter method (5-7). The responses of the TE-TE chamber, which measures the total dose, and the Mg-Ar chamber, which is relatively insensitive to neutrons, are described as follows:

$$R_t' = k_t \cdot D_n + h_t \cdot D_g$$

$$R_u' = k_u \cdot D_n + h_u \cdot D_g$$

In these equations, known as the paired chamber equations, the subscript t refers to the chamber measuring the total dose (TE-TE), and u refers to the neutron-insensitive chamber (Mg-Ar). Each term is defined below.

$R_t', R_u'$  = chamber response (coulombs) in mixed field multiplied by cobalt-60 calibration factor (Gy/coulomb) for each chamber (units: Gy[Co-60])

$k_t, k_u$  = sensitivity of each chamber to neutrons in mixed field relative to its sensitivity to calibration gamma rays (units: Gy[Co-60]/Gy[mixed field]).

$h_t, h_u$  = sensitivity of each chamber to gamma rays in mixed field relative to its sensitivity to calibration gamma rays (units: Gy[Co-60]/Gy[mixed field]).

$D_n, D_g$  = neutron and gamma-ray tissue absorbed dose (or tissue kerma) in Gy. Note: In this report,  $K_n$  and  $K_g$  are used to represent the neutron kerma and gamma-ray kerma, respectively.

The chamber response,  $R'$ (Gray), is calculated from

$$R' = R \cdot \alpha_c \cdot K_s \cdot K_e / K_w$$

where  $R$  = measured ionization charge (coulomb), which is average of readings at + and - polarity, corrected to standard temperature and pressure, and compensated for background noise or drift (average of pre- and postirradiation drifts).

$\alpha_c$  = cobalt-60 tissue-absorbed dose calibration factor.

$\alpha_c = N_x \cdot f_c \cdot K_w$ , where  $N_x$  is roentgen calibration (roentgens/coulomb),  $f_c$  is exposure to tissue-absorbed dose conversion factor for cobalt-60 photons (0.00962 gray/roentgen) (reference 8), and  $K_w$  is wall attenuation and scatter correction factor for cobalt-60 calibration beam.

$K_s$  = saturation correction factor, with measurements made with collecting potentials set at 200 V instead of 400 V. No evidence of saturation was observed; i.e.,  $K_s = 1$ .

$K_e$  = electrometer correction factor (traceable to NBS calibration of electrometer).

$K_w$  = wall attenuation and scatter correction factor in field of measurement, determined by measuring ionization current (R) with various wall thicknesses, and extrapolating graph of wall thickness versus R to zero wall thickness (see Figures 7 and 8).

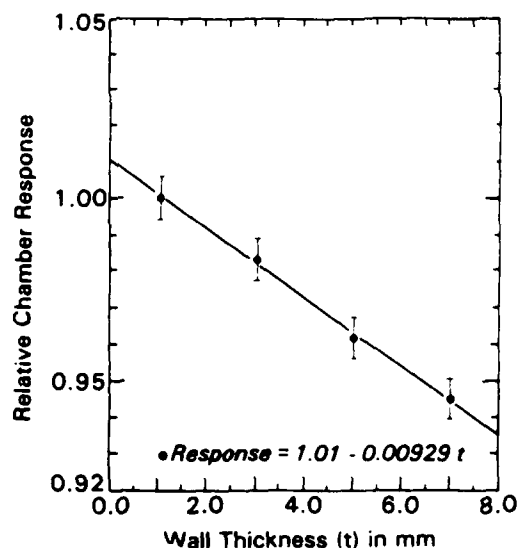


Figure 7. TE-TE wall attenuation and scatter data for FIA dosimetry setup

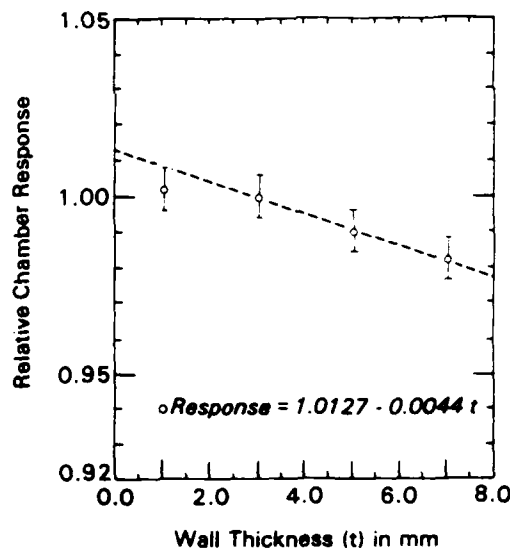


Figure 8. Mg-Ar wall attenuation and scatter data for FIA dosimetry setup

Values of the relative chamber sensitivities ( $k_t$ ,  $h_t$ ,  $k_u$ ,  $h_u$ ) depend on neutron and gamma-ray energies. The sensitivities were evaluated for the bare-core energy spectrum (Table 1 and Figure 1), since this was the only spectral information available. The calculation of  $k_t$  was based on the APRF spectrum (Appendix A),  $k_u$  was determined from data in reference 9, and  $h_t$  and  $h_u$  were set equal to 1 because they are generally close to unity (10). Table 3 summarizes the physical parameters and the chamber constants used for this study.

Each steady-state run was monitored by a 50-cm<sup>3</sup> spherical TE ionization chamber filled with TE gas. One run was performed at 3 kW (instead of 6 kW) to test the linearity of the reactor power monitors. Response of the 50-cm<sup>3</sup> ion chamber monitor (shown in Table 10 in Appendix B) was constant per kW-min for all runs.

Table 3. Physical Parameters Used for Calculations

| Parameter              | Value                                     |
|------------------------|---|
| Average neutron energy | 2.3 MeV                                   |
| $W_n$ , MTE gas        | 31.6 eV                                   |
| $W_c$                  | 29.3 eV                                   |
| K ICRU muscle          | $2.85 \times 10^{-11}$ Gy-cm <sup>2</sup> |
| K MTE gas              | $2.89 \times 10^{-11}$ Gy-cm <sup>2</sup> |
| $k_t$                  | 0.942                                     |
| $k_u$                  | 0.031                                     |
| $h_t$                  | 1.00                                      |
| $h_u$                  | 1.00                                      |

### SULFUR ACTIVATION FOILS

Sulfur activation foils were placed on the converter shield (Figures 6a,b) and between the ionization chambers on the irradiation array for each run. The sulfurs were 2.5 cm in diameter by 0.3 cm thick, and were benchmarked in the NBS californium-252 facility as described in reference 11. Cross-section corrections to account for differences in the APRF spectrum compared to that of the NBS californium source were not applied. However, for the fluence greater than 3 MeV ( $\phi > 3$  MeV, the quantity used in this study), the correction is expected to be negligible.

From the steady-state runs, a sulfur fluence-to-neutron kerma conversion factor was calculated based on the ionization chamber readings, and this factor was used to determine the neutron dose for the pulsed irradiations. The dose uniformity across the phantom array was estimated by stringing sulfur foils across the array for one irradiation (Figure 6b).

### RHODIUM ACTIVATION FOILS

Rhodium activation foils have the potential to be excellent kerma monitors because the reaction cross section of  $^{103}\text{Rh}(n,n')^{103m}\text{Rh}$  compares very well with that of neutron kerma in tissue for neutrons with energies between about 0.7 and 5 MeV (12,13). Two rhodium foils, one with and one without a cadmium cover, were placed in the arrays for four irradiations. A sulfur activation foil was placed alongside each rhodium foil, and the rhodium activity was normalized to the sulfur fluence. A sodium iodide detector connected to a portable multichannel analyzer was used to count the 20-keV X rays from the rhodium decay. The efficiency of the system was based on benchmark irradiations at the NBS californium-252 facility and the use of a cadmium-109 check source.

## CALCIUM FLUORIDE TLD'S

Harshaw (Solon, OH) TLD 200 ( $\text{CaF}_2\text{:Mn}$ ) chips, in 4-mm-thick plastic buildup capsules, were used to measure the gamma-ray component of the kerma in the steady-state and the pulsed irradiations. The TLD's were calibrated in a beam of cobalt-60 gamma rays (calibration directly traceable to NBS [reference 14]), and a correction for fading between the time of readout and irradiation was included in the calculations. This correction was based on a set of control TLD's irradiated in an APRF cobalt-60 unit at approximately the same time the TLD's were irradiated in the reactor. The control TLD's were then read out with the reactor-irradiated TLD's. Each TLD reading represents the average of approximately five TLD chips irradiated together.

## RESULTS

The results of the ionization chamber measurements are shown in Table 4, and the detailed chamber data are provided in Appendix B (Tables 10-12). Ionization chamber precision was about 0.6%, and the absolute accuracy of the paired chamber method is considered to be around 5%-8% (7). The effect of the phantom was to increase the total kerma rate by about 13%, and the neutron and gamma-ray components by 7% and 18%, respectively.

Table 4. Summary\* of Ionization Chamber Results

| Configuration      | Kerma Rate (cGy/kW-min) |                  |                  | $K_g/K_t$ |
|--------------------|-------------------------|------------------|------------------|-----------|
|                    | $K_n$<br>(Neutron)      | $K_g$<br>(Gamma) | $K_t$<br>(Total) |           |
| Free in air (FIA)  | 3.51                    | 4.65             | 8.15             | 0.57      |
| On phantom surface | 3.76                    | 5.49             | 9.25             | 0.59      |
| Phantom FIA        | 3.67                    | 5.18             | 8.85             |           |

\*Summarized from Table 1, Appendix B.

Table 5 summarizes the neutron spectrum data. The neutron spectrum listed is the fluence of neutrons with energies greater than 0.025 eV, averaged over the spectrum averaged cross section. The neutron spectrum was measured on 11/11/77. The counting error for the spectrum was about 1.5%. The neutron spectrum in Figure 9, the field was very uniform, and the neutron spectrum was very uniform, varied from unity by about 1.5%.

Table 5. Summary of Sulfur Results

| Run No.                       | Array   | kW-min | Fluence* (>3 MeV)<br>Per kW-min |                    | Neutron kerma <sup>-</sup><br>Per Fluence (>3 MeV) |              |
|-------------------------------|---------|--------|---------------------------------|--------------------|--|--------------|
|                               |         |        | M3 <sup>†</sup>                 | M1,M2 <sup>§</sup> | M3   | M1,M2        |
| SS 86-99                      | FIA     | 57     | 1.75                            | 3.10               | 1.99   | 11.2         |
| SS 86-100                     | FIA     | 38     | 1.73                            | 3.08               | 2.01   | 11.3         |
| SS 86-101                     | FIA     | 38     | 1.77                            | 3.10               | 2.01   | 11.4         |
| SS 86-102                     | FIA     | 63     | 1.78                            | 3.09               | 1.97   | 11.3         |
| SS 86-103                     | FIA     | 200    | 1.76                            | 3.10               | 2.00   | 11.4         |
| SS 86-104                     | FIA     | 30     | 1.79                            | 3.08               | 1.96   | 11.4         |
| SS 86-105                     | Phantom | 200    | 1.81                            | 3.10               | 2.06   | 12.1         |
| P 86-15                       | Phantom | 24.9   | 1.90                            | 3.41               | —  | —            |
| P 86-16                       | FIA     | 39.5   | 1.84                            | 3.21               | —  | —            |
| Average FIA SS<br>(SEM, 1 SD) |         |        | 1.76<br>1.1%                    | 3.10<br>0.4%       | 1.99<br>1.0%                                       | 11.3<br>0.7% |
| Phantom/FIA                   |         |        | 1.028                           | 1.00               | 1.035  | 1.07         |

\*Units of fluence are  $\text{n/cm}^2/\text{kW-min} \times 10^8$ .

<sup>†</sup> Determined from ionization chamber measurements. Units are  $\text{Gy-cm}^2 \times 10^{-10}/\text{n}$  calculated by dividing ion chamber  $\text{Gy/kW-min}$  (Table 4) by sulfur  $\text{n/cm}^2/\text{kW-min}$  (Table 5).

<sup>‡</sup> M3 = sulfur near ion chambers (counting error  $\pm 1.5\%$  [1 SD]).

<sup>§</sup> M1,M2 = average of sulfurs on converter shield (counting error  $\pm 0.5\%$ ).

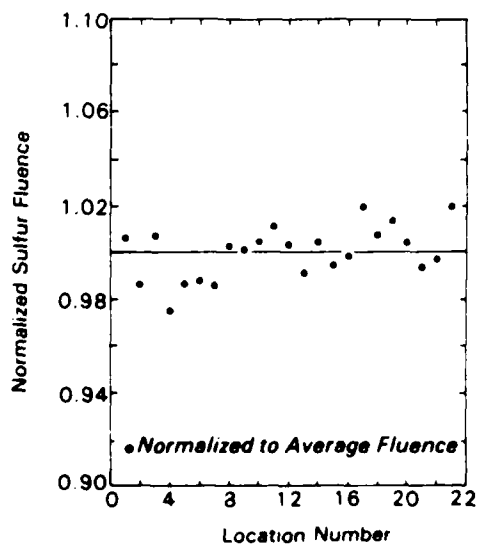


Figure 9. Field uniformity of phantom array

The  $\text{CaF}_2\text{:Mn}$  TLD results are shown in Table 6. The precision shown in the Table is the SEM of the five TLD chips used for each irradiation. Except for run SS 86-103, the precision was very good. In all cases, there was good agreement between the TLD's and the ionization chambers.

Table 6. Summary of  $\text{CaF}_2\text{:Mn}$  TLD Results

| Run No.   | Array   | kW-min | $K_g$ TLD's<br>(cGy/kW-min) | SD<br>(%) | $K_g$ Chambers<br>(cGy/kW-min) |
|-----------|---------|--------|-----------------------------|-----------|--------------------------------|
| SS 86-103 | FIA     | 200    | 4.47                        | 6.9       | 4.72                           |
| SS 86-104 | FIA     | 30     | 4.80                        | 0.8       | 4.67                           |
| SS 86-105 | Phantom | 200    | 5.45                        | 2.5       | 5.51                           |
| P 86-15   | Phantom | 24.9   | 6.22                        | 0.5       | —                              |
| P 86-16   | FIA     | 39.5   | 5.34                        | 0.5       | —                              |

In Table 7, the rhodium data are shown normalized to the sulfur foils and compared to the neutron kerma measured by the ionization chambers. The counting error for the rhodium foils was about 1%, but the consistency from run to run was only about 3.5%. Reasons for this poor precision are not clear at this time, and more work is needed to adapt the Rh system as a kerma monitor.

Table 7. Rhodium Results

| Run No.   | Array   | Rh (No Cd) |   |   | Rh (Cd)   |   |   |
|---|---------|------------|---|---|-----------|---|---|
|   |         | Activity*  | Activity<br>Per Fluence<br>( $>3$ MeV) <sup>†</sup> | Neutron<br>Kerma Per<br>Activity <sup>‡</sup> | Activity* | Activity<br>Per Fluence<br>( $>3$ MeV) <sup>†</sup> | Neutron<br>Kerma Per<br>Activity <sup>‡</sup> |
| SS 86-103   | FIA     | 5.29       | 15.2  | 1.32  | 5.38      | 15.5  | 1.31  |
| SS 86-104   | FIA     | 0.76       | 14.5  | 1.40  | 0.79      | 14.7  | 1.36  |
| SS 86-105   | Phantom | 5.17       | 14.6  | 1.45  | 5.47      | 15.0  | 1.37  |
| P 86-15   | Phantom | 0.73       | 15.4  | —   | 0.73      | 15.7  | —   |
| P 86-16   | FIA     | 1.13       | 15.7  | —   | —         | —   | —   |
| Average activity/fluence ( $>3$ MeV) : $15.1 \times 10^{-11} \mu\text{Ci} \cdot \text{cm}^2/\text{g} \cdot \text{neutron}$<br>SEM (1 SD) : 3.1% |         |            |   |   |           |   |   |
| Average neutron kerma/activity : $1.37 \text{ Gy} \cdot \text{g}/\mu\text{Ci}$<br>SEM (1 SD) : 3.5%   |         |            |   |   |           |   |   |

\*Units are  $\mu\text{Ci/g}$

<sup>†</sup>Units are  $\mu\text{Ci-cm}^2 \times 10^{-11}/\text{g} \cdot \text{neutron}$

<sup>‡</sup>Units are  $\text{Gy} \cdot \text{g}/\mu\text{Ci}$

In Table 8, kerma values determined from the sulfur foils and from  $\text{CaF}_2\text{:Mn}$  TLD's are compared to the ionization chamber results.  $K_g$  was determined directly from the TLD's, and  $K_n$  was determined using the sulfur foil at irradiation position M3 and the fluence-to-kerma conversion factors (Table 5) as follows:

$$\text{FIA: } K_n (\text{Gy}) = 1.99 \times 10^{-10} \text{ Gy/n/cm}^2 \cdot \phi > 3 \text{ MeV n/cm}^2$$

$$\text{Phantom: } K_n (\text{Gy}) = 2.06 \times 10^{-10} \text{ Gy/n/cm}^2 \cdot \phi > 3 \text{ MeV n/cm}^2$$

Table 8. Kerma From Sulfurs and TLD's

|           |         | Kerma (Gray)      |       |       |           |                     |           |
|-----------|---------|-------------------|-------|-------|-----------|---------------------|-----------|
|           |         | Sulfurs and TLD's |       |       |           | Ionization Chambers |           |
| Run No.   | Array   | $K_n$             | $K_g$ | $K_t$ | $K_g/K_t$ | $K_t$               | $K_g/K_t$ |
| SS 86-103 | FIA     | 7.03              | 8.93  | 16.0  | 0.56      | 16.4                | 0.57      |
| SS 86-104 | FIA     | 1.07              | 1.44  | 2.51  | 0.57      | 2.44                | 0.57      |
| SS 86-105 | Phantom | 7.48              | 10.9  | 18.4  | 0.59      | 18.4                | 0.59      |
| P 86-15   | Phantom | 0.98              | 1.55  | 2.53  | 0.61      | —                   | —         |
| P 86-16   | Phantom | 1.45              | 2.11  | 3.56  | 0.59      | —                   | —         |

Note that the M3 sulfur was used as monitor because it was close to the irradiation array and would therefore reflect any minor positioning errors. The sulfurs on the converter shield would more accurately monitor reactor power levels.

## DISCUSSION

The ionization chamber results presented above are based on the APRF bare-core neutron spectrum 15 m from the core. Although the effect of the converter shield is to harden the spectrum, this is not expected to cause significant change in the factor  $k_t$  (TE-TE chamber sensitivity). Table 12 (in Appendix B) gives examples of chamber constants  $k_t$  and  $k_u$  for other neutron energy spectra. Even in the most extreme cases (water and lead shield configurations), the calculated variations in  $k_t$  and  $k_u$  cause total kerma differences of less than 2%. Thus the lack of precise knowledge of the neutron energy spectrum transmitted through the converter shield does not adversely affect the accuracy of kerma measurements presented in this report.



The data in Table 8 indicate that the sulfur foils and  $\text{CaF}_2\text{:Mn}$  TLD's performed well in determining the kerma, differing from the ionization chamber results by 3.5% or less. Table 9 shows that the APRF sulfur results agreed with those of AFRRI. This was expected, because both systems were benchmarked in the same NBS californium radiation field. Table 8 also shows that the gamma-ray component is slightly enhanced for the pulsed irradiations; this was most likely due to the delayed gamma-ray tail. Although the precision of the rhodium data was not ideal, the data in Table 6 show that the ratio of the rhodium activity to sulfur fluence ( $>3$  MeV) was fairly constant for all runs, i.e., steady-state, pulsed, FIA, and on the phantom. The constancy of this ratio indicates that the neutron spectrum (above 0.7 MeV) in the FIA irradiation did not differ much from the phantom irradiation. The ion chamber showed an increase in the neutron component during the phantom irradiation. This is due to albedo neutrons of energies lower than the rhodium 0.7-MeV threshold. In Tables 4 and 6, the ion chambers and the TLD's showed an increase in the gamma component of the dose from the hydrogenous phantom.

Table 9. Comparison of APRF and AFRRI Sulfur Fluence\* Measurements

| Run No.   | Array   | On Converter Shield |      | At Chamber Position |      |
|-----------|---------|---------------------|------|---------------------|------|
|           |         | AFRRI               | APRF | AFRRI               | APFR |
| SS 86-99  | FIA     | 3.10                | 3.11 | 1.76                | 1.76 |
| SS 86-100 | FIA     | 3.08                | 3.12 | 1.73                | 1.73 |
| SS 86-101 | FIA     | 3.10                |      | 1.77                |      |
| SS 86-102 | FIA     | 3.09                |      | 1.78                |      |
| SS 86-103 | FIA     | 3.10                |      | 1.76                | 1.72 |
| SS 86-104 | FIA     | 3.08                |      | 1.79                |      |
| SS 86-105 | Phantom | 3.10                |      | 1.81                |      |
| P 86-15   | Phantom | 3.42                |      | 1.90                |      |
| P 86-16   | FIA     | 3.21                | 3.24 | 1.85                | 1.85 |

\*Units are  $\text{n} \times 10^8/\text{cm}^2 \cdot \text{kW-min.}$

## CONCLUSIONS

A method to provide reference dosimetry for the NATO Dosimetry Study has been developed based on measurements using paired ionization chambers. Sulfur fluence-to-neutron kerma conversion factors have been established, and  $\text{CaF}_2\text{:Mn}$  TLD's have been shown to accurately measure the gamma-ray component of the kerma in the APRF reactor fields to be used in the Study. Ideally, a sulfur foil and a set of  $\text{CaF}_2\text{:Mn}$  TLD's will be placed with each participant's irradiation array. The sulfurs, benchmarked to the NBS californium-252 source, measure the fluence  $>3$  MeV, from which the neutron kerma is calculated as follows:

$$\text{FIA: } K_n (\text{Gy}) = 1.99 \times 10^{-10} \text{ Gy/n/cm}^2 \cdot \phi > 3 \text{ MeV n/cm}^2$$

$$\text{Phantom: } K_n (\text{Gy}) = 2.06 \times 10^{-10} \text{ Gy/n/cm}^2 \cdot \phi > 3 \text{ MeV n/cm}^2$$

$\text{CaF}_2\text{:Mn}$  TLD's in buildup capsules and with cobalt-60 calibration traceable to NBS (and corrections for fading when applicable) are used to measure the photon kerma. In addition, sulfur activation foils are placed on a set location on the converter shield to serve as power monitors. Kermas calculated using this system are within about 3% of those determined by the ionization chambers.

## ACKNOWLEDGMENTS

The authors would like to thank the APRF staff for their help and cooperation.

## APPENDIX A. CALCULATION OF $k_t$

$$k_t = \frac{W_c}{W_n} \frac{(s_{m,g})_c}{(r_{m,g})_n} \frac{[(\mu_{en}/\rho)_t/(\mu_{en}/\rho)_m]_c}{(K_t/K_m)_n}$$

where

subscript c = calibration gamma rays (cobalt-60).

subscript n = neutrons in mixed field.

$W$  = average energy required to produce an ion pair in cavity gas (calculational methods provided in reference 10).

$s_{m,g}$  = wall-to-gas restricted collision mass stopping power ratio = 1.

$r_{m,g}$  = gas-to-wall absorbed dose conversion factor for non-Bragg-Gray cavity conditions generally produced by neutrons = 1.

$(\mu_{en}/\rho)_t/(\mu_{en}/\rho)_m$  = ratio of mass energy absorption coefficient of tissue (ICRU muscle) to chamber material = 1.

$K_t/K_m$  = ratio of spectrum-averaged kerma factor for tissue to that of MTE gas (calculational methods provided in reference 10).

## APPENDIX B. IONIZATION CHAMBER DATA

Table 10. Summary of Ionization Chamber Data at APRF

| Run No.      | Array   | kW | Chamber Response*              |                  | Monitor Response |
|--------------|---------|----|--------------------------------|------------------|------------------|
|              |         |    | cGy/kW-min<br>R <sub>t</sub> ' | R <sub>u</sub> ' | nC/kW-min        |
| SS 86-99     | FIA     | 6  | 7.96                           | 4.75             | 118.5            |
| SS 86-100    | FIA     | 6  | 8.00                           | 4.76             | 118.8            |
| SS 86-101    | FIA     | 6  | 7.99                           | 4.73             | 119.0            |
| SS 86-102    | FIA     | 6  | 7.94                           | 4.78             | 119.1            |
| SS 86-103    | FIA     | 3  | 7.86                           | 4.72             | 118.0            |
| SS 86-104    | FIA     | 6  | 7.96                           | 4.78             | 118.6            |
| SS 86-105    | Phantom | 6  | 9.03                           | 5.61             | 119.2            |
| Average FIA: |         |    | 7.95                           | 4.76             | 118.6            |
| SEM (1 SD):  |         |    | 0.6%                           | 0.6%             | 0.3%             |

\*Includes wall corrections (see Table 11 and Figures 7, 8)

Table 11. Ionization Chamber Factors

| Chamber                         | TE-TE<br>(TE-300) | MG-AR<br>(MG-143) |
|---------------------------------|-------------------|-------------------|
| <b>K<sub>w</sub>:</b>           |                   |                   |
| Cobalt-60                       | 0.988             | 0.990             |
|                                 | 4-mm cap          | 2-mm cap          |
| APRF                            | 0.990             | 0.987             |
|                                 | No cap            | 2-mm cap          |
| K <sub>e</sub>                  | 0.985             | 0.977             |
| K <sub>s</sub>                  | 1.00              | 1.00              |
| N <sub>x</sub><br>(roentgen/nC) | 5.405             | 4.118             |

Table 12. Chamber Constants for Different Radiation Fields

| Field                  | Average<br>Neutron<br>Energy<br>(MeV) | $W_n$<br>MTE gas<br>(eV) | 10 <sup>-11</sup> Gy · cm <sup>2</sup> |                 | $k_t$ | $k_u$ |
|------------------------|---------------------------------------|--------------------------|--|-----------------|-------|-------|
|                        |                                       |                          | K<br>ICRU<br>Muscle                    | K<br>MTE<br>Gas |       |       |
| APRF bare core at 15 m | 1.2                                   | 32.0                     | 1.35                                   | 1.37            | 0.930 | 0.02  |
| APRF (source spectrum) | 2.3                                   | 31.6                     | 2.84                                   | 2.89            | 0.942 | 0.03  |
| HPRR at 3 m:           |                                       |                          |  |                 |       |       |
| Bare core              | 1.9                                   | 31.9                     | 2.11                                   | 2.14            | 0.933 | 0.02  |
| Lucite shield          | 2.4                                   | 31.8                     | 1.64                                   | 1.66            | 0.939 | 0.02  |
| AFRRI at 1 m:          |                                       |                          |  |                 |       |       |
| 15-cm-Pb shield        | 1.0                                   | 32.2                     | 1.52                                   | 1.54            | 0.933 | 0.010 |
| Bare core              | 1.5                                   | 32.0                     | 1.96                                   | 2.00            | 0.944 | 0.020 |
| 30-cm-water shield     | 3.7                                   | 31.7                     | 2.76                                   | 2.80            | 0.956 | 0.024 |
| Californium-252        | 2.5                                   | 31.6                     | 2.90                                   | 2.95            | 0.958 | 0.03  |

For all spectra, assume  $h_t = h_u = 1.00$ .

## REFERENCES

1. Kazi, A. H. Operation of Army Pulsed Radiation Facility reactor core III. Transactions of American Nuclear Society 14: 313, 1971.
2. Kazi, A. H., Heimbach, C. R., Harrison, R. C., and Robitaille, H. A. Comparison of measured and calculated radiation transport in air-over-ground geometry to 1.6 km from a fission source. Nuclear Science and Engineering 85: 371-386, 1983.
3. Robitaille, H. A., and Hoffarth, B. E. A comparison of measured and calculated air-transported radiation from a fast, unshielded reactor. DREO Report No. 835, Defense Research Establishment of Ottawa, Ottawa, 1980.
4. Dooley, M. A., Goodman, L. J., Zeman, G. H., Schwartz, R. B., and Eisenhauer, C. M. Ionization chamber intercomparison in mixed neutron and gamma-ray radiation fields by National Bureau of Standards and Armed Forces Radiobiology Research Institute. Technical Report TR86-3, Armed Forces Radiobiology Research Institute, Bethesda, Maryland, 1986.
5. Goodman, L. J. A practical guide to ionization chamber dosimetry at the AFRRRI reactor. Contract Report CR85-1, Armed Forces Radiobiology Research Institute, Bethesda, Maryland, 1985.
6. Neutron Dosimetry for Biology and Medicine. ICRU Report 26, International Commission on Radiation Units and Measurements, Washington, DC, 1977.
7. Broese, J. J., Mijnheer, B. J., and Williams, J. R. European protocol for neutron dosimetry for external beam therapy. British Journal of Radiology 54: 882-898, 1981.
8. Wycoff, H. O. Reply to corrected f factors for photons from 10 keV to 2 MeV. Medical Physics 10: 715-716, 1983.
9. Waterman, F. M., Kuchnir, F. T., Skaggs, L. S., Kouzes, R. T., and Moore, W. H. Energy dependence of the neutron sensitivity of C-CO<sub>2</sub>, Mg-Ar, and TE-TE ionization chambers. Physics of Medicine and Biology 24: 721-733, 1979.
10. Zeman, G. H., and Ferlic, K. P. Paired ion chamber constants for fission gamma-neutron fields. Technical Report TR84-8, Armed Forces Radiobiology Research Institute, Bethesda, Maryland, 1984.
11. Grundl, J. A., and Eisenhauer, C. M. Compendium of benchmark neutron fields for reactor dosimetry: Standard neutron field entries. NBSIR 85-3151, National Bureau of Standards, Gaithersburg, Maryland, 1986.
12. Ing, H., and Cross, W. G. A criticality neutron dosimeter using the Rh-103(n,n')Rh-103m reaction. Health Physics 25: 291-297, 1973.

13. Zeman, G. H. Rhodium-103 and indium-115 inelastic scattering reactions for fission neutron dosimetry. Technical Report TR84-7, Armed Forces Radiobiology Research Institute, Bethesda, Maryland, 1984.
14. Zeman, G. H., and Dooley, M. A. Performance and dosimetry of Theratron-80 cobalt-60 unit at Armed Forces Radiobiology Research Institute. Technical Report TR84-1, Armed Forces Radiobiology Research Institute, Bethesda, Maryland, 1984.
15. Zeman, G. H., and Bice, W. S, Jr. Kerma factors for use in 37-group neutron spectrum calculations. Technical Report TR83-3, Armed Forces Radiobiology Research Institute, Bethesda, Maryland, 1983.

END

8-87

DTIC